National Library
of Canada

Acquisitions and
Bibliographic Services Branch

395 Wellington Street
Ottawa, Ontario
K1A 0N4

Bibliothèque nationale
du Canada

Direction des acquisitions et
des services bibliographiques

395, rue Wellington
Ottawa (Ontario)
K1A 0N4

Hot Deformation Behaviour of SiC_p/Al Composites and Their Matrices and an Al-Mg-Si Alloy

Peter Sakaris

A Thesis

in

The Department

of

Mechanical Engineering

Presented in Partial Fulfilment of the Requirements

for the Degree of Master of Applied Science at

Concordia University

Montreal, Quebec, Canada

April 1993

ISBN 0-315-84699-2

Name PETER SAKARIS

Dissertation Abstracts International is arranged by broad, general subject categories. Please select the one subject which most nearly describes the content of your dissertation. Enter the corresponding four-digit code in the spaces provided.

Materials Science

SUBJECT TERM

0794

SUBJECT CODE

U·M·I

Subject Categories

THE HUMANITIES AND SOCIAL SCIENCES

COMMUNICATIONS AND THE ARTS

- Architecture 0729
- Art History 0377
- Cinema 0900
- Dance 0378
- Fine Arts 0357
- Information Science 0723
- Journalism 0391
- Library Science 0399
- Mass Communications 0708
- Music 0413
- Speech Communication 0459
- Theater 0465

EDUCATION

- General 0515
- Administration 0514
- Adult and Continuing 0516
- Agricultural 0517
- Art 0273
- Bilingual and Multicultural 0282
- Business 0688
- Community College 0275
- Curriculum and Instruction 0727
- Early Childhood 0518
- Elementary 0524
- Finance 0277
- Guidance and Counseling 0519
- Health 0680
- Higher 0745
- History of 0520
- Home Economics 0278
- Industrial 0521
- Language and Literature 0279
- Mathematics 0280
- Music 0522
- Philosophy of 0998
- Physical 0523
- Psychology 0525
- Reading 0535
- Religious 0527
- Sciences 0714
- Secondary 0533
- Social Sciences 0534
- Sociology of 0340
- Special 0529
- Teacher Training 0530
- Technology 0710
- Tests and Measurements 0288
- Vocational 0747

LANGUAGE, LITERATURE AND LINGUISTICS

- Language
  - General 0679
  - Ancient 0289
  - Linguistics 0290
  - Modern 0291
- Literature
  - General 0401
  - Classical 0294
  - Comparative 0295
  - Medieval 0297
  - Modern 0298
  - African 0316
  - American 0591
  - Asian 0305
  - Canadian (English) 0352
  - Canadian (French) 0355
  - English 0593
  - Germanic 0311
  - Latin American 0312
  - Middle Eastern 0315
  - Romance 0313
  - Slavic and East European 0314

PHILOSOPHY, RELIGION AND THEOLOGY

- Philosophy 0422
- Religion
  - General 0318
  - Biblical Studies 0321
  - Clergy 0319
  - History of 0320
  - Philosophy of 0322
- Theology 0469

SOCIAL SCIENCES

- American Studies 0323
- Anthropology
  - Archaeology 0324
  - Cultural 0326
  - Physical 0327
- Business Administration
  - General 0310
  - Accounting 0272
  - Banking 0770
  - Management 0454
  - Marketing 0338
- Canadian Studies 0385
- Economics
  - General 0501
  - Agricultural 0503
  - Commerce-Business 0505
  - Finance 0508
  - History 0509
  - Labor 0510
  - Theory 0511
- Folklore 0358
- Geography 0366
- Gerontology 0351
- History
  - General 0578
  - Ancient 0579
  - Medieval 0581
  - Modern 0582
  - Black 0328
  - African 0331
  - Asia, Australia and Oceania 0332
  - Canadian 0334
  - European 0335
  - Latin American 0336
  - Middle Eastern 0333
  - United States 0337
- History of Science 0585
- Law 0398
- Political Science
  - General 0615
  - International Law and Relations 0616
  - Public Administration 0617
- Recreation 0814
- Social Work 0452
- Sociology
  - General 0626
  - Criminology and Penology 0627
  - Demography 0938
  - Ethnic and Racial Studies 0631
  - Individual and Family Studies 0628
  - Industrial and Labor Relations 0629
  - Public and Social Welfare 0630
  - Social Structure and Development 0700
  - Theory and Methods 0344
- Transportation 0709
- Urban and Regional Planning 0999
- Women's Studies 0453

THE SCIENCES AND ENGINEERING

BIOLOGICAL SCIENCES

- Agriculture
  - General 0473
  - Agronomy 0285
  - Animal Culture and Nutrition 0475
  - Animal Pathology 0476
  - Food Science and Technology 0359
  - Forestry and Wildlife 0478
  - Plant Culture 0479
  - Plant Pathology 0480
  - Plant Physiology 0817
  - Range Management 0777
  - Wood Technology 0746
- Biology
  - General 0306
  - Anatomy 0287
  - Biostatistics 0308
  - Botany 0309
  - Cell 0379
  - Ecology 0329
  - Entomology 0353
  - Genetics 0369
  - Limnology 0793
  - Microbiology 0410
  - Molecular 0307
  - Neuroscience 0317
  - Oceanography 0416
  - Physiology 0433
  - Radiation 0821
  - Veterinary Science 0778
  - Zoology 0472
- Biophysics
  - General 0786
  - Medical 0760

EARTH SCIENCES

- Biogeochemistry 0425
- Geochemistry 0996
- Geodesy 0370
- Geology 0372
- Geophysics 0373
- Hydrology 0388
- Mineralogy 0411
- Paleobotany 0345
- Paleoecology 0426
- Paleontology 0418
- Paleozoology 0985
- Palynology 0427
- Physical Geography 0368
- Physical Oceanography 0415

HEALTH AND ENVIRONMENTAL SCIENCES

- Environmental Sciences 0768
- Health Sciences
  - General 0566
  - Audiology 0300
  - Chemotherapy 0992
  - Dentistry 0567
  - Education 0350
  - Hospital Management 0769
  - Human Development 0758
  - Immunology 0982
  - Medicine and Surgery 0564
  - Mental Health 0347
  - Nursing 0569
  - Nutrition 0570
  - Obstetrics and Gynecology 0380
  - Occupational Health and Therapy 0354
  - Ophthalmology 0381
  - Pathology 0571
  - Pharmacology 0419
  - Pharmacy 0572
  - Physical Therapy 0382
  - Public Health 0573
  - Radiology 0574
  - Recreation 0575
  - Speech Pathology 0460
  - Toxicology 0383
- Home Economics 0386

PHYSICAL SCIENCES

Pure Sciences

- Chemistry
  - General 0485
  - Agricultural 0749
  - Analytical 0486
  - Biochemistry 0487
  - Inorganic 0488
  - Nuclear 0738
  - Organic 0490
  - Pharmaceutical 0491
  - Physical 0494
  - Polymer 0495
  - Radiation 0754
- Mathematics 0405
- Physics
  - General 0605
  - Acoustics 0986
  - Astronomy and Astrophysics 0606
  - Atmospheric Science 0608
  - Atomic 0748
  - Electronics and Electricity 0607
  - Elementary Particles and High Energy 0798
  - Fluid and Plasma 0759
  - Molecular 0609
  - Nuclear 0610
  - Optics 0752
  - Radiation 0756
  - Solid State 0611
- Statistics 0463

Applied Sciences

- Applied Mechanics 0346
- Computer Science 0984
- Engineering
  - General 0537
  - Aerospace 0538
  - Agricultural 0539
  - Automotive 0540
  - Biomedical 0541
  - Chemical 0542
  - Civil 0543
  - Electronics and Electrical 0544
  - Heat and Thermodynamics 0348
  - Hydraulic 0545
  - Industrial 0546
  - Marine 0547
  - Materials Science 0794
  - Mechanical 0548
  - Metallurgy 0743
  - Mining 0551
  - Nuclear 0552
  - Packaging 0549
  - Petroleum 0765
  - Sanitary and Municipal 0554
  - System Science 0790
- Geotechnology 0428
- Operations Research 0796
- Plastics Technology 0795
- Textile Technology 0994

PSYCHOLOGY

- General 0621
- Behavioral 0384
- Clinical 0622
- Developmental 0620
- Experimental 0623
- Industrial 0624
- Personality 0625
- Physiological 0989
- Psychobiology 0349
- Psychometrics 0632
- Social 0451

CONCORDIA UNIVERSITY

DIVISION OF GRADUATE STUDIES

This is to certify that the thesis prepared

By: Peter Sakaris

Entitled: Hot Deformation Behavior of SiC_p/Al Composites and Their Matrices and an Al-Mg-Si Alloy

and submitted in partial fulfillment of the requirements for the degree of

Master of Applied Science

complies with the regulations of this University and meets the accepted standards with respect to originality and quality.

Signed by the Final Examining Committee:

Dr. X. Xiao — Chair

Dr. G.H. Vatistas — Examiner

Dr. L.M. Landsberger (Electrical & ComputerEngineering) — External to the Program

Dr. H.J. McQueen — Supervisor

Approved by

Dr. R.B. Bhat, Graduate Program Director
Department of Mechanical Engineering

Dr. M.N.S. Swamy, Dean
Faculty of Engineering & Computer Science

April 14, 1993

ABSTRACT

Hot Deformation Behaviour of SiC_p/Al Composites and Their Matrices and an Al-Mg-Si Alloy

Peter Sakaris

Isothermal hot torsion tests were performed on two metal matrix composites (15v/o SiC_p/A356 Al and 15v/o SiC_p/6061 Al), a casting aluminum-silicon matrix alloy (A356) and an aluminum-magnesium-silicon alloy (6201). The composites and matrix alloy were tested over the range 300 to 540°C and 0.1 to 5.0 s^{-1}. Flow stress (σ) and strain-to-failure (ε_f) data were determined and compared with published results. The flow stresses decrease monotonically with increasing deformation temperature (T), following the same relationship as the published data. At very high temperatures, σ is similar for all materials but as T falls to 300°C, the A356 rises more rapidly than 6061. Flow stresses for the composites rise more rapidly than the matrix alloys, the A356 composite more than the 6061 composite. The ductility of all materials increases as T increases although it did not rise nearly as much for A356 as for 6061. However, ε_f rises more rapidly for SiC_p/A356 Al than ε_f for SiC_p/6061 Al. The decreased reduction in ε_f in the A356 materials compared to the 6061 materials indicates that the SiC particles have much less effect as additional crack initiators in A356. The plot of log $\dot{\varepsilon}$ versus log sinh $\alpha\sigma$ were approximately linear over the narrow range of strain rates tested. Also the plots of log sinh $\alpha\sigma$ versus 1000/T revealed straight line relationships so that single activation energies (Q_{HW}) can be computed for each material.

Testing of 6201 Al was conducted at 200 to 500°C for overaged specimens and at 300 to 600°C for the solutioned ones at rates of 0.1 to 4.0 s^{-1}. The activation energy for the precipitated alloy is about 192 kJ/mol which is higher than that of pure aluminum. The alloy is somewhat stronger than aluminum because of the particles at low temperatures and the increased level of solute at high ones. The solutioned specimens had high peak stresses and considerable work softening at 300°C due to dynamic formation and coalescence of precipitates. The Q_{HW} was higher but poorly defined because of variations in precipitation during heating. The ductility increased as T rose and $\dot{\varepsilon}$ decreased and was higher for precipitated than for solutioned specimens. The reduction of flow stress was confirmed to be dynamic recovery by the presence of elongated grains.

PREFACE

The work described in this thesis was carried out by the author in the Department of Mechanical Engineering, Concordia University and the Department of Mining and Metallurgy, McGill University between September 1990 and December 1992, under the supervision of Dr. H. J. McQueen. No part of this thesis has been previously been submitted for a degree at this or any other university. The data used in this thesis if they are from other research work has been duly acknowledged in the text. A list of references is included at the end of this thesis. Parts of this work have been presented at the Advanced Composites '93 Conference in Wollongong, Australia, in February 1993, at the 31st Annual Canadian Institute of Mining and Metallurgy Conference, Edmonton, Canada, in August 1992, at the ICAA3 Conference, Trondheim, Norway, in June 1992 and at the First Canadian International Composites Conference and Exhibition, Montreal, Canada, in September 1991.

ACKNOWLEDGEMENTS

The author wishes to express his gratitude and appreciation to his supervisor Dr. Hugh J. McQueen who provided guidance and encouragement throughout this research project. Special thanks go to Dr. John Bowden and Dr. Terry Maccagno who, willingly, gave technical assistance with respect to the mechanisms of the testing system and computer programming. The author gratefully acknowledges the cooperation of Mrs. Janet Bowles with respect to the metallographic work presented in this thesis. He is also grateful to Dr. David J. Lloyd of Alcan International Limited for providing the machined aluminum-matrix composites and the A356 Al alloy specimens. The SCR®-6201 Al test samples were supplied by Southwire Co., Carrolton, Georgia. He would like to thank la Formation de Chercheurs et l'Aide à la Recherche (FCAR) for providing the funds in making this research project possible.

TABLE OF CONTENTS

Page

Page

APPENDIX

LIST OF FIGURES

FIGURE

Page

FIGURE

Page

FIGURE

Page

FIGURE

LIST OF TABLES

NOMENCLATURE

A: Material Constant [s^{-1}]

L_o: Specimen Gauge Length [mm]

m: Strain Rate Sensitivity Exponent

N: Number of Turns

n: Stress Exponent

n'': Strain Hardening Exponent

Q_c: Activation Energy for Creep [kJ/mol]

Q_{HW}: Activation Energy for Hot Working [kJ/mol]

R: Universal Gas Constant [8.314 J/mol-K]

r: Specimen Gauge Radius [mm]

Z: Zener-Hollomon Parameter [s^{-1}]

α: Stress Multiplier [MPa^{-1}]

γ: Torsional Strain

ε: Equivalent Strain

$\dot{\varepsilon}$: Strain Rate (s^{-1})

σ: Equivalent Flow Stress [MPa]

τ: Shear Stress [MPa]

1. INTRODUCTION

The objective of this research is to determine the hot working behaviour of two silicon carbide reinforced aluminum-matrix composites (SiC/Al), an aluminum-magnesium-silicon alloy (Al-Mg-Si) and a casting aluminum-silicon alloy (Al-Si) under continuous deformation conditions. Torsion is the method of testing employed and has the advantage compared to tension and compression in that a large strain can be applied to a specimen at a relatively constant rate. The drawback of the torsion test is that the strain and strain rate are not constant across the section of the specimen.

The project involves the determination of stress-strain curves and fracture strains at typical hot working temperatures and strain rates. General characteristics of SiC/Al composites, Al-Mg-Si and cast Al-Si alloys will be examined in Chapter 2. The literature which describes the general hot working characteristics of the above materials then follows in Chapter 3. A description of the hot torsion machine along with its operating procedure are presented in Chapter 4. A full description of the experimental procedures adopted in the present study is also given. Chapter 5 details all experimental results and a discussion of the results follows in Chapter 6. Finally, in Chapter 7, conclusions are drawn concerning the hot deformation characteristics of the materials based on the present work.

2. GENERAL MATERIAL CHARACTERISTICS

2.1 Aluminium-Matrix Composites

Aluminum alloys reinforced with silicon carbide (SiC/Al) are advanced materials engineered to overcome the limitations of conventional aluminum alloys. These composites yield substantial improvements in stiffness and strength [1-3]. Compared to the unreinforced alloy, SiC/Al generally offers other advantages including high temperature deformation, low coefficient of thermal expansion, improved abrasion resistance and better fatigue properties [1,4,5]. Table 2.1 compares mechanical data of various aluminum alloy composites fabricated by powder metallurgy as a function of the amount of SiC [6]. The density of SiC is only slightly higher than that of aluminum but the improvement in stiffness and thermal dimensional stability make these materials more attractive than other low density alloys for aerospace applications [1,3,7]. Although the strengths of particulate composites are usually inferior to composites with continuous fibers, their isotropic properties prove to be advantageous. Moreover, fabrication by conventional metalworking practices such as extrusion, forging and rolling without major modifications in the standard process is possible [2,6,8,9].

The development of SiC/Al composites has been slow due to the high cost of producing the silicon carbide fibers. Advancements over the past decade include the fabrication of less expensive SiC fibers and particles. The availability of SiC coupled with the potential of lightweight and structurally efficient components make these materials very attractive for use in many applications [10,11].

Table 2.1: Typical mechanical properties of SiC particulate reinforced aluminum alloy composites fabricated by powder metallurgy [6].

Material (v/o SiC)	Modulus of Elasticity (GPa)	Yield Strength (MPa)	Ultimate Tensile Strength (MPa)	Ductility (%)
6061				
0 (Wrought)	68.9	275.8	310.8	12.0
15	96.5	400.0	455.1	7.5
20	103.4	413.7	496.4	5.5
25	113.8	427.5	517.1	4.5
30	120.7	434.3	551.6	3.0
35	134.5	455.1	551.6	2.7
40	144.8	448.2	586.1	2.0
2124				
0 (Wrought)	71.0	420.6	455.1	9.0
15	--	--	--	--
20	103.4	400.0	551.6	7.0
25	113.8	413.7	565.4	5.6
30	120.7	441.3	593.0	4.5
35	--	--	--	--
40	151.7	517.1	689.5	1.1
7090				
0 (Wrought)	72.4	586.1	634.3	8.0
15	--	--	--	--
20	103.4	655.0	724.0	2.5
25	115.1	655.0	724.0	2.5
30	127.6	703.3	772.2	1.2
35	131.0	710.2	724.0	0.90
40	144.8	689.5	70.2	0.90

2.1.1 Composite System

Aluminum-matrix composites are not a single material but a family of materials whose stiffness, strength, density, thermal and electrical properties can be adjusted for specific applications [4,5]. The matrix alloy and the type, size, volume fraction and location of the reinforcement are chosen to match desired properties [12]. In general, the ductility and fracture toughness are controlled by the matrix alloy composition and heat treatment while the stiffness and strength are determined by the reinforcement. Silicon carbide reinforcements can be in the form of continuous filaments, discontinuous whiskers and discontinuous particles. The choice depends on the required properties, cost and the matrix material [4,5,12,13].

Continuous filaments, ranging from 3 to 200 μm in diameter, provide the greatest improvement in strength but are also the most expensive to fabricate [4,5,10]. Discontinuous whiskers are needle-like fibers with very small diameters and lengths ranging from 10 to 100 μm. The length-to-diameter ratio of these crystals is typically between 50 and 150. Whiskers are used to produce the highest strength discontinuous reinforced metal matrix composite (MMC) [1,3,5]. Particles provide the least improvement in strength and stiffness but are the least expensive reinforcement to produce. Ranging in diameter from 3 to 200 μm, they produce more isotropic properties, while continuous fibers and discontinuous whiskers yield more directional properties [4,5]. Using particles of around 10 μm reduces the propensity for particle fracture which occurs readily in coarse particles. The composite ductility is very sensitive to the distribution of particles, with voids opening up in particle clusters. Since

SiC particles are pushed ahead of the liquid-solid interface, the particle distribution is dependent on the solidification conditions or casting process used. Figure 2.1 compares the as-cast microstructures of 20v/o SiC_p/A356 Al produced by investment and by pressure die casting. The particle distribution is more uniform for pressure die casting. Any secondary fabrication, such as extrusion, further modifies the particle distribution [9].

In a composite system, the best properties are obtained when the reinforcement and the matrix alloy are as physically and chemically compatible as possible [1]. Although SiC can be used with other metals, its combination with Al alloys offers improved strength to weight ratio [4]. The selection of the matrix alloy is based on the characteristics desired in the final product. The 6xxx series alloys are widely used because of their high formability and overall good mechanical properties. The 7xxx and 2xxx series alloys are selected where strength is required. For improved castability, Al-Si alloys such as A356 can be used [13].

2.1.2 Fabrication

Two processes are commonly used to produce SiC/Al: liquid metal fabrication and powder metallurgy. Liquid metal fabrication is a simple process but can be difficult because the liquid metal may not wet the reinforcement and hence does not penetrate between every particle thus causing clustering [8,9,11,14]. This problem can be overcome by precoating the particles which improves wettability (molecular or atomic bonding taking place over the entire surface of the reinforcement). However for combinations with good wetting, it is possible that the liquid metal dissolves the

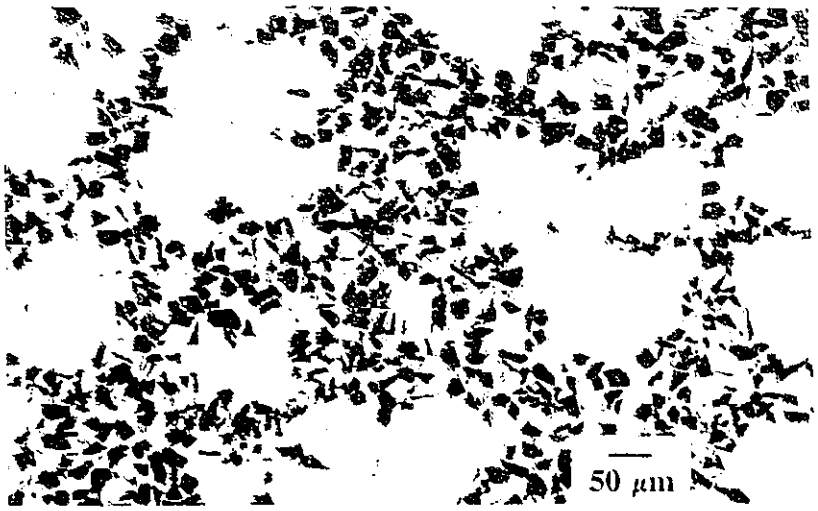

(a)

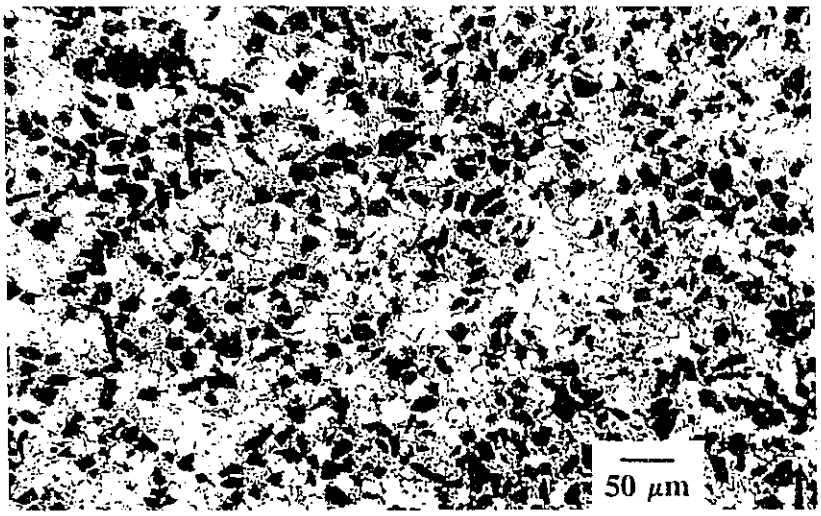

(b)

Figure 2.1: SiC particle distribution in 20v/o SiC/A356 Al: (a) investment and (b) pressure die casting [14].

reinforcement non-uniformly or dissolves into it thus weakening it. Aluminum alloy and SiC particle combinations have been produced successfully by the DURALCAN® molten metal mixing method. Since the composites are produced in the molten state, they can be processed using conventional casting and fabrication techniques and can also be cast to shape. However, problems of segregation occur as the particles increase in size and volume fraction [8,9,11]. The uniformity of distribution is improved by faster cooling to reduce the spacing of the dendrite arms. This method is less expensive than powder metallurgy but the particles are larger and less well distributed, thus leading to reduced strength. Spray deposition of atomized liquid metal and reinforcing particles ensure a liquid layer around every particle and rapid solidification. However, a low density of voids requires subsequent consolidation. In compo-casting, the fibers are arranged in a preform at the beginning of infiltration but are pressed together when the matrix is partly solidified to eliminate voids at relatively low pressures. For near net shapes, the preform can be infiltrated in a mold but voids are left at low pressures. If the fibers are not preheated, damage may result due to thermal shock from the molten metal [8,11].

Powder metallurgy (P/M) (Figure 2.2) begins with the mixing and blending of pre-alloyed metallic powder and ceramic material, followed by heating and degassing and finally consolidation into intermediate or final product forms [1,8,11]. The ceramic powders employed may be finer (about 5 μm) than those in solidification processing. This process is unlikely to yield complete density of the powders if the initial compaction is cold which can mechanically damage the reinforcements. Hot isostatic pressing is an effective process in eliminating voids with limited damage [8,11]. P/M manufacture

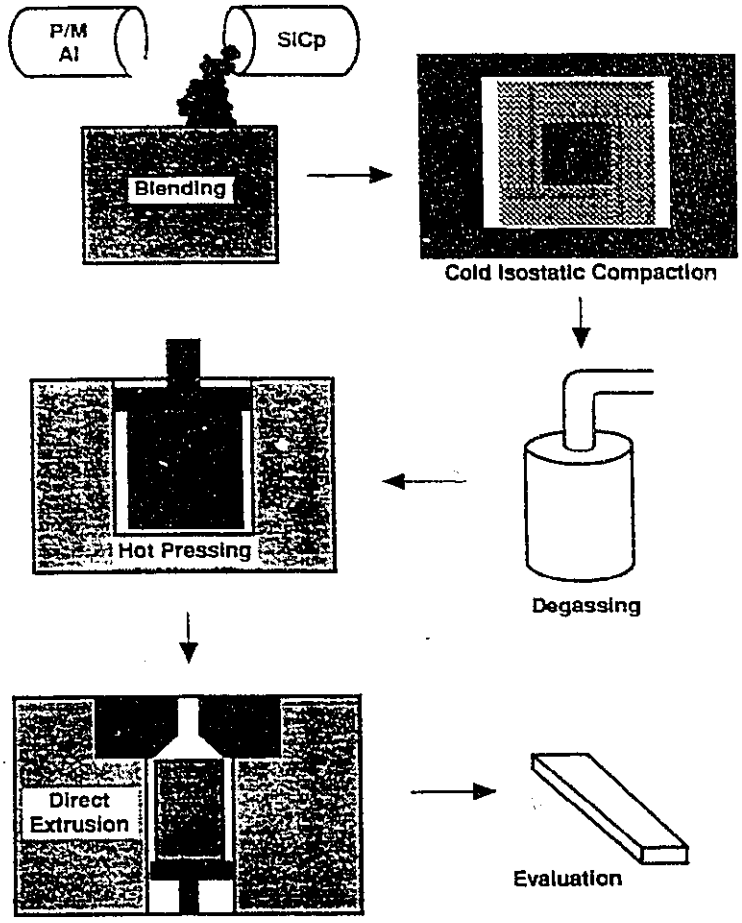

Figure 2.2: Powder metallurgy fabrication route for discontinuously reinforced composites [11].

generally yields improved mechanical properties compared to liquid melt fabricated composites. When composites are produced by P/M, the reinforcement is either never exposed to molten metal or exposed to short contact times during sintering. However, in molten metal processing, because of the relatively long exposure times, the liquid metal may react with the reinforcing material and degrade it. This is the case with unprotected SiC, which is unstable in most aluminum alloys [11,14]. The main reaction between liquid aluminum and SiC is:

$$4Al + 3SiC \rightleftharpoons Al_4C_3 + 3Si \qquad (2.1)$$

The formation of Al_4C_3 is deleterious from several viewpoints. Obviously, it degrades the reinforcement and is susceptible to corrosion. It increases the silicon level of the alloy, modifying the composition and metallurgy of the matrix, which may be detrimental to the final properties. However, the extent of the reaction can be limited by increasing the Si level of the matrix alloy. An alternative method of limiting the reaction is to give the SiC particles a protective surface treatment which also enhances wettability [14].

2.1.3 Mechanical Properties

The mechanical properties of SiC reinforced aluminum are better than those of the unreinforced advanced alloys in several ways, being stronger and more wear resistant. The enhanced properties of the composites allow for the use of components with lower sectional thickness and therefore less weight. Unfortunately, these advantageous properties are accompanied by low ductility and fracture toughness [1,3].

2.1.3.1 Strength and Stiffness

Silicon carbide composites offer improvements in elastic modulus and strength over the metal alloys used as their matrices (Table 2.1) [2,3,6]. Figure 2.3 shows the stress-strain curves for 6061 and A356 Al composite along with their matrix counterparts under two heat treatment conditions. Figure 2.4 shows that yield strength, tensile strength and stiffness values increase as the amount of reinforcement increases [1,6,15,16]. The SiC whiskers offer both very high modulus values and yield strengths. In objects requiring multi-directional reinforcement, SiC particles outperform whisker or fiber reinforced composites due to their isotropic behaviour [6].

Composites respond very well to heat treatment. Figure 2.5 shows that aging times to achieve peak strength are reduced for SiC/Al composites [6]. The difference in aging behaviour of the reinforced materials and the unreinforced alloys suggest that the matrix behaves in a particular way, as a consequence of the presence of the reinforcement [17]. The increase in yield stress and the reduced aging time is attributed to the presence of high diffusive interfaces in the composite and to the high dislocation density as a result of the differences in coefficients of thermal expansion of the matrix and the reinforcement [16,17].

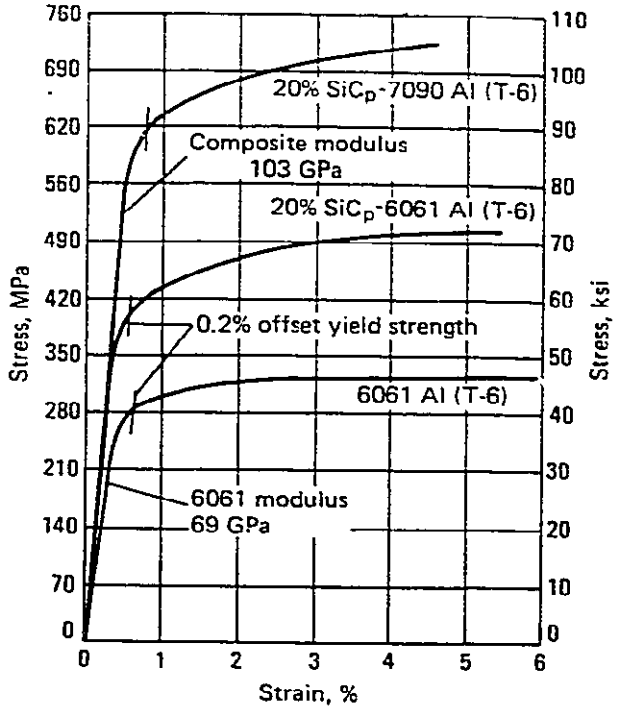

(a)

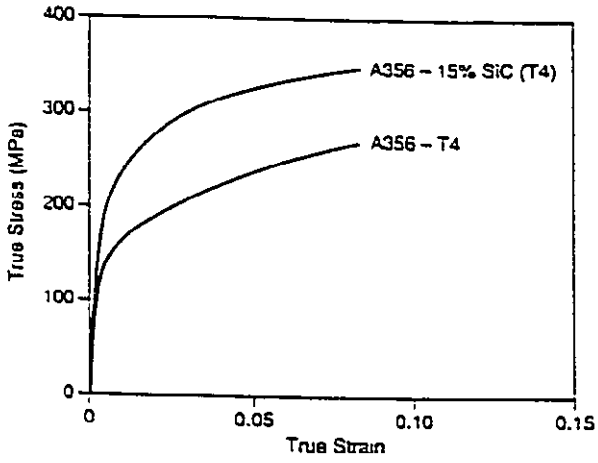

(b)

Figure 2.3: Stress-strain curves: (a) 6061 Al and (b) A356 Al based materials [6,9].

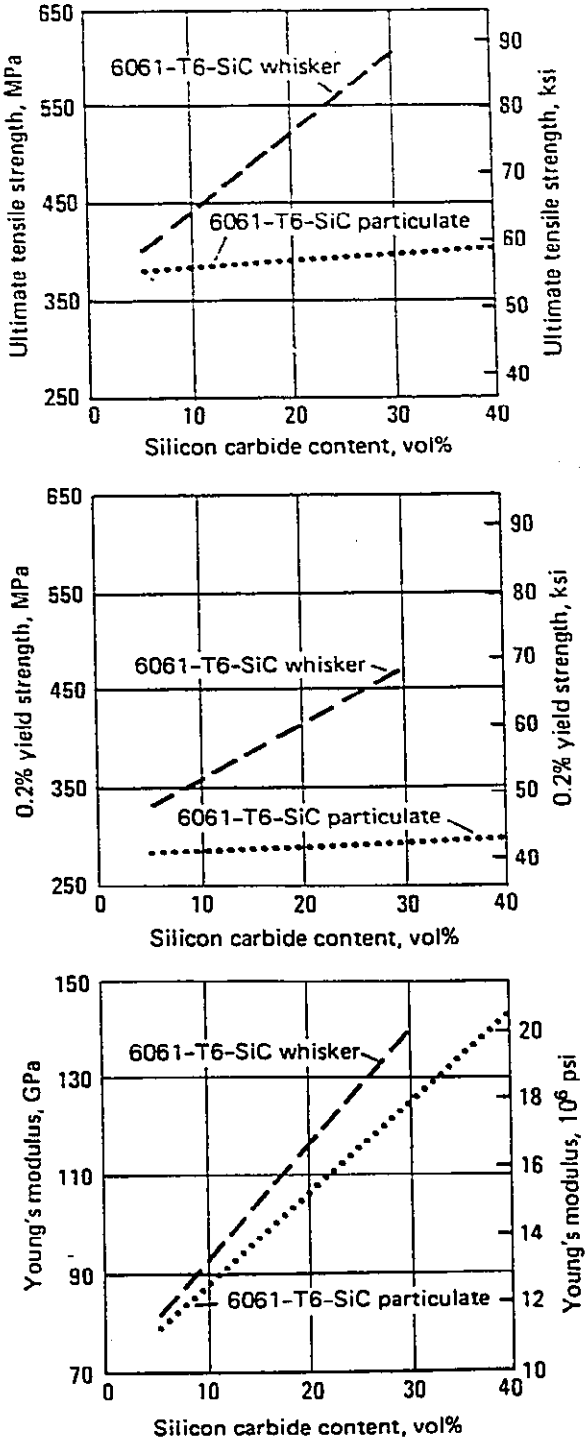

Figure 2.4: Effects of SiC content on tensile properties of 6061 MMC [6].

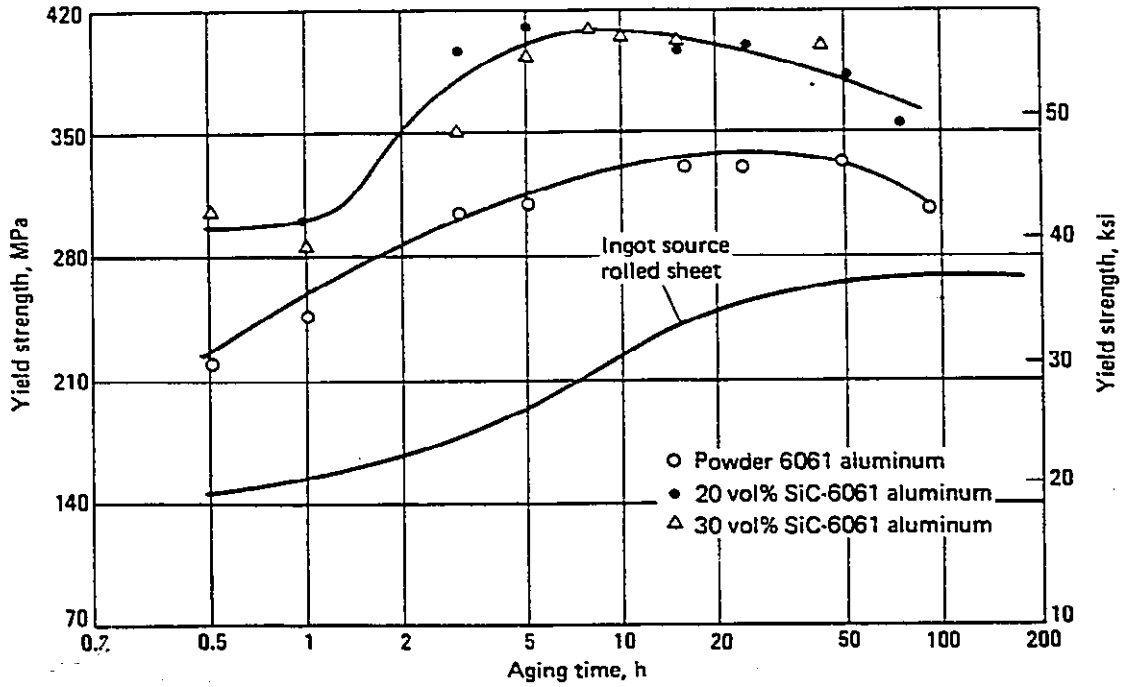

Figure 2.5: Aging response for 6061 Al and SiC/6061 Al composites, aged at 160°C [6].

2.1.3.2 Ductility

Ductility decreases as the amount of reinforcement increases (Table 2.1) [6]. Table 2.2 shows the percent elongation data for various SiC/Al forms and matrix alloys. Percent elongation decreases as the amount of SiC increases but rises with T6 heat treatment. At constant volume fractions, ductility enhancement requires the minimization of the sizes of the SiC and the constituent phases [3,8]. The ductility of SiC particulate composites is much greater than it is for continuous fiber composites. Hot rolling increases the strength of P/M particulate composites notably by redistributing clustered SiC particles and by bringing them all into contact with the matrix (Figure 2.6) [3,8,15]. After rolling, the composite has a very uniform distribution of Al and SiC. Ductility rises with the amount of hot work but declines with rising SiC content (Figure 2.7) [8,15].

Figure 2.8 compares the tensile elongations at different strength levels of unreinforced A356 Al and SiC/A356 in both the as-cast condition and after extruding with a 70:1 extrusion ratio. The tensile elongation of the as-cast composite is around 1% which is much lower than the unreinforced alloy. However, after extrusion the composite ductilities are comparable or better than the unreinforced alloy while also being considerably stronger. This behaviour suggests that the tensile ductility is controlled by matrix failure under high stresses associated with particle clusters [9].

Table 2.2: Tensile properties of SiC/Al product forms and relation to wrought alloys [15].

Material	Modulus of Elasticity (GPa)	Yield Strength (MPa)	Ultimate Tensile Strength (MPa)	Ductilty (%)
20v/o SiC_w/6061-T6				
(Rolled Sheet 2.5 mm)				
Longitudinal[1]	124	372	434	2.4
Transverse	93	338	407	7.0
(Extruded Tube 30 mm O.D.)				
Longitudinal[1]	100	386	462	14.5
Typical 6061-T6	69	276	310	10.0
20v/o SiC_w/6061-O				
(As-Pressed Billet 150 mm dia. x 150 mm)				
Axial	87	117	228	4.1
Radial	88	124	269	2.7
Typical 6061-O	69	55	124	30.0
25v/o SiC_p/2024				
(As-Pressed Sheet 0.5 mm)				
Longitudinal[1]	124	--[2]	--[2]	--[2]
Transverse	120	331	345	2.5
(Typical 2024)				
Annealed	73	76	186	21.0
T3	--	345	476	18.0

[1] Longitudinal to the extrusion direction
[2] Longitudinal sheet taper caused failure within the thinner of the two grip sections

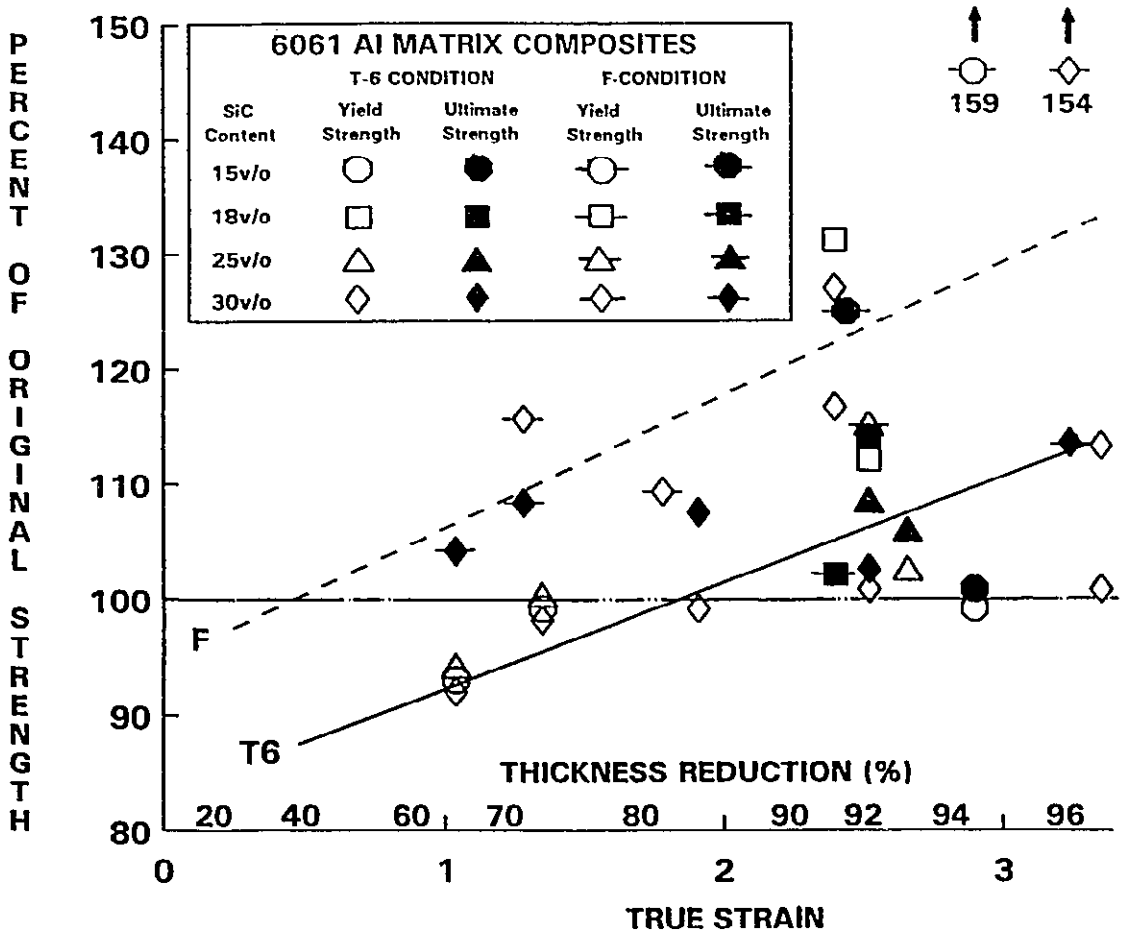

Figure 2.6: The strength of T-6 heat treated MMCs increase as rolling reduction rises above 83% to 96%. The increase in strength is much higher for F-treated material because of the high level of matrix strain hardening [8,15].

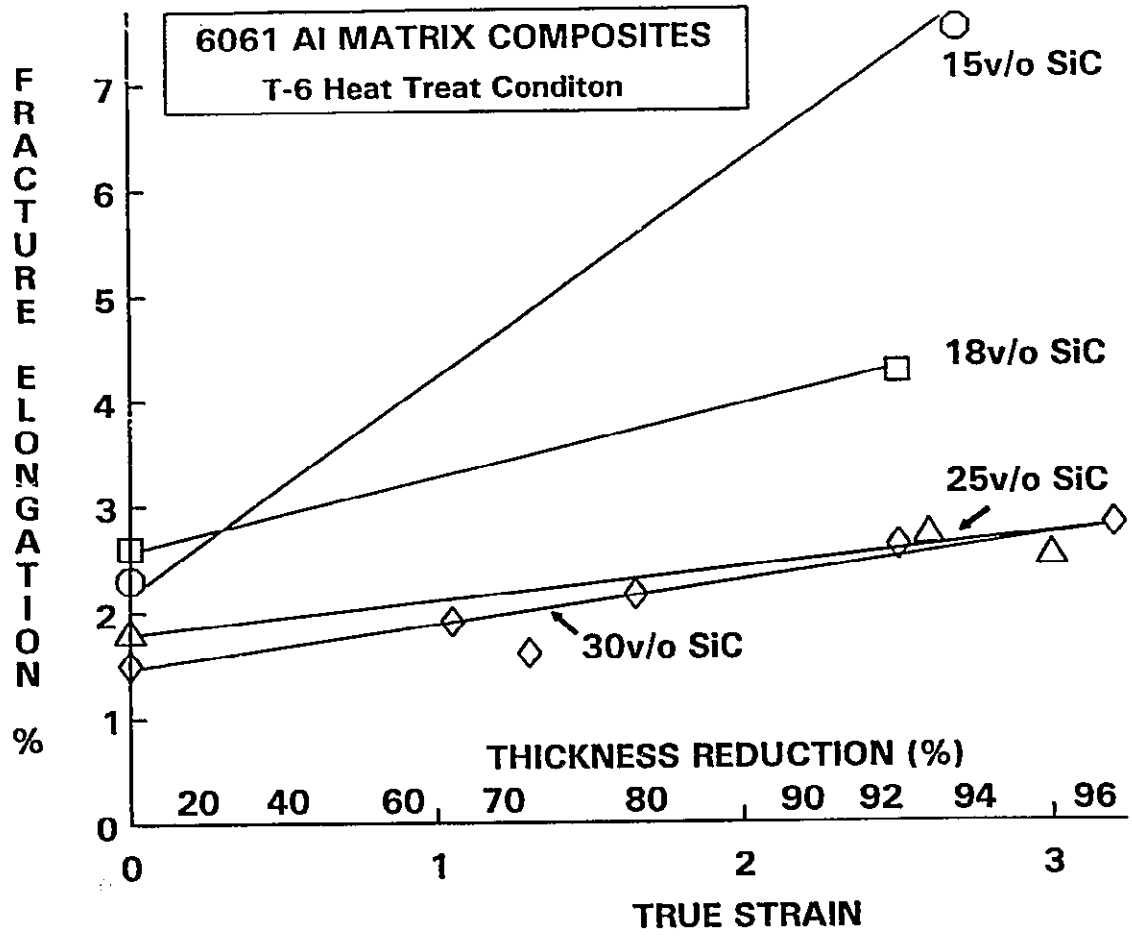

Figure 2.7: Ductility increase due to elimination of fissures between particles and increased particle-matrix bond surface with rising strain [8,15].

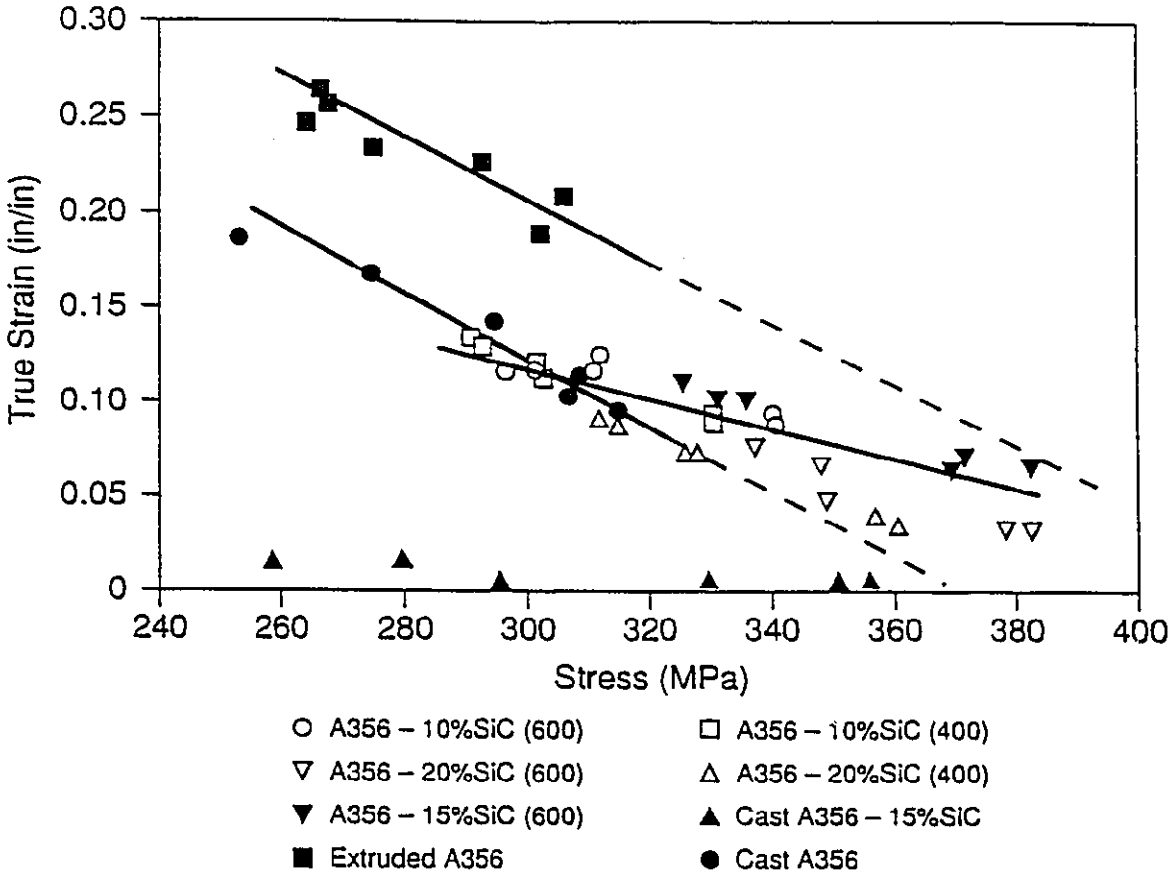

Figure 2.8: Tensile elongation to fracture against tensile strength for A356 and SiC/A356 Al composites [9].

2.1.3.3 Fracture Toughness

Fracture toughness values of the composite are approximately one-half to one-third lower than that of the matrix alloy. The fracture toughness values are higher for particulate than whisker reinforced composites (Figure 2.9). It is also a function of matrix alloy chemistry. Modification of the alloy composition can help prevent the formation of undesirable phases that could act as void initiation sites [10].

The site of crack nucleation depends on the mechanical properties of the matrix, interface cohesion and fracture of particles or gaps in the middle of clusters [7,18]. Crack nucleation sites can occur as microcracks in low strength matrices between SiC particles or as interface decohesions and broken particles in age hardened alloys. Figure 2.10 shows crack initiation and propagation consisting of two stages: breaking of particles and decohesion and linking of these defects through ductile fracture of the matrix [18].

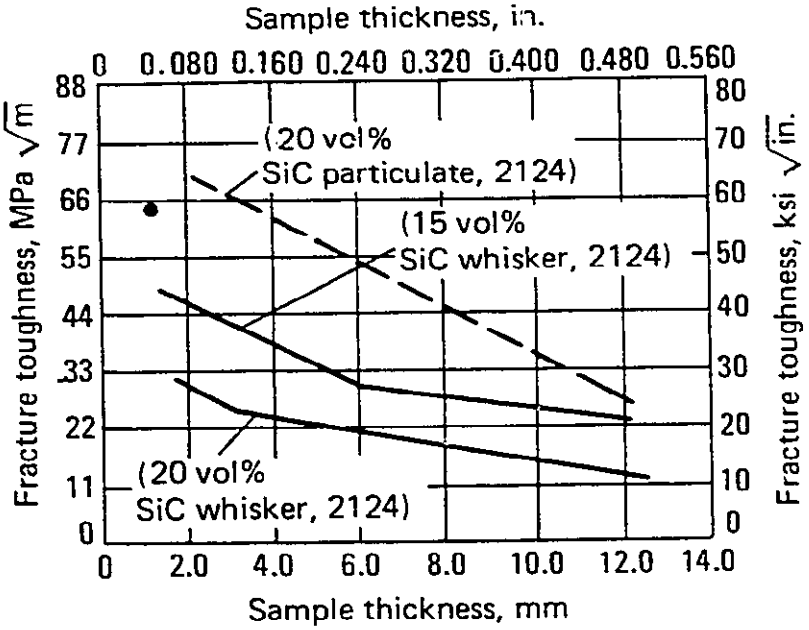

Figure 2.9: Fracture toughness as a function of sample thickness [6].

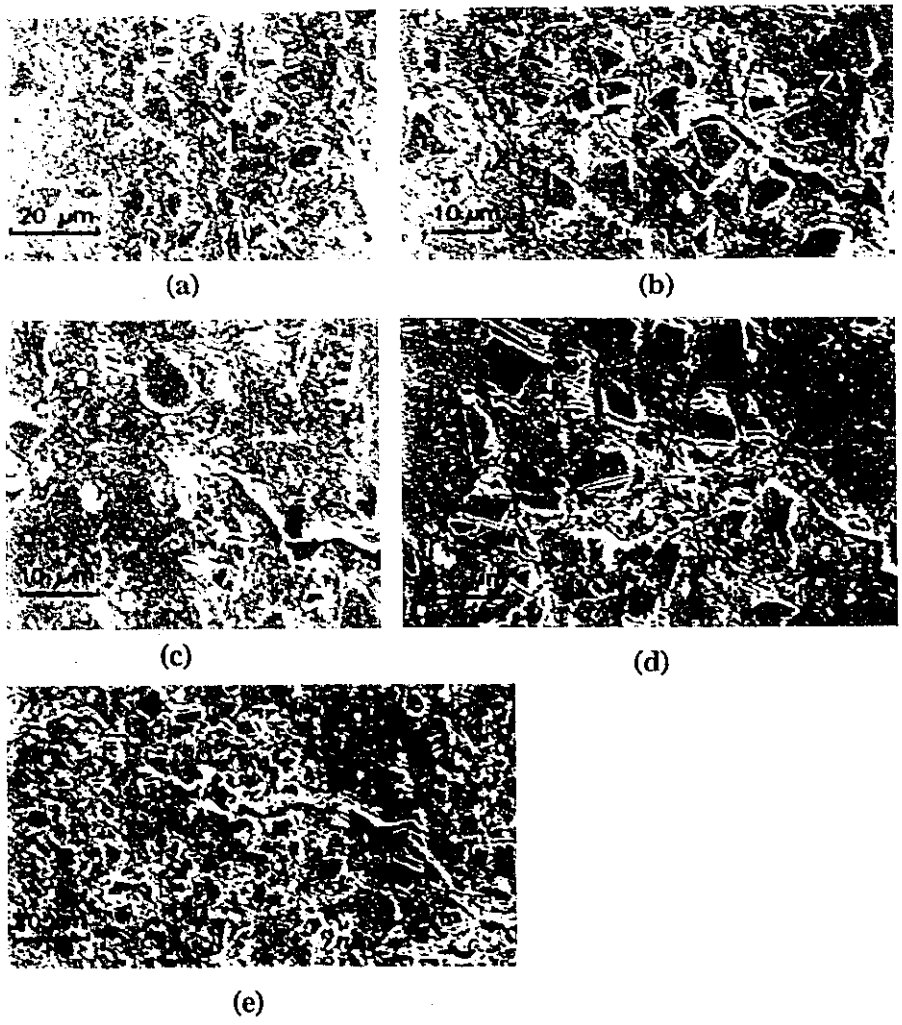

Figure 2.10: Tensile crack initiation and propagation in 6061-T4 alloy with 25v/o SiC_p: (a) decohesion at the notch tip, (b) matrix ligaments are broken, (c) few decohesions are visible, (d and e) crack propagates through the damaged zone [18].

2.2 Aluminum-Magnesium-Silicon Alloys (6xxx Series)

Al-Mg-Si alloys are widely used as medium strength structural alloys which have the additional advantages of good weldability, corrosion resistance and resistance to stress corrosion cracking [19,20]. The 6xxx series are used for the majority of extrusions with smaller quantities being available as sheet, plate and rod. Magnesium and silicon are added either in balanced amounts to form quasi-binary Al-Mg_2Si alloys (Mg:Si = 1.73:1) or with an excess of silicon above that needed to form Mg_2Si [19,21,22]. The commercial alloys may be divided into three groups.

The first group comprises alloys with balanced amounts of magnesium and silicon adding up to between 0.8 and 1.2%. These alloys can be readily extruded and offer a further advantage in that they may be quenched at the extrusion press when the product emerges hot from the die, thereby eliminating the need to solution treat as a separate operation. Moderate strength is developed by age hardening at 160-190°C and one alloy, 6063 (Al-0.6Mg-0.4Si), is the most widely used of all Al-Mg-Si alloys. These alloys are used for architectural and decorative finishes [20,23].

The other two groups contain magnesium and silicon in excess of 1.4%. They develop higher strength on ageing and are quench sensitive. It is usually necessary to solution treat and water quench as separate operations after extrusion or rolling. Alloys that fall under this category are 6061 (Al-1Mg-0.6Si) and 6201 (Al-0.8Mg-0.7Si). Copper is added to improve the mechanical properties together with chromium to offset any detrimental effect copper may have on corrosion resistance. These alloys are widely used as structural materials. The alloys in the other group contain silicon in excess of

that needed to form Mg_2Si. The excess silicon promotes an additional response to age hardening by both refining the size of the Mg_2Si particles and precipitating as silicon. Unfortunately, it can reduce the ductility by causing intergranular cracking which is attributed in part to its tendency to segregate to the grain boundaries. The presence of chromium and manganese helps to offset this effect by promoting fine grain size and inhibiting recrystallization during solution treatment. In addition to extrusions, the alloys are used as forgings [20,23].

2.2.1 SCR® Al-Mg-Si Process

Southwire Company has perfected the processing of 6201 in a continuous operation which yields an intermediate rod product of high quality and a high degree of uniformity in its mechanical and electrical properties. The rod is produced from a 49 cm^2 bar at a production rate of 12 metric tonnes per hour and can be processed to wire at relatively high speeds. Alloys such as 6201, used for overhead conductor wires, are being fabricated using the SCR® (Southwire Continuous Rod) process [24].

The SCR® system for processing Al-Mg-Si alloy results in a rod which is produced in the solution treated condition in one continuous operation as shown in Figure 2.11(a). This process eliminates several steps of heat treatment and handling which results in economic savings and a decrease in physical damage due to additional handling that are necessary in conventional processes (Figure 2.11(b)). An important element of this process is the continuous filtration of the molten metal prior to casting which eliminates wire breakage due to large inclusions. Results of the intermediate rod product with mechanical and electrical properties which are uniform throughout the coil length

can be observed in Figure 2.12. Conventional processes which utilize reheating and quenching the rod coil after rolling, in a separate process, yields a coil of solution treated rod with less uniform properties. This effect is a result of the differential quenching rate that takes place from the outside to the inside of the coil. The SCR® process offers great processing advantages and results in a final wire product with equal mechanical and electrical properties to the conventional product [24].

2.2.2 Stability and Drawability

The natural aging behaviour of the SCR® Al-Mg-Si aluminum alloy rod is shown in Figure 2.13. Partial precipitation of Mg_2Si begins within hours after solution treatment. After a short period of time, it becomes stable allowing the rod to be kept for long periods of time without adverse effects on ductility, drawability or mechanical properties. This behaviour is the result of small, finely dispersed Mg_2Si precipitates. Metallographic examination of the rod after 7 days reveals no significant morphological differences in the structure of either subgrains or precipitated particles [24].

The stability of SCR®-6201 alloy allows it to be drawn at the drawing machine manufacturer's rated speeds (Table 2.3) to desired sizes. Cold drawing can be performed at any time after rolling (Figure 2.11) without affecting drawing speeds or properties of the produced wire. SCR® Al-Mg-Si alloys can be drawn on both "slip" and "non-slip" type drawing machines with satisfactory results. A higher degree of work hardening is obtained with the non-slip type drawing machine since there is more heat dissipation occurring between dies and immediately after deformation; generation of heat through friction on the "slip" drawing drums promotes partial recovery of the matrix [24].

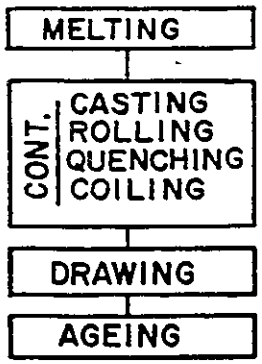

(a)

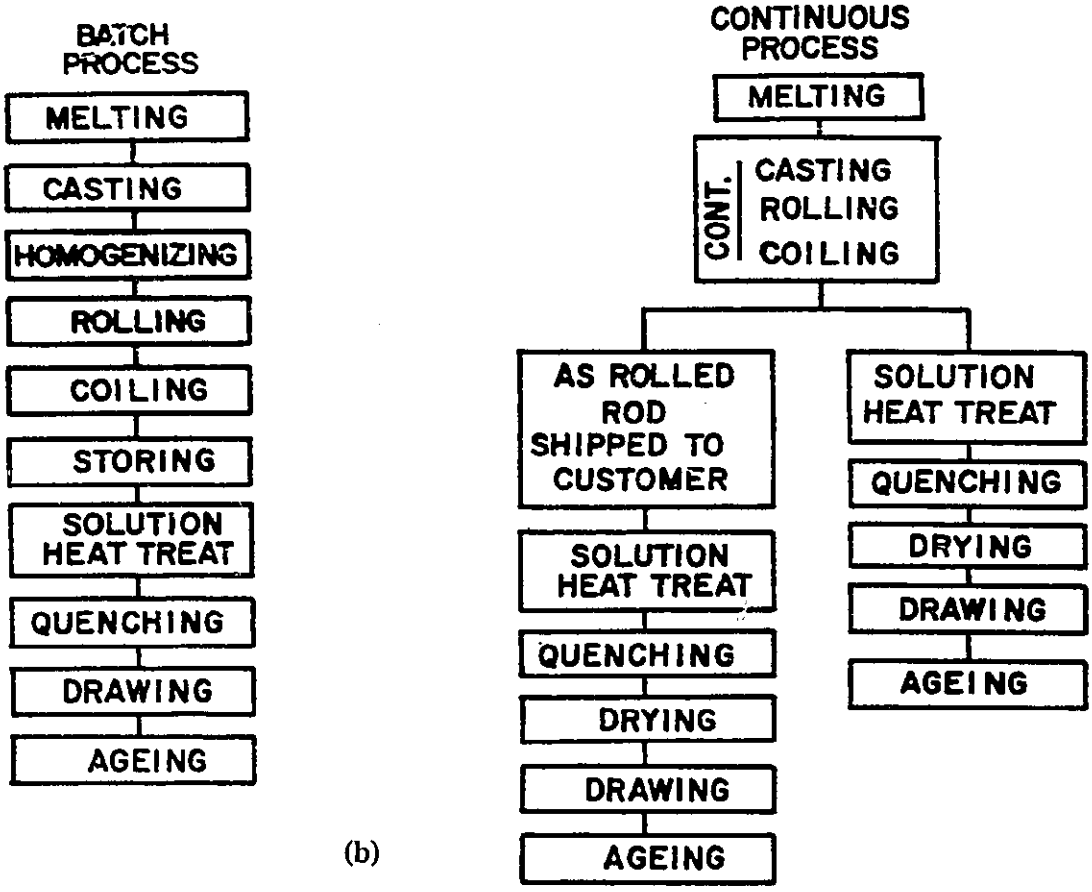

(b)

Figure 2.11: Al-Mg-Si alloy rod production methods: (a) Southwire's SCR® process and (b) conventional Al-Mg-Si alloy processes (batch or continuous) [24].

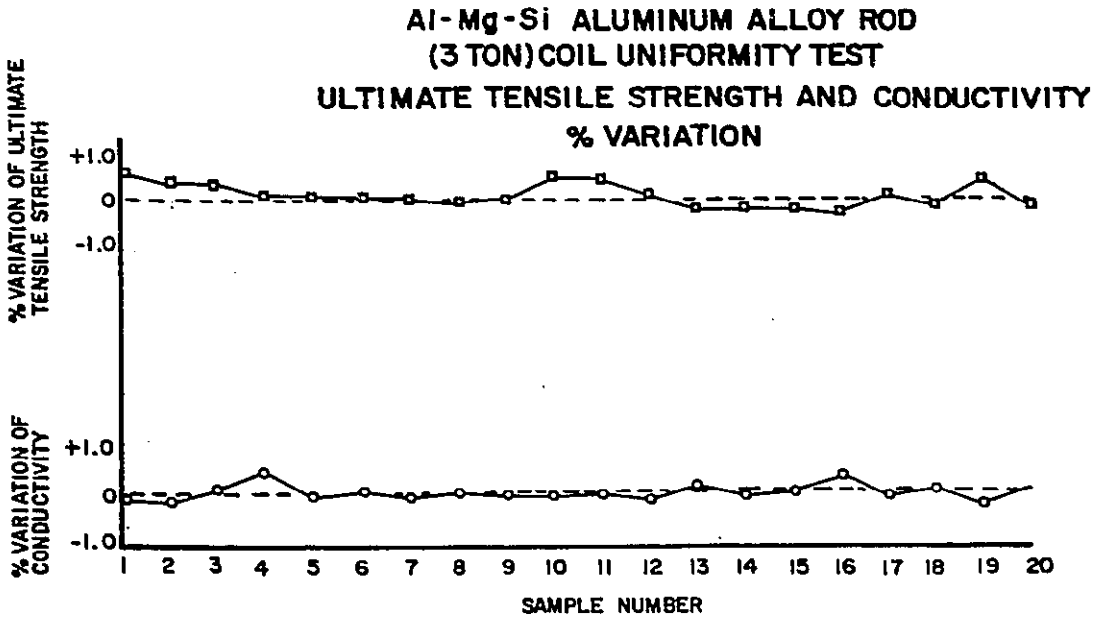

Figure 2.12: Al-Mg-Si alloy rod (3 ton) uniformity test [24].

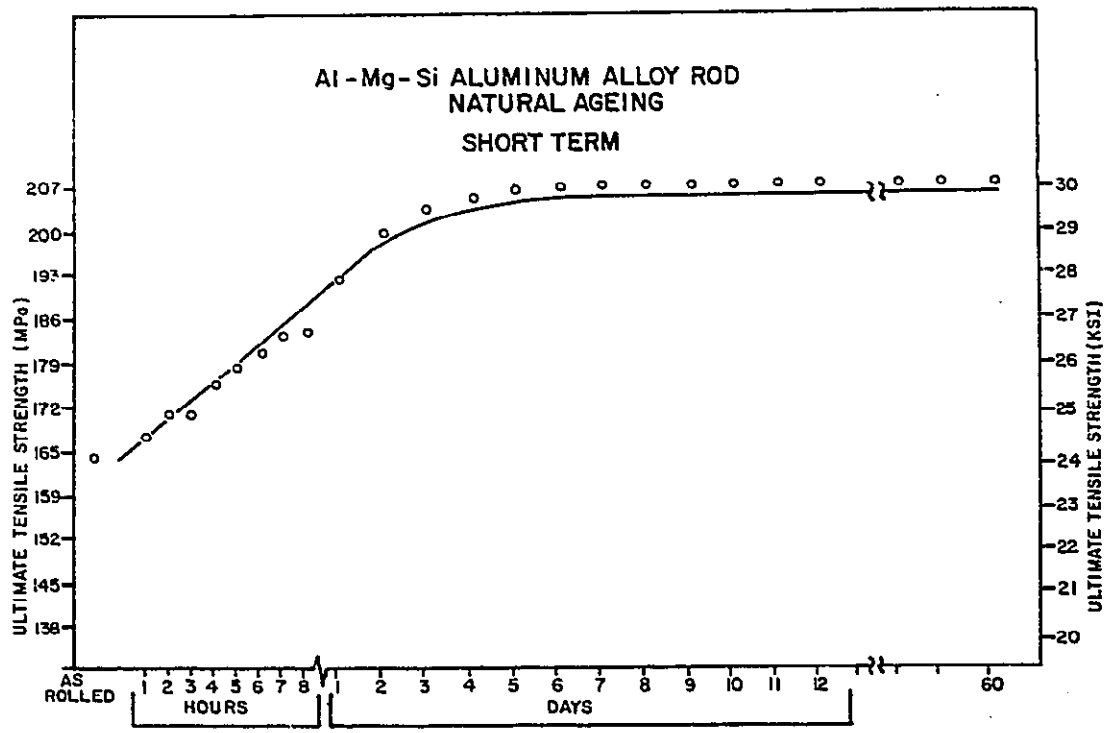

Figure 2.13: Al-Mg-Si alloy rod natural aging (short term) [24].

Table 2.3: High drawing speeds obtained in the drawing of SCR® Al-Mg-Si alloy rod [24].

SCR® - 6201 ALLOY	
Wire Diameter (mm)	Drawing Speed Range (m/s)
2.1	41-45
2.7	32-35
3.4	25-30
4.1	20-25

2.2.3 Artificial Aging

During artificial aging, precipitation of the Mg_2Si particles takes place uniformly in the wire when the wire is treated at temperatures ranging from 138 to 160°C. This treatment also produces recovery of the subgrain structure which takes place simultaneously with the precipitation process. The result is a wire product with improved tensile strength, yield strength, electrical conductivity and elongation. Figure 2.14 shows the behaviour of artificial aging from 1 to 10 hours at 132 and 154°C. Precipitation starts immediately and reaches a maximum after 4 hours at 154°C and starts to overage thereafter. In this stage, Mg_2Si particles become larger and incoherent with the matrix, thereby decreasing the strength but increasing electrical conductivity [24].

2.2.4 Wire Properties

Table 2.4 summarizes typical properties of SCR®-6201 alloy which are compared with some aluminum alloy electrical conductor wires. 6201 exhibits higher strengths compared to the other alloys, however, ductility and conductivity are considerably lower. Al-Mg-Si alloys obtain their strength from a combination of precipitation of the Mg_2Si particles and the work hardening induced by the severe cold work during the wire drawing operation. Although Al-Mg-Si alloys are used as electrical conductors for a number of applications, their conductivity is relatively low ($\leq$ 55% IACS). In general, alloying elements which are either in solid solution or as finely dispersed precipitates cause significant increases in resistivity so that these strengthening mechanisms are unfavourable for aluminum conductors. Work hardening is less harmful, however, conductors strengthened in this manner tend to exhibit poor thermal stability [24].

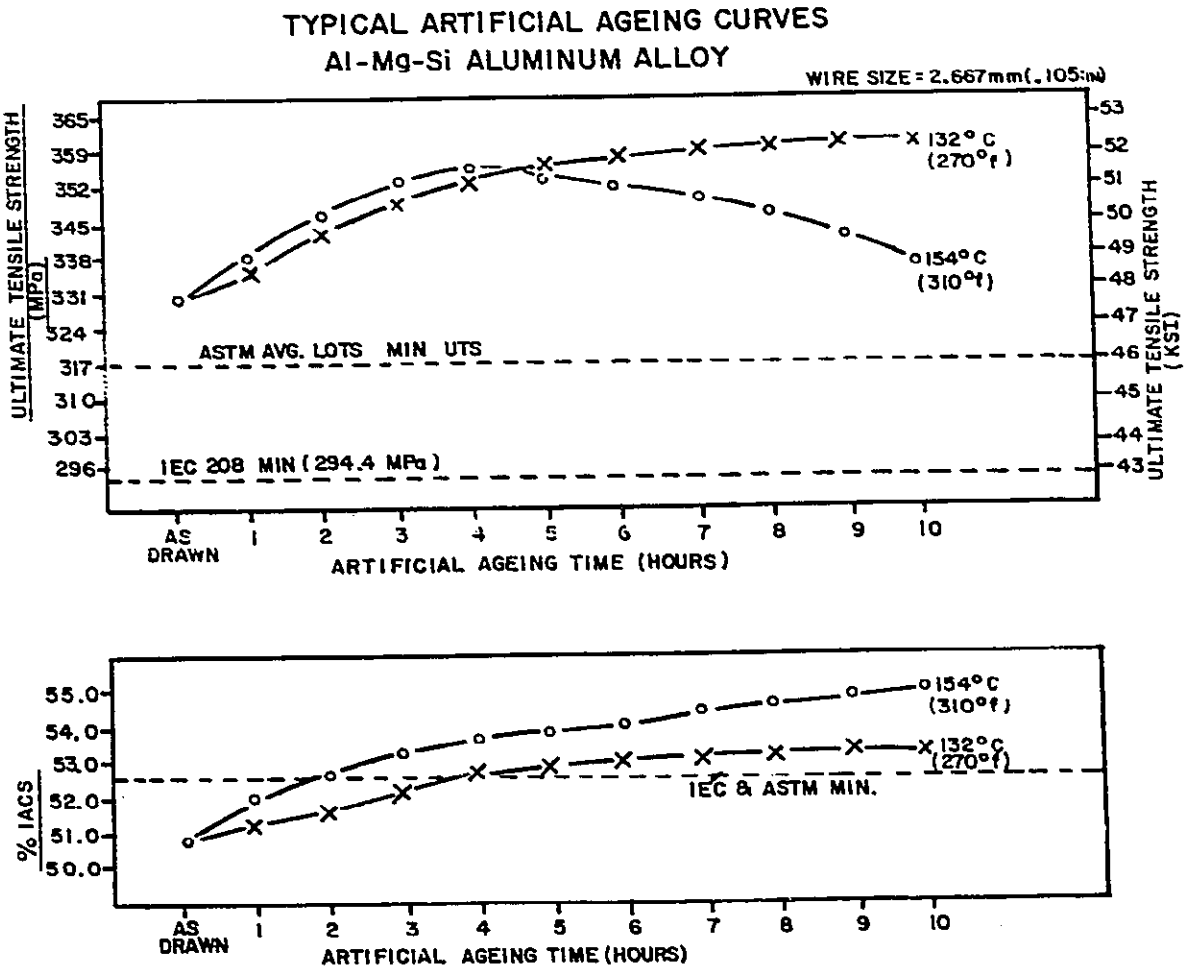

Figure 2.14: Typical artificial aging curves of Al-Mg-Si alloy [24].

Table 2.4: Comparisons and typical properties of some aluminum alloy electrical conductor wires [23].

Alloy	Yield Strength (MPa)	Tensile Strength (MPa)	Elongation in 250 mm (%)	Electrical Conductivity (% IACS)
EC (99.6 Al)	28	83	23	63.4
5005-H19	193	200	2	53.5
6201-T81	303	317	3	53.3
Triple E (Al-0.65Fe)	68	95	33	62.5
Super T (Al-0.5Fe-0.5Co)	109	129	25	61.1
8076	61	109	22	61.5
Stabiloy (Al-0.6Fe-0.22Cu)	54	114	20	61.8
Nico (Al-0.5Ni-0.3Co)	68	109	26	61.3
X8130 (Al-0.6Fe-0.08Cu)	61	102	31	62.1

2.3 Cast Aluminum-Silicon Alloys

Alloys with silicon as the major alloying addition are the most important of the aluminum casting alloys because of the high fluidity due to the low melting point of large amounts of Al-Si eutectic. Other advantages of these castings are high resistance to corrosion, good weldability and the fact that silicon reduces the coefficient of thermal expansion. However, machining may present difficulties because of the presence of hard silicon particles in the microstructure. Commercial alloys are available with hypoeutectic, eutectic and hypereutectic compositions. The most commonly used processes for these alloys are sand casting, permanent mold casting and cold-chamber pressure die casting [19,20,25].

The eutectic is formed between aluminum solid solution containing slightly over 1% Si and pure Si as the second phase. Slow solidification of a pure Al-Si alloy produces a very coarse microstructure in which the eutectic consists of large plates or needles of silicon in a continuous aluminum matrix (Figure 2.15). Alloys having this coarse eutectic exhibit low ductility because of the brittle nature of the large silicon plates. Rapid cooling refines the microstructure and the Si phase has a fibrous form resulting in improved strength and ductility [20,25]. The eutectic may also be refined by the process known as modification.

Modification of Al-Si alloys is usually achieved by the addition of small amounts of sodium. Much research has been done on the mechanism by which the size and form of the silicon phase is modified. Sodium depresses the eutectic temperature by as much as 12°C and a finer microstructure is expected because the rate of nucleation is greater

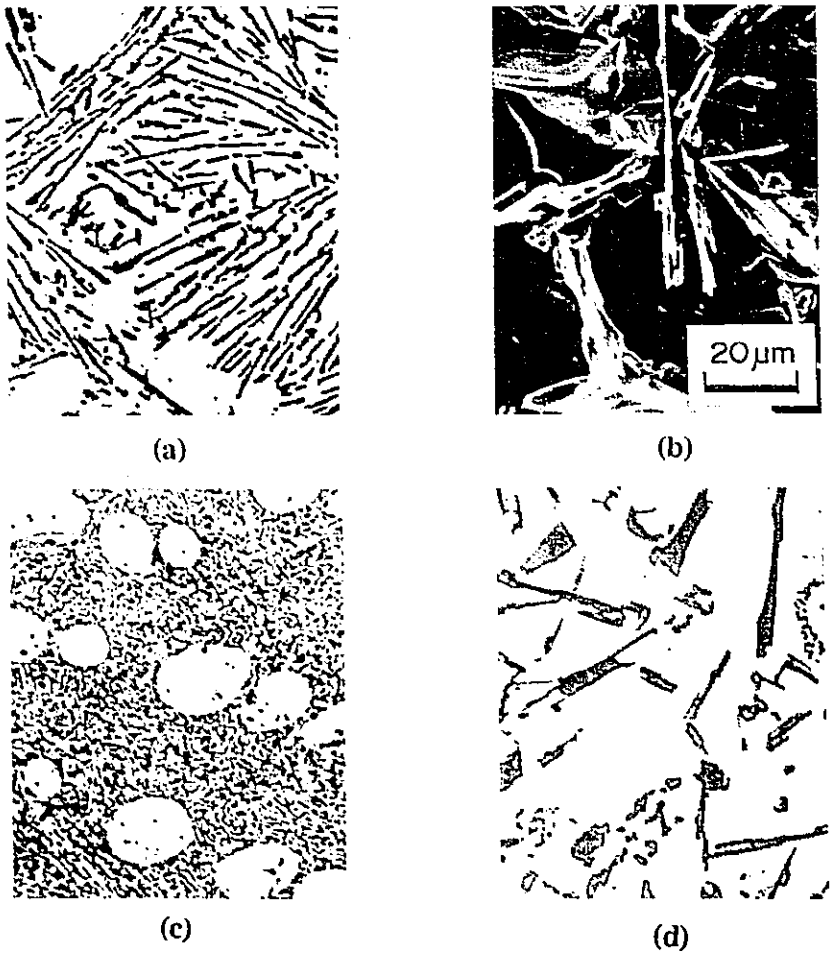

Figure 2.15: As-cast binary Al-Si alloys in the following conditions: (a) 12% Si unmodified, (b) 7% Si unmodified (SEM), (c) 12% Si modified with sodium and (d) 12% Si with excess phosphorous [(a), (c), (d) x400 and (b) x600] [20].

in the under-cooled condition. Depression of the eutectic temperature means that the sodium reduces the potency of silicon nucleation sites. The use of sodium presents casting problems such as reduced fluidity but its major disadvantage is the rapid loss of the element by evaporation or oxidation. However, adding an excess amount can lead to over-modification, in which the formation of another compound AlNaSi provides sites for the easy nucleation of coarse silicon particles. The effects of modification are lost if Al-Si castings are remelted; the same reason prevents foundries being supplied with pre-modified ingots. However, studies have shown that replacing sodium with strontium is very successful. The addition of this element produces a refined Al-Si eutectic and the tensile properties of castings are comparable with those obtained when sodium is used. Loss of strontium during melting is much less and the modified microstructure is retained after remelting. Over-modification is also less of a problem with strontium since excess amounts of this element are taken into the compound $SrAl_3Si_3$ which has little effect on the size of the silicon particles in the eutectic [26-27].

2.3.1 Binary Al-Si Alloys

Binary Al-Si alloys up to the eutectic composition have good ductility providing the iron content is controlled to minimize the formation of large, brittle plates of the compound α-AlFeSi. Additions of manganese have been found to be beneficial since it aids formation of spheroidal ß-AlFeSi. If the silicon content is below 8%, refining the eutectic composition is not necessary to achieve good ductility because the primary Al phase is present in large amounts. The eutectic composition, which has high fluidity and low shrinkage on solidification, has application for thin-walled castings. When as-cast

alloys containing large amounts of silicon are subjected to elevated temperatures, they suffer growth due to precipitation of silicon from solid solution. Dimensional stability can be achieved by heating for several hours in the temperature range 200-250°C prior to use [19,20].

Although binary Al-Si alloys show some response to heat treatment because the Al phase can be supersaturated with Si by rapid cooling, much greater strengthening is possible by the addition of other alloying elements such as Mg. Large quantities of sand and permanent mold castings are made from Al-Si-Mg alloys such as A356 (Al-7Si-0.3Mg) in which the relatively small addition of magnesium can induce age hardening through precipitation of Mg_2Si in the aluminum matrix. The yield strength of A356 in the heat treated condition is double that of the binary alloy containing a similar amount of silicon. In addition, Al-Si-Mg alloys display excellent corrosion resistance. These alloys find use in aircraft and automotive applications [19,20].

3. HOT WORKING CHARACTERISTICS

Hot working is considered to be deformation at a temperature above 0.5 T_m (melting temperature, K) and strain rate between 10^{-3} to 10^{3} s^{-1}. The strains may vary from 0.1 to as high as 50. At these temperatures, most metals have low flow stress and high ductility. Both dynamic and static softening mechanisms take place during the hot working process which includes the preheating, deformation and subsequent cooling. Hot working is employed because metals can be subjected to large and rapid changes in shape without cracking. The perennial need for improved processes and products generates continued and growing interest in high temperature deformation [28-30].

3.1 Restoration Mechanisms on Hot Working

Deformation of any metal causes an increase in dislocation density within its grains, which serves to strain harden the material and will ultimately lead to fracture if some form of restoration mechanism is not active to alleviate stress concentrations. In any deformation process, one or all of the following restoration mechanisms may be active:

(i) Dynamic Recovery (DRV)

(ii) Dynamic Recrystallization (DRX)

(iii) Static Recovery (SRV)

(iv) Static Recrystallization (SRX)

Restoration occurring during deformation is called dynamic and in the absence of stress

or strain on the material is termed static. The major factor that determines whether recovery or recrystallization will take place during hot working is the stacking fault energy (SFE). Their initiation and control is dependent on both material properties and on the selection of such parameters as time, temperature, strain and strain rate [28-30].

3.1.1 Dynamic Recovery

A simple flow curve in which there is decreasing strain hardening to a steady state plateau, is characteristic of pure DRV (Figure 3.1). The flow curve exhibits three distinct stages. During the first, the elastic strain is increasing from zero to the yield stress. Strain hardening takes place during the second stage; however, the slope of the curve continually decreases as the rate of work hardening diminishes. The amount of work hardening and the strain to the end of this stage decreases as the temperature is raised and the strain rate lowered. In the third stage, the work hardening rate has reached zero and the flow stress has levelled off at an equilibrium steady state value. Therefore, in hot working, the temperature, the strain rate and the flow stress are constant in the steady state regime. In practice, the flow curve may decrease after the plateau has been reached as the result of other factors such as deformation heating or precipitate coarsening [28-31].

During the initial loading stage of the flow curve, some dislocation multiplication takes place, increasing slightly the dislocation density. In the strain hardening stage, the dislocations increase greatly and become entangled into a substructure within the grains. As deformation continues in metals with high SFE, the sub-boundaries increase in number and dislocation density and so does the rearrangements by DRV until a dynamic

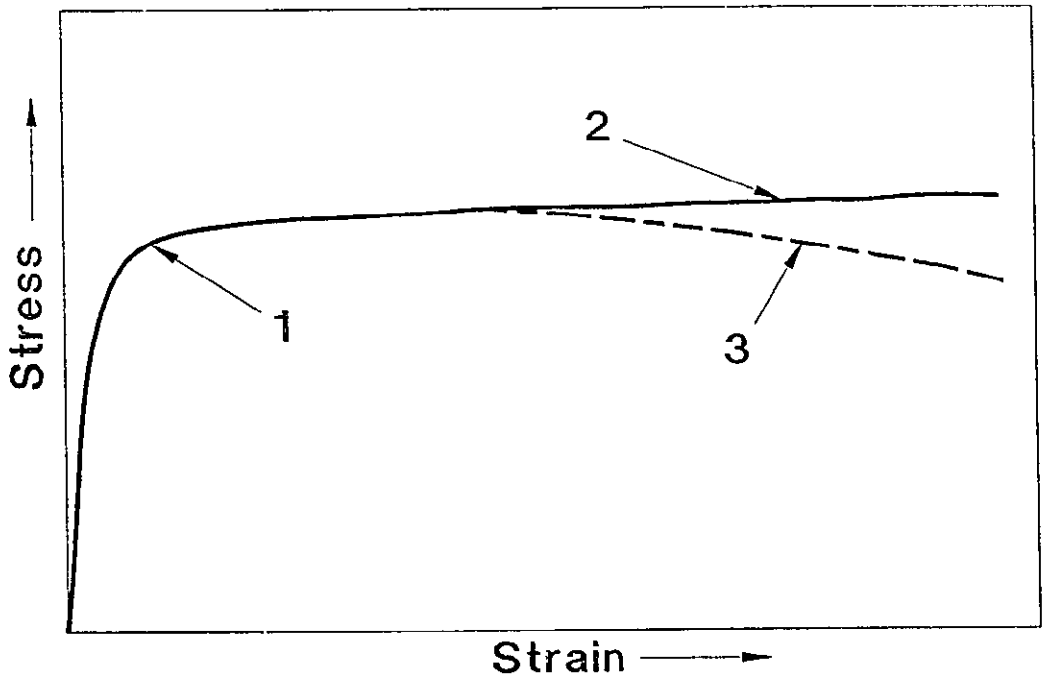

Figure 3.1: Typical dynamic recovery flow curve: after an initial strain hardening phase (1), there is a region of steady state deformation without strain hardening (2). In practice, the flow curve may decrease as the result of deformation heating or precipitation coalescence (3) [28].

equilibrium is reached between dislocation generation and annihilation. At this point where the subgrains reach the equilibrium size, a steady state is established in which the flow stress remains constant. While the grains are deforming in correspondence with the external shape, the subgrains remain equiaxed even after large strains, indicating that the individual sub-boundaries are being broken up and reformed. This dynamic regeneration termed repolygonization explains the absence of any distorted subgrains even after very large strains. The subgrains become larger in size as the deformation temperature is increased or as the strain rate is decreased. Such larger subgrains and their boundaries, both contain less dislocations [28-32].

The description of DRV up to this point refers to metals in which it occurs to a high degree. In the case of two-phase alloys, where the particles are small and insoluble and are not sheared by the dislocations, they serve as obstacles which stabilize the substructure. Examples of this are fine equilibrium Mg_2Si precipitates or $FeAl_3$ eutectic rods (0.2 μm) [49]. In some cases the subgrain diameter may be reduced to the size of the inter-particle spacing which lead to high flow stresses. However, when the spacing is very small, they may inhibit the formation of subgrains; such is the case in underaged aluminum alloys. If the particles are partially soluble, they can coalesce into fewer and larger particles during deformation, leading to a decreasing flow stress over a prolonged strain. At higher temperatures and lower strain rates, the particles are larger when steady state flow is achieved. Fine and uniformly distributed particles which would limit the degree of recovery, tend to decrease the ductility. Large non-deformable particles such as constituent $MnAl_6$ or α-AlFeSi (>0.6 μm) or SiC particles in MMCs cause

additional deformation in the surrounding matrix and the development of very fine subgrains. The dense dislocation substructure can give rise to particle stimulated nucleation (PSN) of recrystallization. Large particles can also lead to the nucleation of voids or cracks which then link up to cause failure. If the amount of particles is high, then the crack density may be so great that their growth counters the ductility enhancement of the recovery or recrystallization mechanisms [31,32].

3.1.2 Dynamic Recrystallization

The typical flow curve of a material undergoing DRX is shown in Figure 3.2. Several distinguishing characteristics of Figure 3.2 are:

(i) The initiation of recrystallization after a critical strain denoted by a decrease in work hardening rate to a distinct peak in the flow curve.

(ii) A flow softening due to the growth of DRX grains which are also being deformed.

(iii) The flow stress levelling off at a steady state value due to strain hardening, DRV and repeated uniformly distributed DRX.

At higher strain rates, DRX is continuous after giving rise to a single peak stress value and produces grain refinement. However, at lower strain rates, the mechanism is periodic with each stress-decreasing recrystallization wave followed by a degree of work hardening. The result is a cyclic pattern of decreasing amplitude and grain coarsening [31-33].

DRX is generally observed in metals with low SFE whereas in metals with high SFE, it seldom occurs because DRV produces a low dislocation density. When the

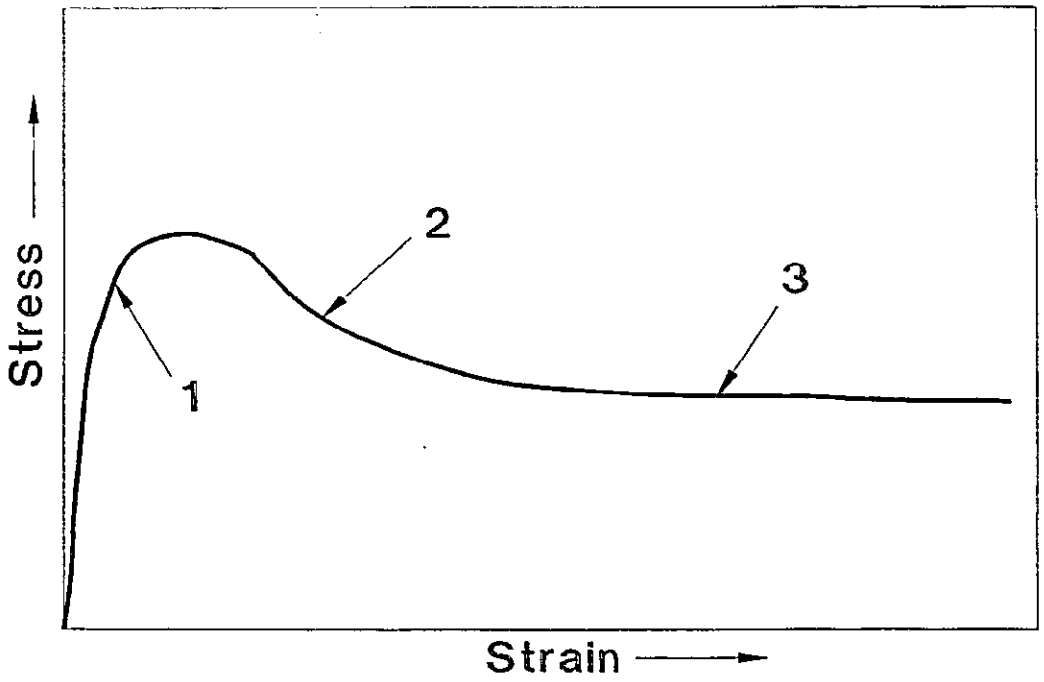

Figure 3.2: Typical dynamic recrystallization flow curve: the accumulation of dislocations is sufficiently great that recrystallization is nucleated during deformation (1). Since the recrystallized grains have a lower density of dislocations (2) than the unrecrystallized material (1), there is work softening. These recrystallized grains are continually reworked and repeatedly recrystallized giving the steady state flow stress (3) [28].

dislocation density builds up to a critical level, it is the critical strain at which DRX occurs. At lower strain rates nucleation possibly occurs by the bulging of existing grain boundaries. Migrating grain boundaries leave behind dislocation-free regions in which the dislocation density once again increases as strain proceeds until recrystallization is again nucleated. At high strain rates, a fine and dense tangled cellular structure is developed throughout the grains but more strongly at the grain boundaries and deformation bands. Nuclei develop initially along grain boundaries where there are high misorientations between the subgrains. The dislocation densities at the centre of the new grains increase sufficiently that nucleation occurs again before any wave of recrystallization is complete. As a result, there is a distribution of dislocation substructures which maintains the average flow stress at a steady state between the yield stress of statically recrystallized material and the peak stress [31-33].

3.1.3 Static Recovery and Recrystallization

At the end of a high temperature deformation, there is a dislocation substructure with an associated stored energy which is capable of driving static restoration mechanisms. These are static recovery and static recrystallization [31,32].

SRV is the annihilation and rearrangement of dislocations in the sub-boundaries followed by growth of the subgrains. This process is the sole mechanism of softening if the critical stored energy is not surpassed and always occurs during the incubation period before the appearance of recrystallization nuclei. As the stored energy increases, the incubation period for SRX decreases so that there is less opportunity for SRV. An increase in temperature or strain energy (higher $\dot{\varepsilon}$ or ε) increases the rate of SRV while

the addition of alloying elements decreases it [31,32].

SRX is the elimination of dislocations as a result of the motion of high angle boundaries. SRX is preceded by an incubation period for nucleation, i.e. formation of regions with low dislocation density surrounded by mobile high angle boundaries. The new grains grow until all the deformed grains are replaced. A critical strain is required for SRX to take place; it rises as the temperature rises and the strain rate falls. At higher strains or strain rates, the driving forces are higher making the rate of recrystallization faster. Part of this results from the reduction of the subgrain size and increase in sub-boundary density so that there is a higher density of nucleation sites [31,32].

The effects of second phases are varied depending on their size and spacing. If they are small and numerous, they tend to stabilize the substructure, thus both limiting SRV and preventing nucleation of recrystallization. Larger particles distributed along the grain boundaries, may prevent their migration and consequently recrystallization without altering recovery. However, large and rigid particles ($>0.6\ \mu$m) which cause additional flow in the surrounding matrix, create nucleation sites for SRX [31-33].

3.2 Interdependence of Stress, Strain Rate and Temperature

A number of mathematical expressions have been proposed to describe the relationship between flow stress (σ), strain rate ($\dot{\varepsilon}$) and temperature (T in Kelvin). In creep, the increase of $\dot{\varepsilon}$ in the steady state region as T rises and σ increases can be expressed by a power law and an Arrhenius relationship:

$$\dot{\varepsilon} = A_1 \sigma^{n'} \exp(-Q_C / RT) \tag{3.1}$$

where A_1 : Empirical Constant

R : Universal Gas Constant (8.314 J/mol-K)

Q_C : Activation Energy for Creep

For aluminum, the relationship holds over eight orders of magnitude from 10^{-8} to 10^{-2} s^{-1}. The value of Q_C is approximately equal to that for self diffusion indicating that the rate controlling mechanism is dependent on vacancy migration [28-33].

The interrelationship between the three parameters σ, $\dot{\varepsilon}$ and T can also be written in the hot working form and with different stress functions:

$$A_1 \sigma^{n'} = \dot{\varepsilon} \exp(Q_{HW} / RT) = Z \tag{3.2}$$

$$A_2 \exp(\beta \sigma) = \dot{\varepsilon} \exp(Q_{HW} / RT) = Z \tag{3.3}$$

$$A_3 [\sinh(\alpha \sigma)]^n = \dot{\varepsilon} \exp(Q_{HW} / RT) = Z \tag{3.4}$$

where A_i, α, ß, n, n' : Empirical Constants

Z : Zener-Hollomon Parameter

Q_{HW} : Activation Energy for Hot Working

These equations hold for DRV or DRX but Q_{HW} would be different for the two

mechanisms. The power law (Equation 3.2) works satisfactorily for low stresses and the value of n is usually in the range of 4 to 5. The exponential law (Equation 3.3) is useful for high stresses and ß (= $\alpha n'$) has values in the range of 1 to 1.5×10^{-3} MPa^{-1}. The hyperbolic sine law (Equation 3.4) covers the entire stress range (10^{-8} to 10^{2} s^{-1}) (Figure 3.3). The Z parameter is a temperature compensated strain rate which increases as T decreases. In hot working tests, Z is constant since T and $\dot{\varepsilon}$ are the controlled variables [28-33].

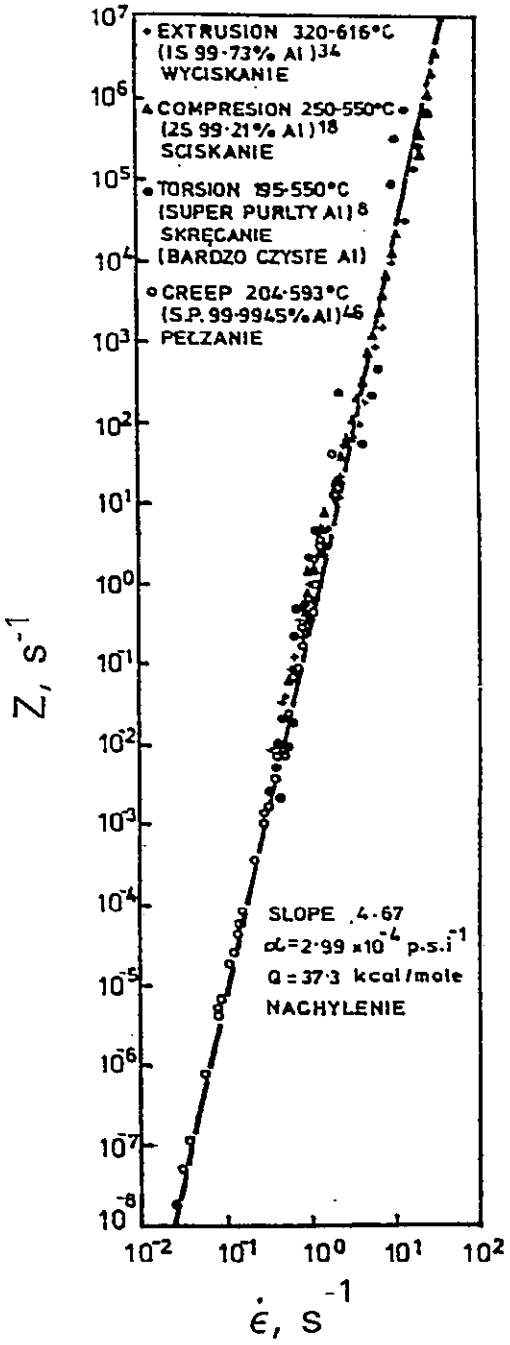

Figure 3.3: The application of Equation 3.4 to aluminum is confirmed over the strain rate range 10^{-2} to 10^{2} s^{-1} between 195 and 616°C [31].

3.3 High Temperature Deformation of Particulate MMCs

The mechanical behaviour of particulate MMCs at high temperatures is very important since they may be produced as billets which are subsequently mechanically shaped. Due to their limited low temperature ductility, working at elevated temperatures is necessary; the most relevant aspects of this will be discussed in this section [8,34,35].

Deformation processing of discontinuously reinforced composites is usually carried out at higher temperatures where the ductility is greater and the flow stress lower although it remains significantly higher than the matrix alloy [2,8,15,34-38]. Above 200-300°C, the work hardening rate of the matrix is reduced primarily by DRV [8,34,35,39]. The particles in composites are sufficiently large that they do not interact with dislocations but being much harder than the matrix, they do force it to undergo additional shear thus raising the strain hardening [8,34,35]. At temperatures near melting (aluminum: T_m = 660°C), the flow stress of the composite may fall below that of the matrix alloy and the strain rate sensitivity may increase. These effects have been attributed to grain boundary sliding in fine grained composites [8,38]. Powder based composites are usually hot worked following consolidation to improve the mechanical behaviour by eliminating unmixed regions of reinforcement and matrix thus augmenting the reinforcement-matrix bond. The distribution of the second phase in the matrix becomes more uniform as the amount of deformation is higher. Elevated temperature improves matrix flow and reduces particle degradation [9,11,15,39,40]. Such behaviour in hot working indicates that it would be much more suitable than cold working for the fabrication of composites since the matrix has more ability to flow around the particles

without damaging them [2,8,34,35,39].

There are distinct failure mode changes with temperature in particulate MMCs. At 200-300°C, uniform elongation decreases but there is a considerable amount of necking and the total ductility increases. At 500°C, there is a peak in the ductility as observed in SiC/6061 Al composite. The fracture surfaces of specimens are generally similar to those specimens deformed at lower temperatures, however, there is some evidence of intergranular failure at 500°C. These observations discussed above suggest that there are three distinct temperature regimes in aluminum composites [38,39]:

(i) $T < 200\text{-}300°C$: High work hardening, high flow stress, low ductility

(ii) $500°C > T > 300°C$: Low work hardening rate, improved ductility

(iii) $T > 500°C$: Lower ductility, fracture related to grain boundary

3.3.1 Superplasticity

Superplastic forming is an attractive option for particulate MMCs, as it is suitable for low volume specialised production. This is usually a near net shape process which reduces both the machining costs and the waste of expensive material. Conventional superplastic alloys have a grain size of less than 10 μm and either have duplex microstructures in which both phases are deformable at the deformation temperature or contain a dispersion of very small particles which act to prevent grain growth. The principal mechanism of superplasticity in these types of material is grain boundary sliding [7,38,39]

Although small grain sizes may be achieved in MMCs after cold or hot work followed by recrystallization, superplasticity of different types can occur under certain

condition in particulate reinforced composites containing large undeformable particles. Mahoney and Ghosh [7] have demonstrated that superplasticity can occur in aluminum MMCs containing 10v/o of 5 μm diameter SiC particles when processed to a fine grain size. Nieh et al. [41] found superplasticity in AA 2124 containing SiC in whisker or particulate form. The superplastic deformation occurs at high temperatures and strain rates and is thought to involve some liquid phase. This is somewhat similar to results obtained by Weill and Wyon [50] who found low temperature superplasticity in 10v/o Al_2O_3/Al composites after liquefying the grain boundaries by gallium diffusion. The formation of a very small grain size by particle stimulated nucleation during recrystallization of particulate composites containing large volumes of small ceramic particles, is clearly an important factor for these materials to deform superplastically [38,39].

3.4 High Temperature Deformation of Al-Mg-Si Alloys

In hot working of Al-Mg-Si alloys, the evolution of precipitates with temperature and strain rate produces a strong influence on both workability and mechanical properties of the final products. Their workability is generally superior to Al-Mg alloys or other heat treatable alloys because their total solute levels are quite low [42,51,52]. Homogenization after solidification of Al-Mg-Si alloys improves the hot ductility by reducing the size and number of non-equilibrium constitutive particles. Hot workability is further improved by a slow cooling to precipitate and spherodize large Mg_2Si particles which do not hinder the movement of dislocations as does a fine distribution of

precipitate [42]. Overaging to large equilibrium precipitates has a similar effect. In such a precipitated condition, the hot workability is reduced as a function of rising excess Mg content while excess Si has much less effect. They exhibit similar mechanical behaviour to pure aluminum such as strain hardening to a plateau as a result of subgrain formation through DRV. However, this is not the case after solution treatment because numerous, fine, dynamically precipitated particles pin dislocations diminishing substructure cellularity [42,44,51,52]. Since such strengthening is relatively larger at lower temperatures, there appears to be very high temperature dependence of the flow stress. This is illustrated in the results of Evangelista et al. [45] in which high peaks and rapid work softening is exhibited as will be explained later.

3.4.1 Hot Torsion Testing of Al-Mg-Si Alloys

Al-Mg-Si alloys from 0.49 to 1.11 Mg and 0.42 to 0.75 Si (in wt%) were tested in torsion at 1.8 s^{-1} by Espedal et al [21]. These alloys were balanced in Mg and Si to provide after homogenization 0.81 to 1.75 Mg_2Si on assumption of 0.14 excess Si combined with 0.21 Fe to produce Fe-Si particles. After solution at 560°C, the alloys were quenched and reheated to 450°C where they were aged for increasing time before being deformed. As the concentration of Mg_2Si rose, the peak strength of the aging curves were higher and declined more rapidly reaching a common value after holding time of 15 to 30 min (Figure 3.4). When held for 1200 min, the flow stress decreased to the level of the alloy with solvus at 450°C. During the transient, the strengthening of the particles diminished rapidly as they coalesced at small sizes and it gradually became negligible at larger sizes [21,42].

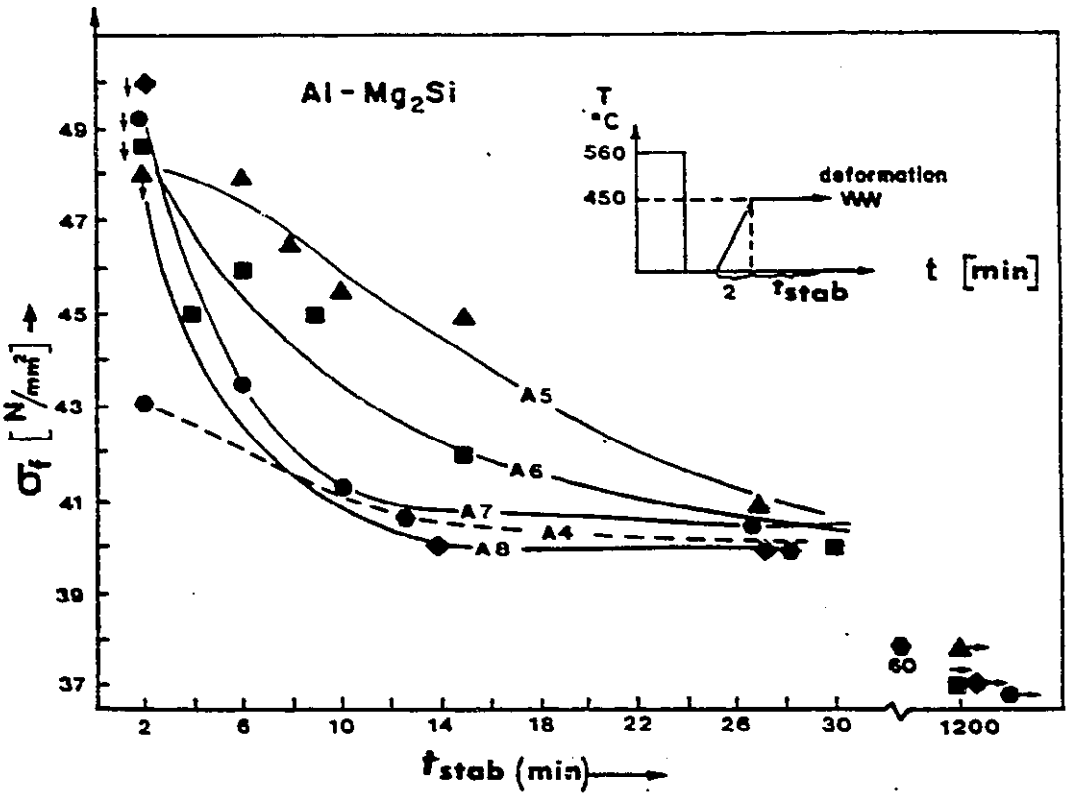

Figure 3.4: Flow stress of Al-Mg-Si alloys at 450°C, 1.8 s^{-1} versus stabilization time at test temperature after quenching [21].

For Al-Mg-Si alloys, the solute behaved in the presence of particles as if they were not present. Magnesium, as explained previously, is a strengthener raising the strength of aluminum two-fold with a 1% addition. However, the same amount of silicon will only raise it by one-third. For alloys up to 1.11% Mg and 0.75% Si with the corresponding stoichiometric ratio of Mg_2Si, the constitutive equation for hot working of Al-Mg-Si alloys in the single-phase region has been derived as [21]:

$$\dot{\varepsilon} = \exp[20.3 - 2.5(wt\% Mg_2Si)]\exp(0.22\sigma)\exp(-Q_{HW}/RT) \qquad (3.5)$$

so that only the first exponential varied with solute content. The activation energy (Q_{HW}) was 150 kJ/mol similar to that for pure aluminum. A study on Al-Mg alloys showed that for 1% Mg, the activation energy is about 150 kJ/mol. The addition of silicon at 500°C raised the strength but at 350°C it lowered the strength due to precipitation [21,42].

In torsion tests of 6015 (0.97Mg-0.29Si-0.19Cu) by Evangelista et al. [45], the alloy was solution-treated, quenched and reheated to various test temperatures in 20 min. At 300 and 350°C, the flow stresses were very high as a result of fine ß (Mg_2Si) rods (Figure 3.5). These led to a low level of DRV which reduced accommodation of grain boundary sliding and hence increased grain boundary cracking. At 400-500°C, rapid overaging and coalescence of the ß (Mg_2Si) led to large and widely separated particles; the associated DRV caused extensive work softening. The activation energy was 170 kJ/mol for 400-500°C but was apparently 460 kJ/mol for 300-350°C (Figure 3.6) as a result of the major differences in precipitate distribution and substructure. At the elevated temperatures, a highly dynamically recovered and equiaxed substructure with

well dispersed particles formed; the original grains lengthened progressively and thinned down until they broke up into equiaxed crystallites. The accommodation of grain boundary sliding due to high DRV inhibited cracking which gave rise to very high ductilities [42,45]. In Al-0.8Si-0.66Mg, solution treated, quenched and aged for 1 hour at 300°C, a peak stress of 87 MPa followed by work softening to 60 MPa during torsion testing at 300°C and 2.1 s^{-1} was observed by Farag and Sellars [46]. The large drop in flow stress is most likely related to change in particle distributions.

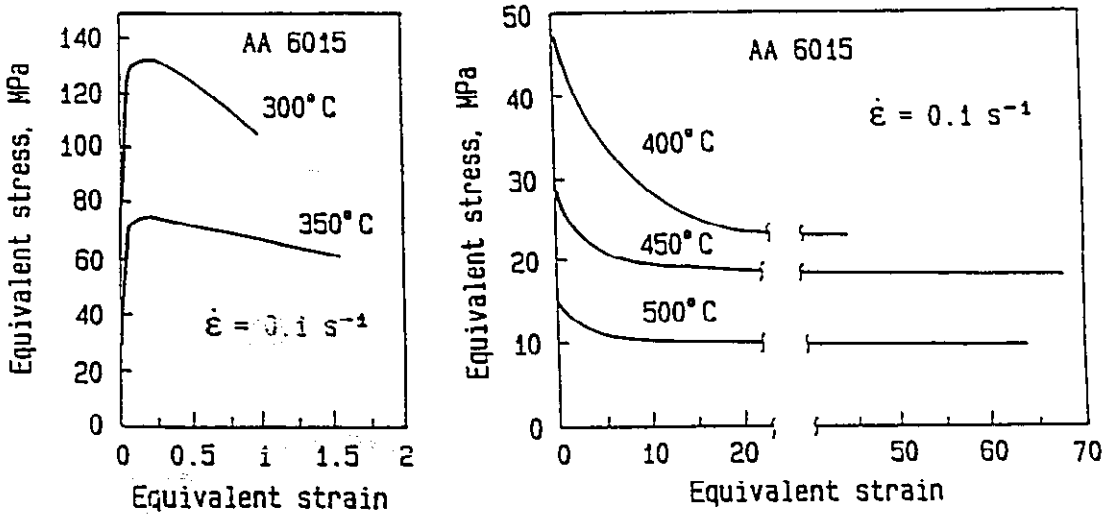

Figure 3.5: Typical equivalent stress-strain curves of 6015 Al alloy after homogenization at 560°C and quenching [45].

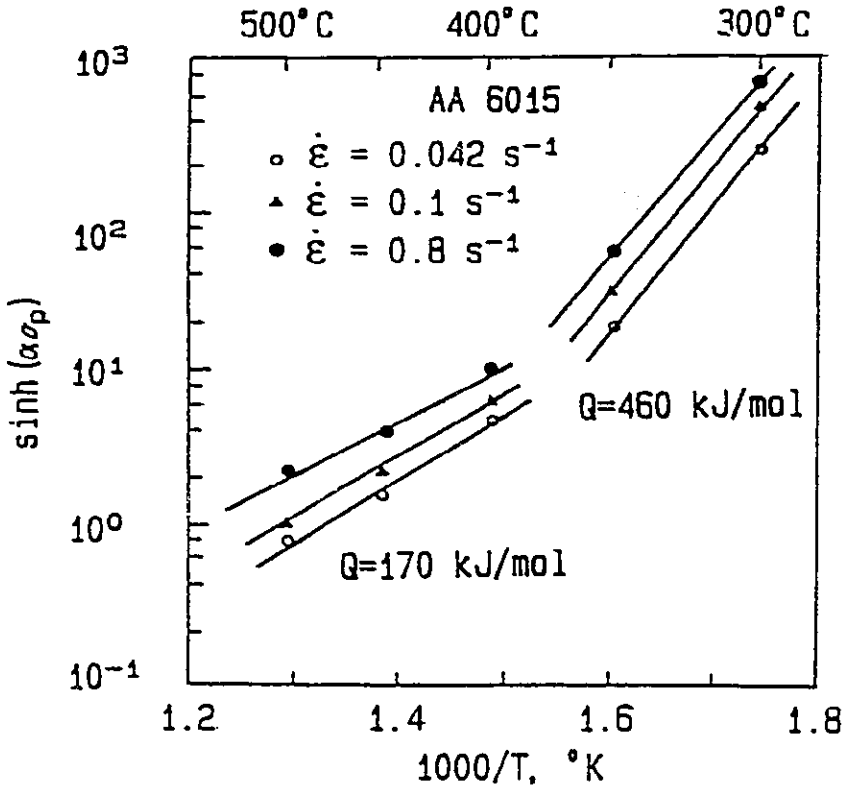

Figure 3.6: Determination of activation energies of 6015 Al alloy. Different slopes are indicative of two different microstructures [45].

4. EXPERIMENTAL PROCEDURE

4.1 Torsion Testing

In recent years, hot torsion testing of solid cylindrical specimens has become more reliable in determining optimum hot working parameters such as strain, strain rate and temperature [2,8,21,22,33-35,42-45]. Although high strains can be achieved at a constant strain rate, there is a linear variation of strain and strain rate from zero at its centre to maximum at the surface. If necessary, the effects of this variation can be reduced by use of a specimen with a tubular cross section. The major advantage of torsion over tension and compression testing is that there is no change in geometry of the specimen during deformation. In light of this fact, true strain and strain rate are equal to the engineering strain and strain rate in torsion. In tension, a sample undergoes localized necking, while a compression specimen suffers from barrelling due to frictional forces at the anvils. In the present work, the torsion test was used to determine the hot working properties of two silicon carbide reinforced aluminum matrix composites and an Al-Mg-Si and an Al-Si alloy.

Torsion testing data are usually recorded in the form of torque versus angle of twist diagrams. Torque is converted to maximum torsional surface shear stress (τ) by using the Fields Backofen equation [47]:

$$\tau = \Gamma(3+m+n')/2\pi r^3 \qquad (4.1)$$

where Γ : Torsional Moment

m : Strain Rate Sensitivity

n'' : Strain Hardening Exponent

r : Specimen Gauge Radius

Since all testing was conducted above 0.5 T_m, n'' is generally taken as zero for the peak or steady state. However as T increases, m varies approximately from 0.01 to 0.2 for each of the materials tested. The variation of m with temperature has only a minor influence ($<10\%$) on the calculated stress because it is added to a larger factor in Equation 4.1.

Torsional strain is defined as the amount of relative rotation, by reference points on the surface of the specimen divided by the distance between them. Therefore, the torsional strain on the surface (γ) is [47]:

$$\gamma = 2\pi r N / L_o \tag{4.2}$$

where N : Number of Turns

L_o : Original Gauge Length

In order to compare torsion data with tension and compression tests, the torsional shear stress and strains are converted to effective stresses and strains using the von Mises criterion for plastic yielding [47]:

$$\sigma = \sqrt{3}\tau \tag{4.3}$$

$$\varepsilon = \gamma/\sqrt{3} \qquad (4.4)$$

where σ : Equivalent Flow Stress

ε : Equivalent Strain

4.2 Testing System and Equipment

Specimens were deformed in a servo-controlled, closed loop torsion machine designed by Sandor Fulop [47] in the Department of Mining and Metallurgy of McGill University (Figure 4.1). In this MTS electro-hydraulic system, torque is applied to a specimen through a rotary hydraulic actuator mounted on a converted lathe bed. Hydraulic power for the system is provided by a 3000 psi supply. On the torsional frame, the test piece is held by two coaxial superalloy bars with attached grips. One end of the test piece is twisted a measured amount by the hydraulic motor controlled by a servo-valve while the other end is held fixed by a torque cell.

The specimen is heated by a quadruple elliptical radiant furnace connected to programmable controller with varied power input. The furnace is water-cooled and capable of temperatures up to 1200°C with rapid heating rates. A transparent quartz tube runs through the furnace enclosing the specimens, grips and bars. Argon is circulating through the tube during heating and testing to prevent oxidation. The temperature is measured by an alumel-chromel (K-type) thermocouple, insulated with double bore ceramic tubing, extending along the stationary test piece shoulder and attached to the specimen with alumel-chromel wire to maintain thermal contact. The location of the

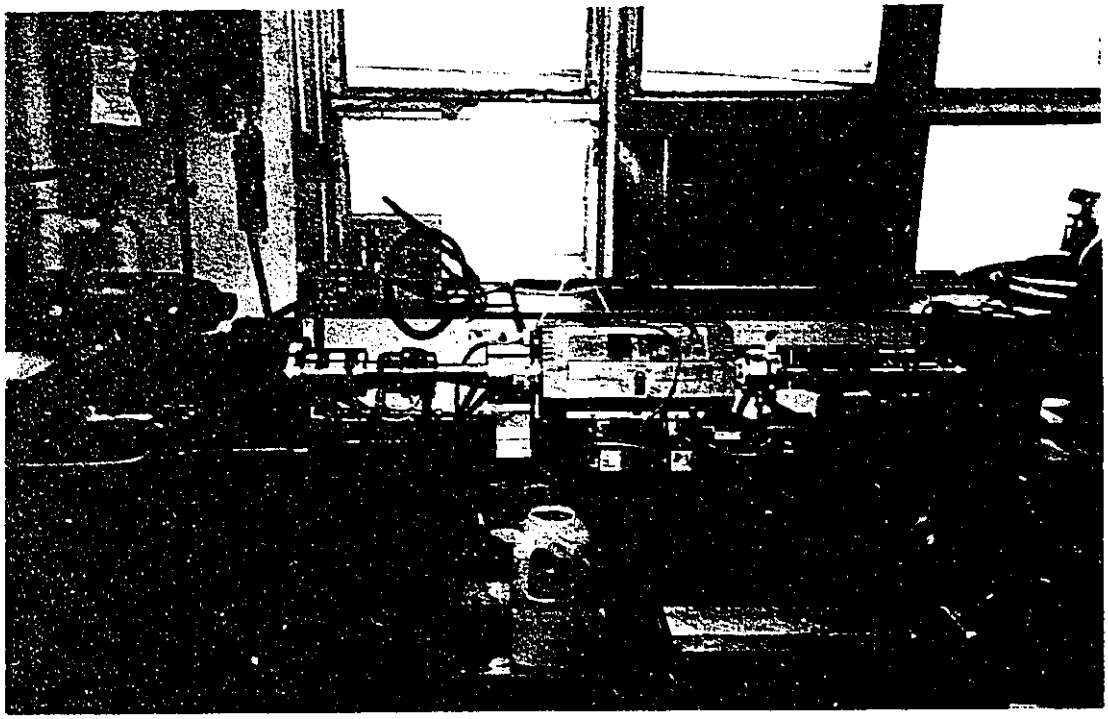

(a)

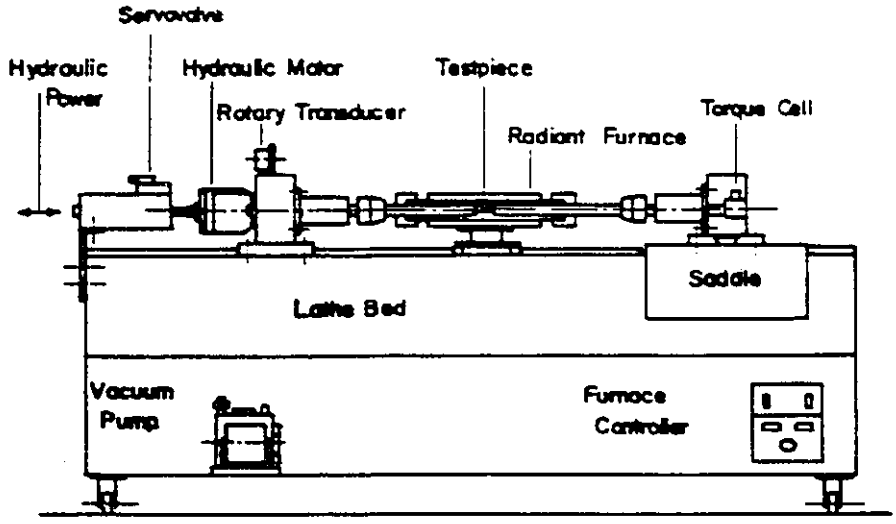

(b)

Figure 4.1: Servo-controlled hot torsion machine: (a) photograph and (b) schematic [47].

thermocouple tip on the gauge section at the fixed end of the specimen was determined to be satisfactory since the thermocouple could be rigidly fixed to the specimen yet underwent only a small fraction of its total revolutions without suffering damage [47].

4.2.1 Control Loop System

A closed loop system provides communication between a command and an operation. The communication lines are via voltage levels set within assigned limits. The command voltage enters as a manually set or pre-programmed value and is converted to a proportional driving force to perform a desired operation (Figure 4.2). In turn, the magnitude of the operation being performed is translated into a voltage level and fed back into the control unit where the progress of the operation may be assessed and varied to meet requirements of the original command voltage [48].

The torsion machine can be operated on either rotary displacement or torque feedback mode. The former was used for the present experiments. The driving signal controls a servo-valve which, through regulating flow of hydraulic oil, controls the position of the hydraulic motor and hence the torsion deformation of the specimen to which it is connected. Torsional displacement is monitored by a dual gang potentiometer and torque by a reaction torque cell, both of which develop proportional voltages to be fed back to their respective channels in the control unit. This system is capable of torsional testing metal specimens at speeds from zero to 1500 rpm, with a maximum torque of 1000 in-lb (113 N-m) for a maximum of fifty turns [48].

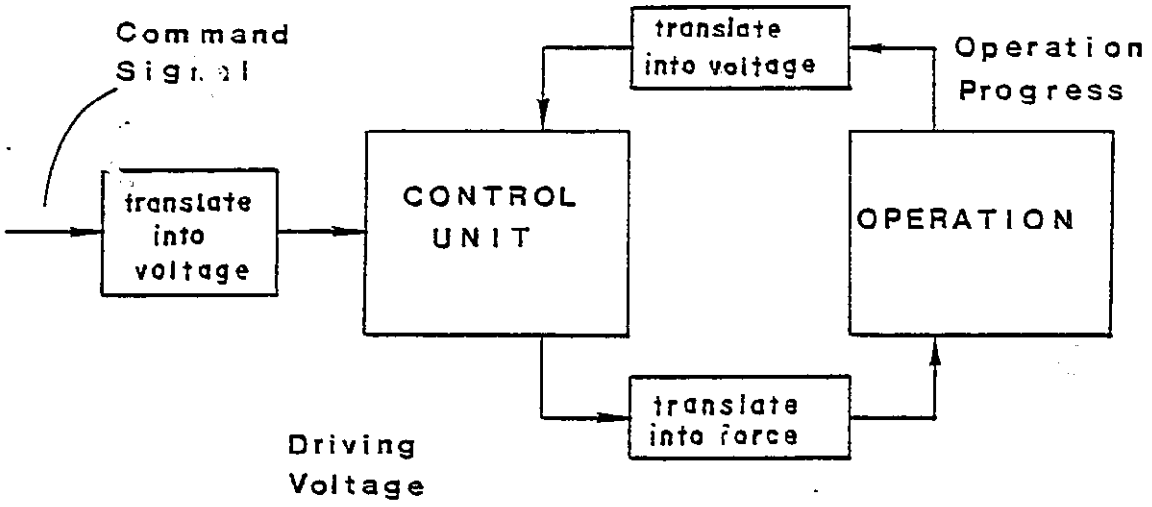

Figure 4.2: Logic of a closed-loop controlling operation [48].

The control unit as shown in Figure 4.3, functions in the MTS system via four basic components with the following individual functions [48]:

(i) Transducer Conditioner : supplies a regulated D.C. voltage to excite the transducer to which it is connected, i.e. the strain or torque transducer, and amplifies the transducer signal to send to the Feedback Selector.

(ii) Feedback Selector : selects the signal from the Transducer Conditioner which the program currently dictates to be the controlled variable and directs this signal to the Servo-Controller.

(iii) Servo-Controller : detects any discrepancy between the command signal and the controlled variable feedback signal and forwards a proportional voltage to the Valve Driver.

(iv) Valve Driver : accepts the error signal from the Servo-Controller and provides a control signal capable of driving the servo-valve to which it is connected.

4.2.2 Computer Operation and Programming

The MTS system incorporates a PdP 11 mini-computer hooked up to a Tektronix® graphics terminal and uses BASIC as its software communication means. In a programmable system, the variations of all controllable parameters are entered via the program for the entire sequence which is then initiated. The responsibilities of the computer may be viewed in terms of the following four categories:

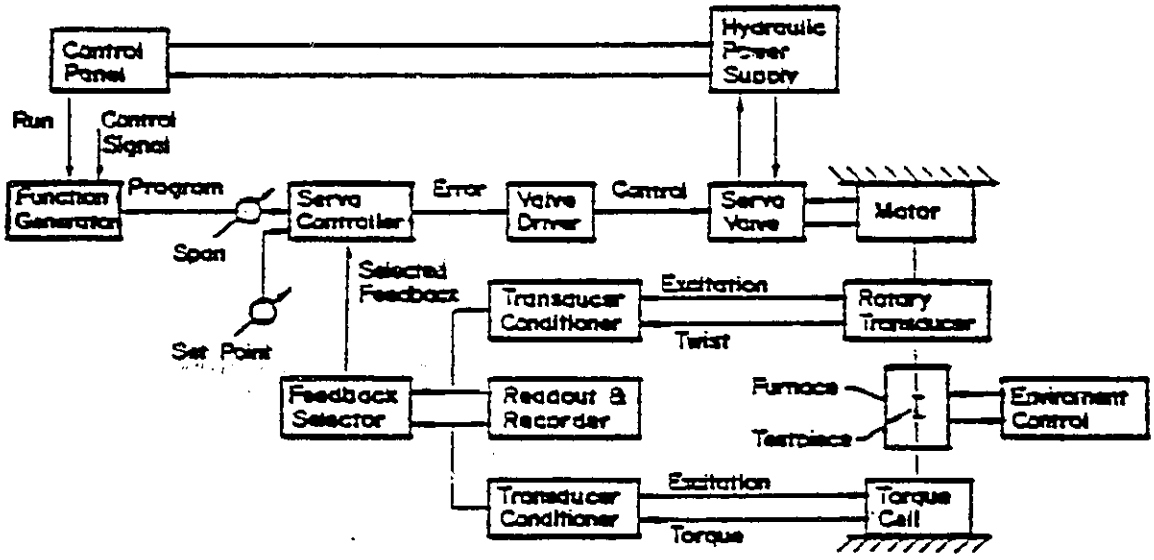

Figure 4.3: Block diagram of typical MTS system [47].

(i) Accept and interpret all test parameter information from the user.

(ii) Use the input information to activate the required hardware devices which will in turn send the appropriate command signals to the closed loop system and drive the test.

(iii) Monitor and record all output feedback information from the transducers within the closed loop system as the run is being executed.

(iv) Interpret the transducer output information and arrange it so it may be presented in a legible manner to the user.

The first step involves allocating and identifying a region of memory space for parameter input; arithmetic values are consequently interpreted entirely by their magnitudes and location in memory. The second step is to convert the arithmetic input which is stored in its memory to an analog output, i.e. an analog voltage output to serve as a command signal to the closed loop system previously discussed. The third step converts the analog voltage transducer signals to some representative arithmetic values which were stored in memory. The final step calls up these transducer values and arranges them in a legible manner to be output to the user usually in the form of a graph [48].

The software component of this system must provide for a number of basic functions [48]:

(i) Interact with user and accept test information parameters.

(ii) Interact with the Hardware Segment Generator to command the servo-controller and drive the torsion machine.

(iii) Accept the feedback information from the servo-controller.

(iv) Present the feedback information to the user in graphical form.

(v) Record and recall data.

Appendix A shows a working copy of a program which fulfils the necessary requirements to run a torsion test on this system followed by flow chart for its operation in Figure Appendix B.

4.3 Test Materials

Four different materials were used in the present studies of which two were commercial aluminum alloys (6201 and A356) while the other two were composites of aluminum alloys 6061 and A356 reinforced with 15v/o SiC particles having an average size of 12 μm. The 6201 Al alloy, which had been Properzi continuously cast and hot rolled into rods of 0.375 in. diameter (SCR® process), was supplied by Southwire Co., Carrolton, Georgia. The rest of the materials were provided by Dural Aluminum Composite Corporation through Alcan Laboratories in Kingston, Ontario in the as-cast condition using the DURALCAN® molten metal mixing method and bar extruded. The chemical composition of the materials are shown in Table 4.1. Torsion specimens with axes parallel to the rolling or casting direction were machined to close tolerances, especially in the gauge section, in order that twisting would be uniform. The test specimen design is shown in Figure 4.4. One end of the test piece is threaded, while the other end has a rectangular section which fits into a slot. This arrangement allows for easy mounting and removal without accidentally straining the specimen.

Two heat treatments were employed to study the hot working behaviour of SCR-6201 alloy; (i) solution treated for four hours at 520°C in an argon atmosphere and quenched in relatively hot water (55-80°C) and (ii) over aged at 300°C for two hours and air-cooled. For the rest of the materials, no post heat treatment was done prior to testing.

4.4 Test Procedures

Before starting any test, the reflecting surfaces of the furnace were cleaned with gauze so that the test temperature would be reached as quickly as possible. For the 6201 Al alloy, isothermal continuous tests were conducted at 300 to 600°C for the solution-treated specimens and at 200 to 500°C for the overaged material at torsional shear strain rates ($\dot{\varepsilon}$) of 0.1, 1.0 and 4.0 s^{-1} to a strain (ε) of 2.5 or to fracture. In the case of the Duralcan® materials, tests were performed at three different $\dot{\varepsilon}$ between 0.1 and 5.0 s^{-1} and four temperatures between 300 and 540°C. The samples were twisted without interruption to fracture. All tests were carried out in a controlled atmosphere of high purity argon. Every specimen was heated to desired temperature and held constant ten minutes prior to deformation. All specimens were quenched in water less than ten seconds after deformation was completed.

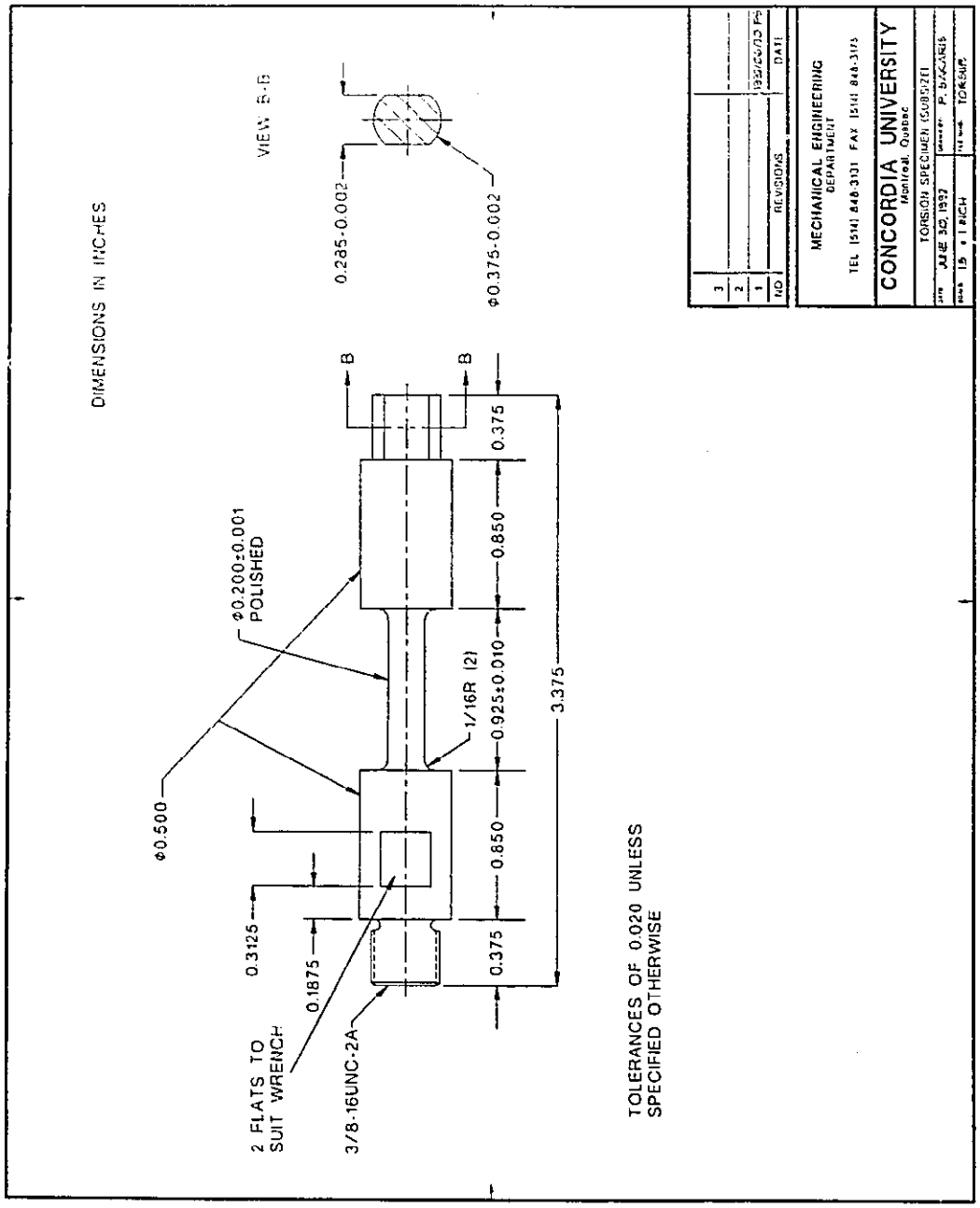

Figure 4.4: Torsion specimen design.

Table 4.1: Chemical Compositions (wt%) [20].

Material	Si	Fe	Cu	Mn	Mg	Cr	Zi	Ti	Al
6201	0.8	0.5	0.1	0.03	0.7	0.03	0.1	--	rem
6061	0.6	0.7	0.3	0.15	1.0	0.1	0.25	0.15	rem
A356	7.0	0.2	0.2	0.1	0.35	--	0.1	0.20	rem

4.5 Metallographic Procedure

In order to investigate the change in structure with deformation, the gauge lengths were sectioned using a diamond blade on a low speed saw to reveal tangential, longitudinal and transverse sections. These were mounted in cold curing resin mold and ground on 240, 320, 400 and 600 grit silicon carbide papers. For the Duralcan® materials, the samples were then polished using 6 μm and 1 μm diamond paste and finally magnesium oxide. Samples were then viewed in the optical microscope in the as-polished condition with the exception of the 6061 composite, where it was etched in 0.5% HF. For the 6201 Al alloy, samples were anodized in a solution of 4-5 ml HBF_4 and 200 ml H_2O using a stainless steel cathode and the sample as the anode for 10 min at 10 mA. They were then viewed in the optical microscope using polarized light.

5. EXPERIMENTAL RESULTS

5.1 Data Analysis

5.1.1 Stress-Strain Curves

The torque and twist data were converted through the use of Equations 4.1 to 4.4 to equivalent σ and ε, in order to compare them to the findings of other researchers. The value of m was taken as the slope of log Γ versus log $\dot{\varepsilon}$ (Figure 5.1). The m values vary from about 0.01 at 200 to 300°C up to 0.17 near T_m for all four materials. The equivalent σ-ε curves for the four materials are presented in Figure 5.2. The values of n' were taken as zero which is valid only at the peak and during steady state.

Strength comparisons of 15v/o SiC_p/6061 Al and the unreinforced alloy (6061 Al) [2] show that the 6061 composite is approximately 25 to 50% higher than that of the matrix between 300 and 400°C tested under compression. The 15v/o SiC_p/A356 Al composite is similarly stronger than A356 Al at 300°C but not as much at 400°C and even less at 500°C. There is a progressive rise in the flow stress when the strain rate is increased for all temperatures. Similar behaviour is observed for both composites and the unreinforced alloy such that below 300°C, they strain harden to failure. A slight degree of flow softening to a steady state regime before fracture is observed at higher temperatures; however, distinct peak stresses are seen in the flow curves for both composites at 500°C which might indicate DRX; otherwise, it is considered to be the result either of some particle coalescence or of greater deformation heating at 300°C than at 400°C. There is also the possibility of the initiation of cracking in the material.

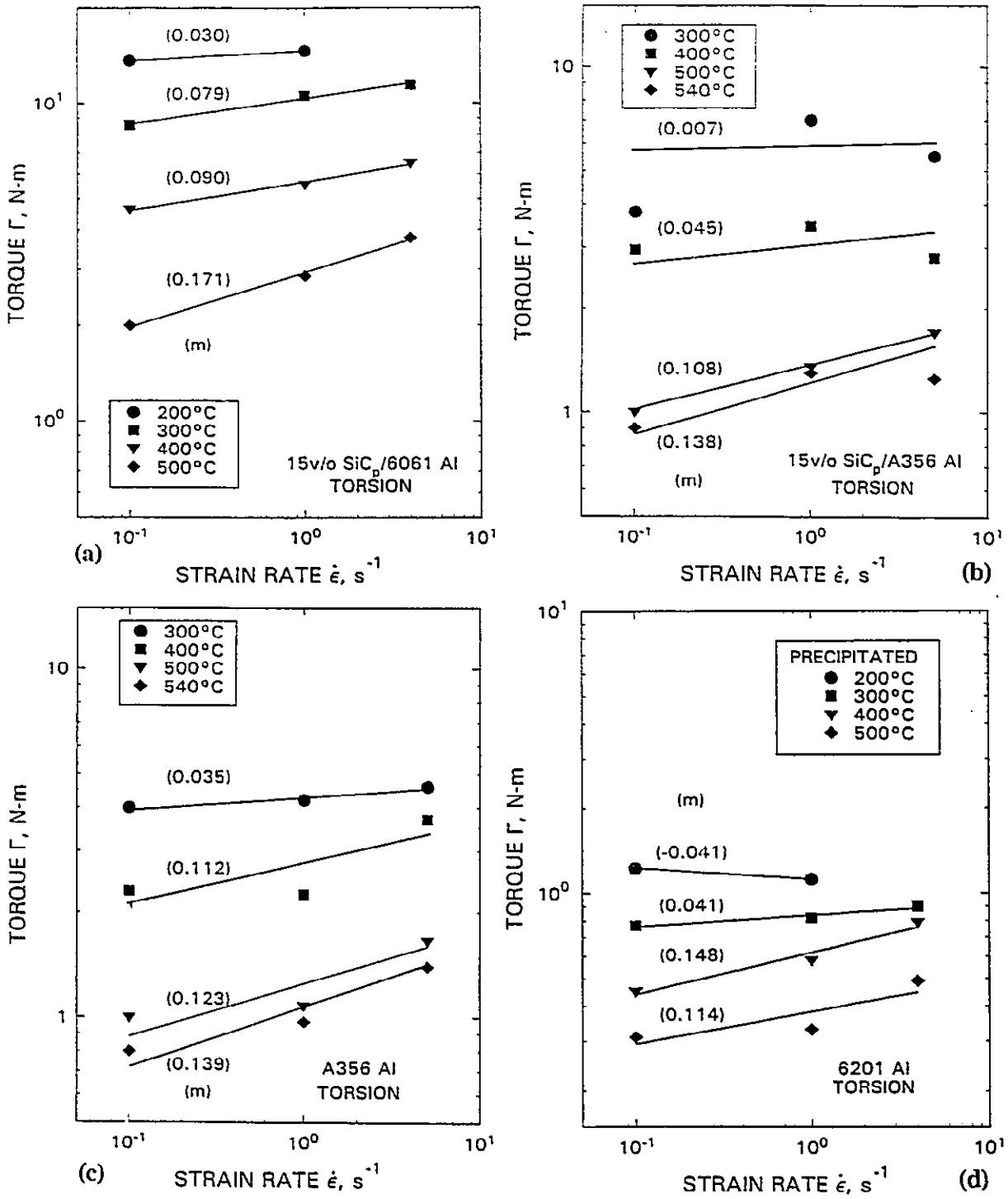

Figure 5.1: Plot of log Γ versus log $\dot{\varepsilon}$ was used to calculate m for: (a) 15v/o SiC$_p$/6061 Al, (b) 15v/o SiC$_p$/A356 Al, (c) A356 Al and (d) 6201 Al.

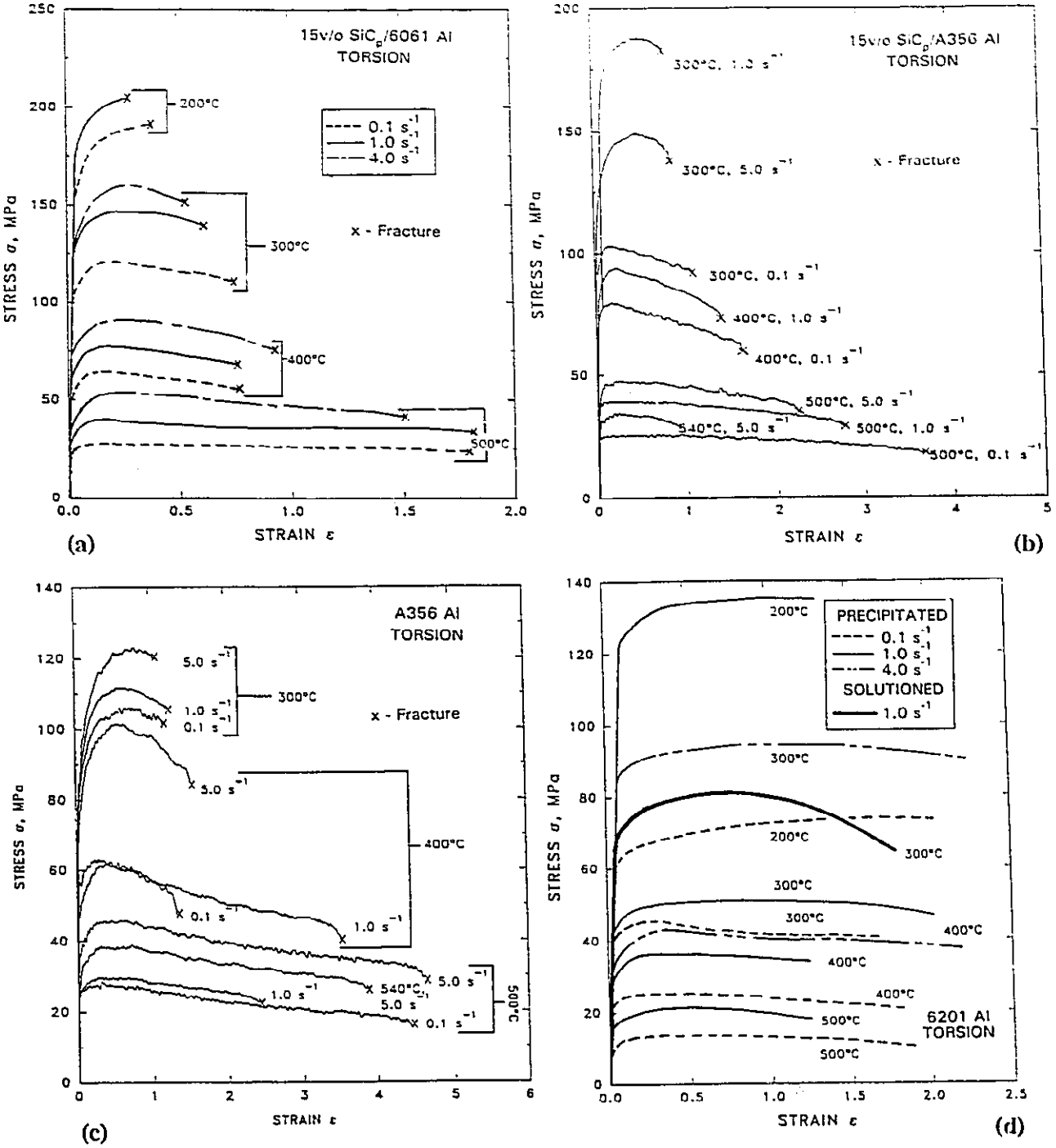

Figure 5.2: Representative σ-ε curves for: (a) 15v/o SiC$_p$/6061 Al, (b) 15v/o SiC$_p$/A356 Al, (c) A356 Al and (d) 6201 Al. The steady state stress rises with rising $\dot{\varepsilon}$ or declining T.

The solution treated 6201 Al alloy at 300°C exhibits a high peak stress followed by some work softening. However, the peak becomes much attenuated as the temperature increased. For the precipitated condition, the stress rises progressively to a steady state regime; the usual form for materials which dynamically recover as explained in Chapter 3. The solutioned material shows significantly higher strength than the precipitated at lower temperatures but as T rises the difference becomes negligible.

5.1.2 Ductility

In torsion tests, the number of turns to fracture represent the ductility which can be found in Figure 5.2. Torsional ductilities of the four materials are shown as graphs of strain to failure versus test temperature (Figure 5.3). Generally, ductility increases with decreasing strain rate and increasing temperature. The fracture strain (ε_f) of 15v/o SiC_p/6061 Al rises to a maximum at 400°C of about 1.5 at 0.1 s^{-1}. The torsional ductility is much lower than that of its matrix alloy although it is much higher than tensile failure strains. For 15v/o SiC_p/A356 Al, ε_f rises to a maximum of about 4.2 above 400°C at 0.1 s^{-1}. The ductility of the A356 composite is about 20 to 30% less than A356 matrix alloy. Fracture strains for this particular composite increase until 500°C for all strain rates and declines slightly as the temperature rises to 540°C. Unlike the composite material, A356 Al displays rising ductility to 540°C and a peak failure strain of 4.7 for 5.0 s^{-1} between 500 and 540°C. With a limited testing strain of 20, 6201 Al for both heat treatments did not fracture at T equal to and greater than 400°C. At 300°C for all three strain rates, the precipitated material failed when ε was between 7 and 8 while the solutioned specimen fractured at about half that value.

The flow stresses decrease with increasing deformation temperature rapidly below 400°C and more slowly above that for all four materials as illustrated in Figure 5.4. The composites are much stronger than the matrix alloy at low temperatures but only slightly so above 500°C. The flow stress does not diminish very rapidly at high temperatures. For 6201 Al alloy, the rate of decline rises with increasing strain rate because of starting from higher stress levels. Furthermore, the decline rate for the solutioned alloy at 0.1 s^{-1} is similar to that of the precipitated material at 1.0 s^{-1}.

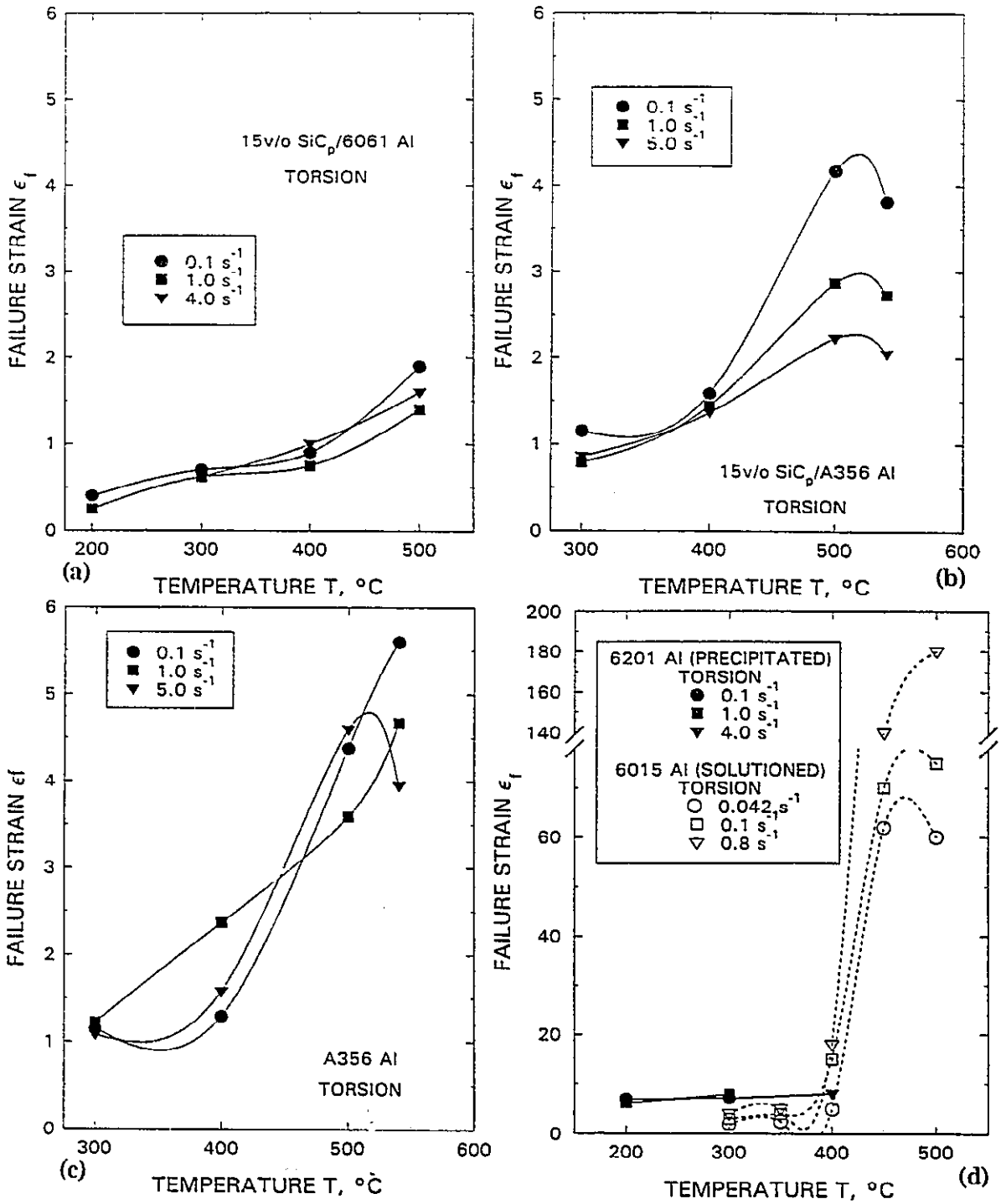

Figure 5.3: Ductilities for: (a) 15v/o SiC$_p$/6061 Al, (b) 15v/o SiC$_p$/A356 Al, (c) A356 Al and (d) 6201 Al increase with rising T to pass through maxima near 500°C.

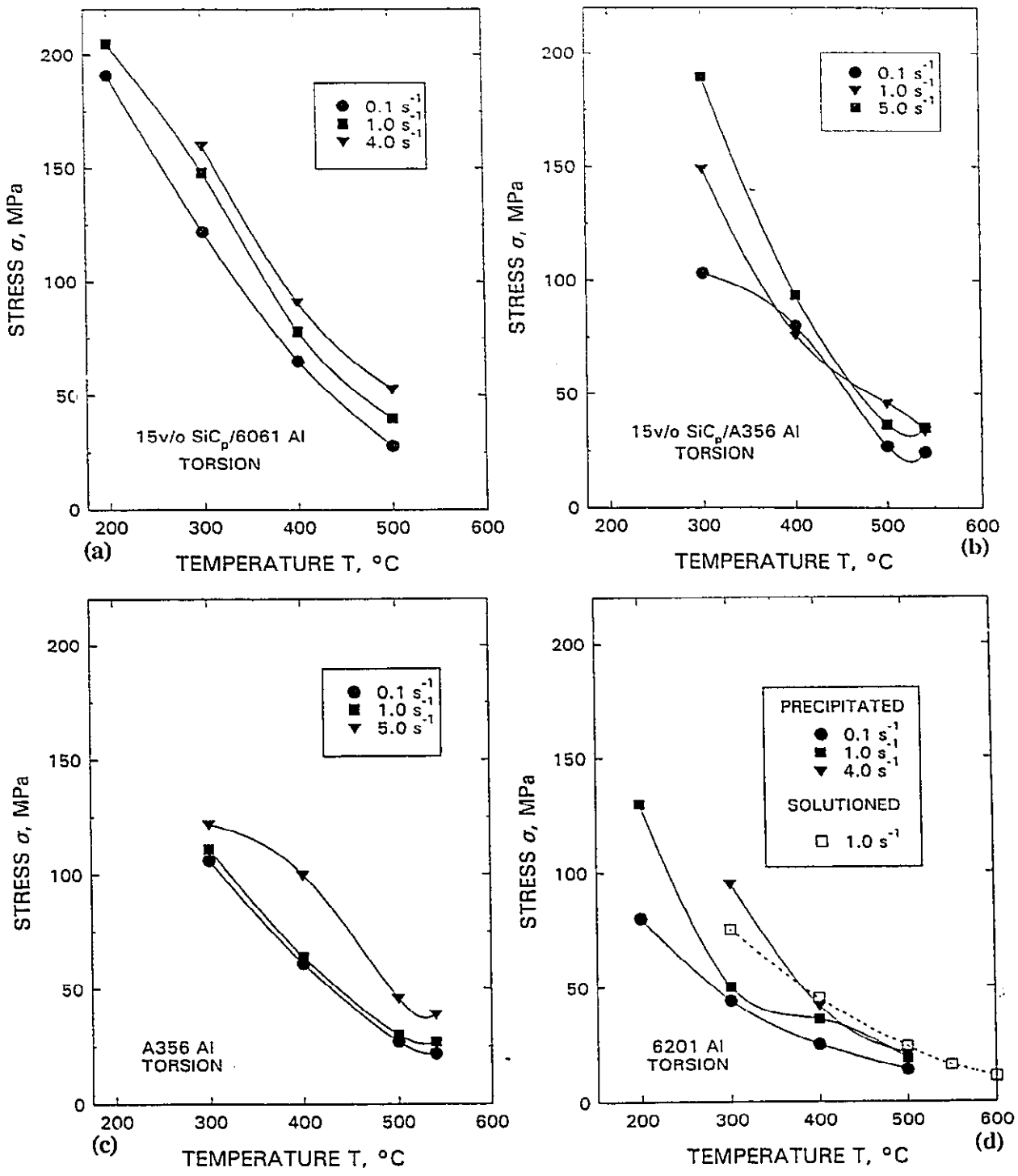

Figure 5.4: Strengths for: (a) 15v/o SiC_p/6061 Al, (b) 15v/o SiC_p/A356 Al, (c) A356 Al and (d) 6201 Al decrease uniformly with rising T.

5.1.3 Constitutive Plots

The effect of temperature and strain rate on flow stress was analyzed and adequately expressed by Equation 3.5. In the hyperbolic sine analysis, the optimum α should result in the constant temperature lines in plots of log $\dot{\varepsilon}$ versus log sinh $\alpha\sigma$ (Figure 5.5) being close to parallel, however, it is normal practice to take the value of α from similar alloys as found in the literature; this facilitates the comparison of Q_{HW} and of data by graphical means. Consequently, a value of $\alpha = 0.052$ MPa^{-1} was used for the composites and A356 Al in Figure 5.5 where the slope n was determined. From the plots of log sinh $\alpha\sigma$ versus 1/T (Figure 5.6), the activation energies were calculated using the following relationship:

$$Q_{HW} = 2.3Rns \qquad (5.1)$$

where s : Slope of log sinh $\alpha\sigma$ versus 1000/T

First order regressions were performed on both the constant temperature and strain rate data to determine the values of the slopes n and s respectively. The average of n and s was calculated from the individual slopes which in turn were fitted back to the data as illustrated in Figures 5.5 and 5.6. It is apparent that these average slopes do not give the best fit lines especially at the low temperatures. At 200°C, the material may not be undergoing any hot working mechanisms which lead to very low and inconsistent fracture strains and consequently large scatter in the flow stress. The separations between some of the data points and the lines indicate experimental error. The values of n, s and Q_{HW} for each material are summarized in Table 5.1.

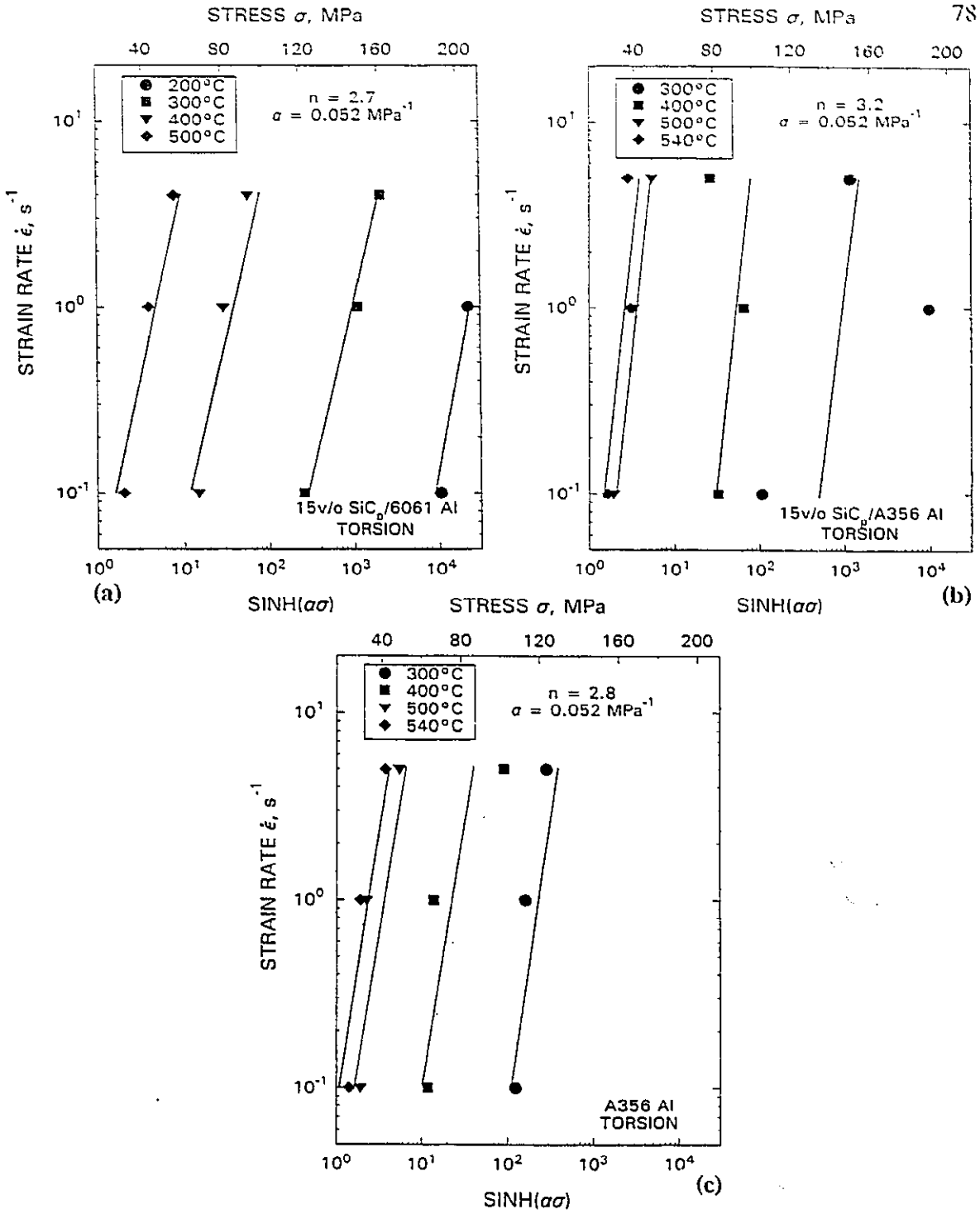

Figure 5.5: Plot of log $\dot{\varepsilon}$ versus log sinh $\alpha\sigma$ (α = 0.052 MPa^{-1}) for: (a) 15v/o SiC_p/6061 Al (b) 15v/o SiC_p/A356 Al and (c) A356 Al. A356 materials are slightly stronger than 6061 materials.

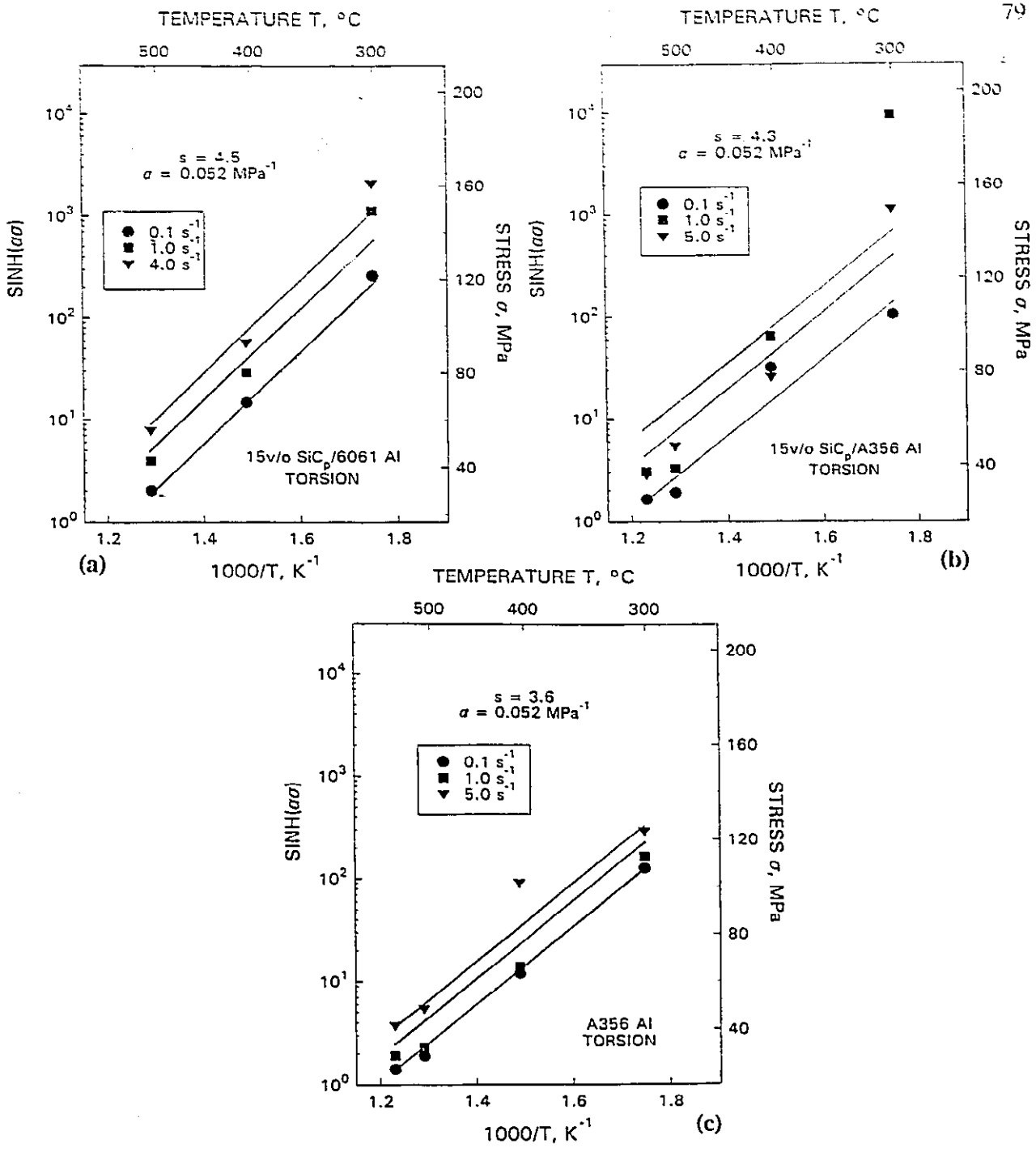

Figure 5.6: Arrhenius relationships linking σ and T suit the data of: (a) 15v/o SiC_p/6061 Al and (b) 15v/o SiC_p/A356 Al data reasonably well such that straight lines can be drawn and a single Q_{HW} can be calculated. The activation energy for (c) A356 Al is comparable with other Al alloys.

Table 5.1: Summary of stress exponents (n), slope (s) and activation energies (Q_{HW}) for composite and bulk matrix alloys.

Material	$n_{200°C}$	$n_{300°C}$	$n_{400°C}$	$n_{500°C}$	$n_{540°C}$	n
15v/o SiC_p/6061 Al	3.5	1.9	2.7	2.7	--	**2.7±0.5**
15v/o SiC_p/A356 Al	--	3.4	-0.5	4.3	5.6	**3.2±1.9**
A356 Al	--	3.8	1.1	3.0	3.4	**2.8±0.9**
Material	$s_{0.1\ s-1}$	$s_{1.0\ s-1}$	$s_{4.0\ s-1}$	$s_{5.0\ s-1}$		s
15v/o SiC_p/6061 Al	4.2	4.7	4.7	--		**4.5±0.3**
15v/o SiC_p/A356 Al	3.1	5.7	--	4.2		**4.3±0.9**
A356 Al	3.6	3.5	--	3.6		**3.6±0.03**
Material	Q_{HW}, (kJ/mol)					
15v/o SiC_p/6061 Al	**233±3**					
15v/o SiC_p/A356 Al	**263±33**					
A356 Al	**199±1**					

With progress in computational techniques, optimization of Equation 3.5 to fit the data is possible by selecting the most suitable combination of α, n and Q_{HW}. However, due to the wide variety of α obtained, difficulty arises in finding any rational relationship between constitutive constants and the alloy composition. In the literature, there are often different values of α for the same alloy making comparable plots of log $\dot{\varepsilon}$ versus log sinh $\alpha\sigma$ difficult. To alleviate this problem, in the case of 6201 alloy, constitutive analysis is repeated with values of α which range from 0.01 to 0.08 MPa^{-1} (Table 5.2). In order to show distinct effects of varying α, the data was plotted for only 0.02, 0.06 and 0.08 MPa^{-1}: both log $\dot{\varepsilon}$ versus log sinh $\alpha\sigma$ (Figure 5.7) and log sinh $\alpha\sigma$ versus 1000/T (Figure 5.8). In Figure 5.7, the sets of lines for increasing α values move to higher values of log sinh $\alpha\sigma$ and to lower n values. The linearity of the data for each temperature changes because the sinh function is not raised as a simple multiple of rising α. A plot of n versus α (Figure 5.9) indicates that there is a tendency towards saturation in n as α increases. Moreover in a plot against α, the slope s increases linearly as α rises but at a higher rate for higher strain rate (Figure 5.10). Meanwhile the solution treated 6201 has slightly higher strength than the overaged alloy at all temperatures; although no comparison can be made for 550 and 600°C since both are above the solvus. Using Equation 5.1, Q_{HW} was calculated for all α values and appears in Table 5.2. Due to large scatter, data points of 200°C, 1.0 s^{-1} and 300°C, 4.0 s^{-1} were omitted from the analysis. In the range 0.01 to 0.04 MPa^{-1}, Q_{HW} for the precipitated material rises towards stabilization at 192 kJ/mol between 0.06 and 0.08 MPa^{-1}.

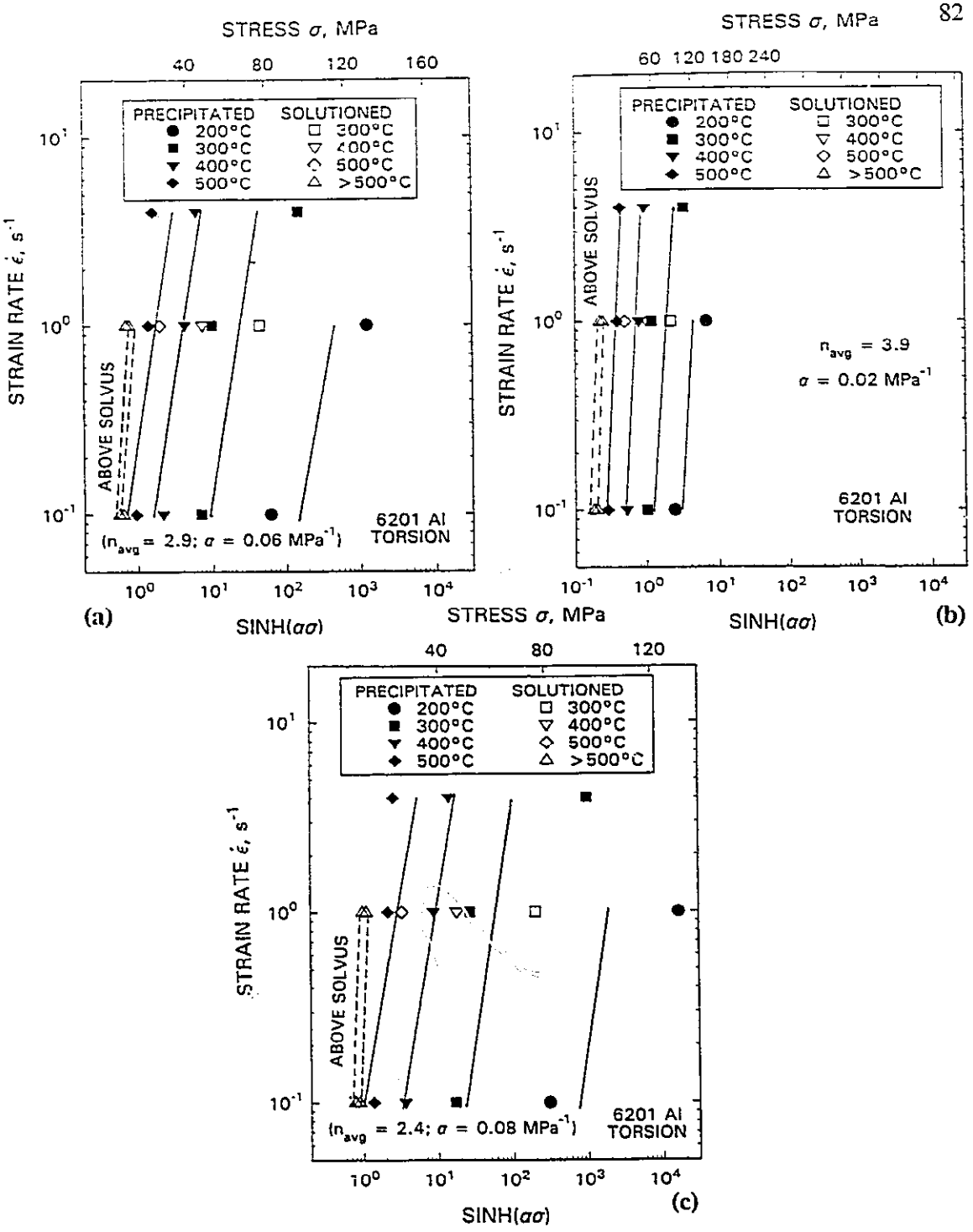

Figure 5.7: Plots of log $\dot{\varepsilon}$ versus log sinh $\alpha\sigma$ for 6201 Al with: (a) $\alpha = 0.06$ MPa^{-1}, (b) $\alpha = 0.02$ MPa^{-1} and (c) $\alpha = 0.08$ MPa^{-1} exhibit parallel lines for constant T which confirm Equation 3.4.

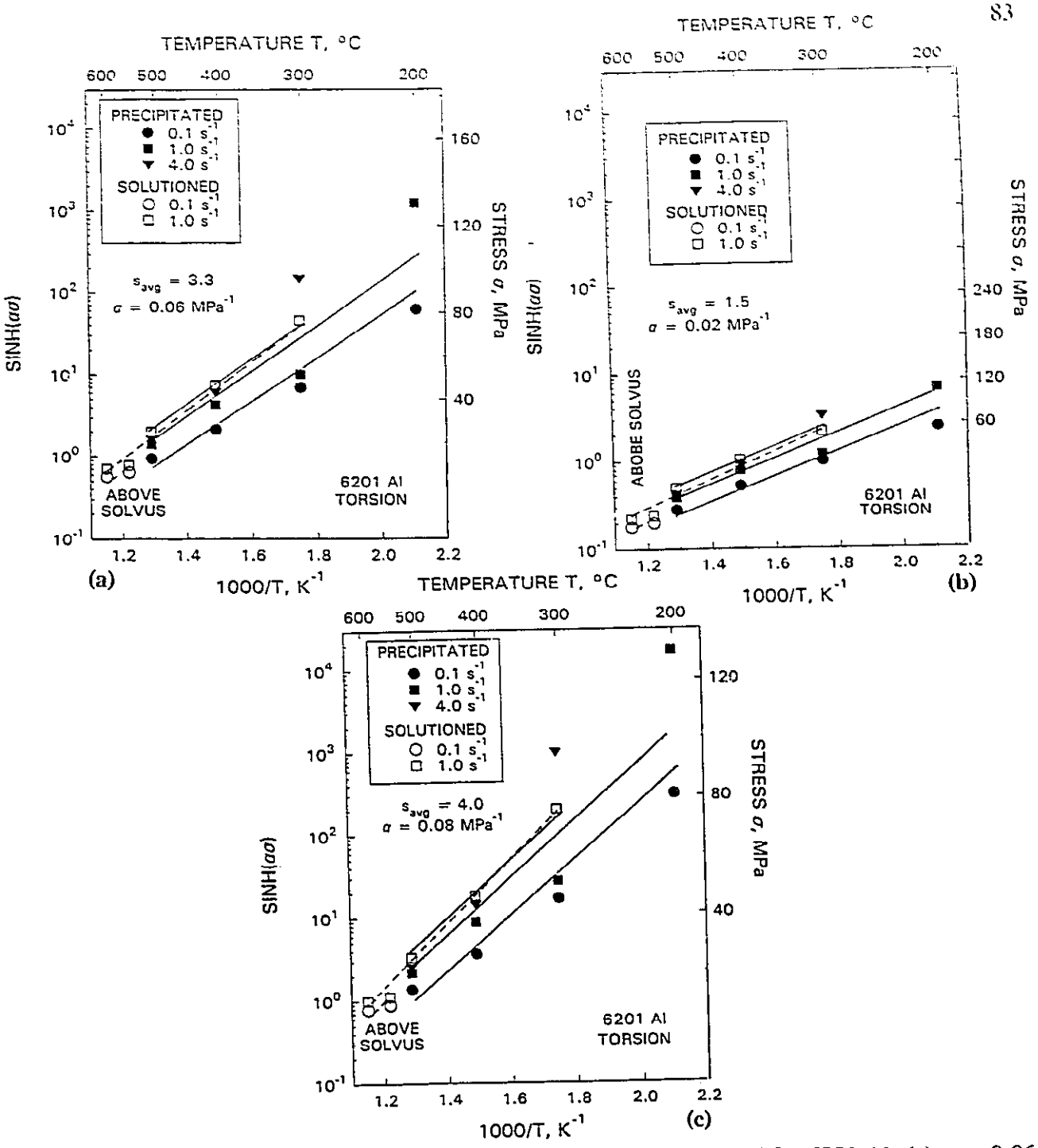

Figure 5.8: Arrhenius relationship linking σ and T is found for 6201 Al: (a) $\alpha = 0.06$ MPa^{-1}, (b) $\alpha = 0.02$ MPa^{-1} and (c) $\alpha = 0.08$ MPa^{-1} according to Equation 3.4. Data points: 200°C, 1.0 s^{-1} and 300°C, 4.0 s^{-1} were disregarded here and in Figure 5.7 for 6201 Al.

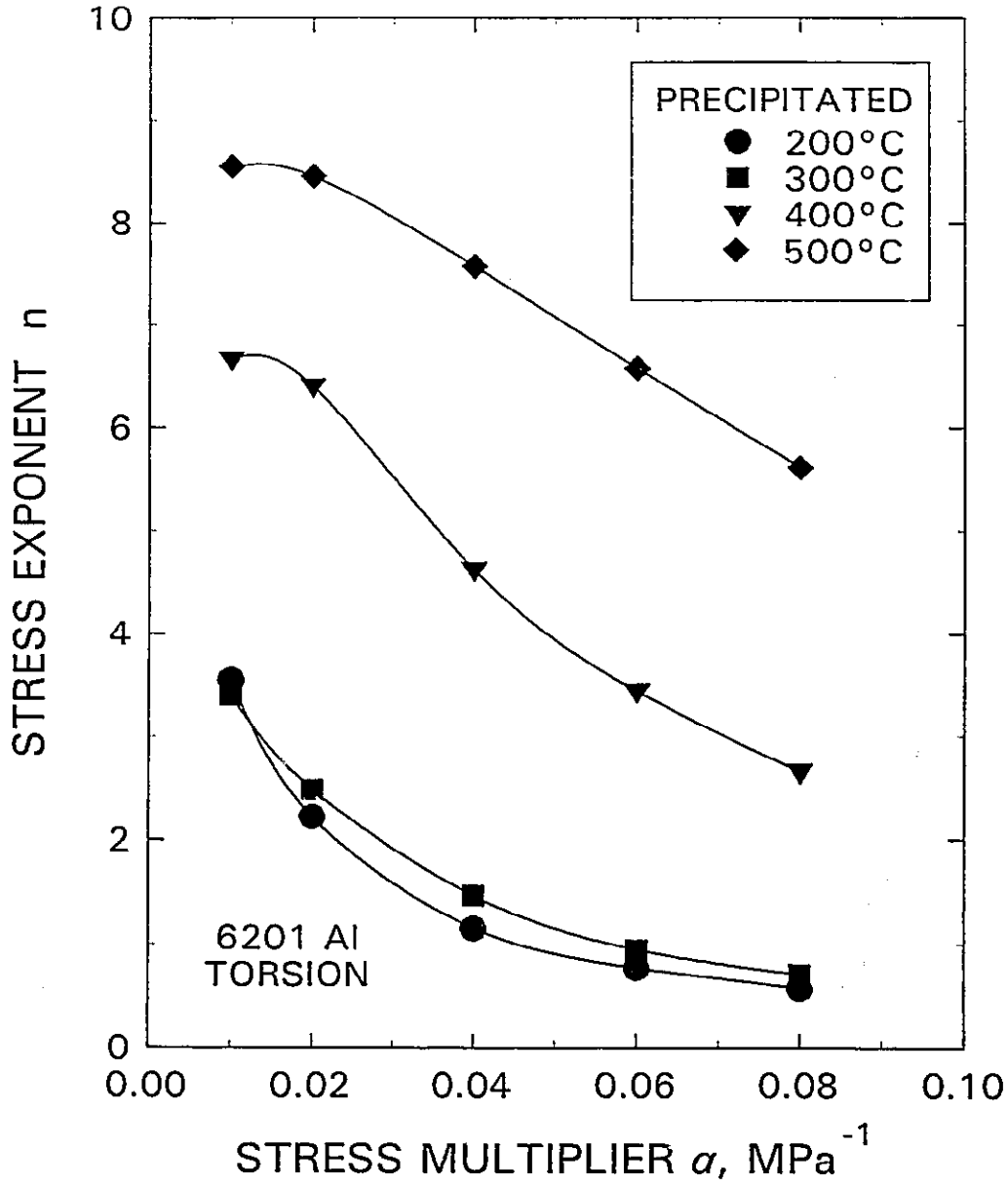

Figure 5.9: Plot of n versus α indicates that n declines at a diminishing rate as α increases for 6201 Al.

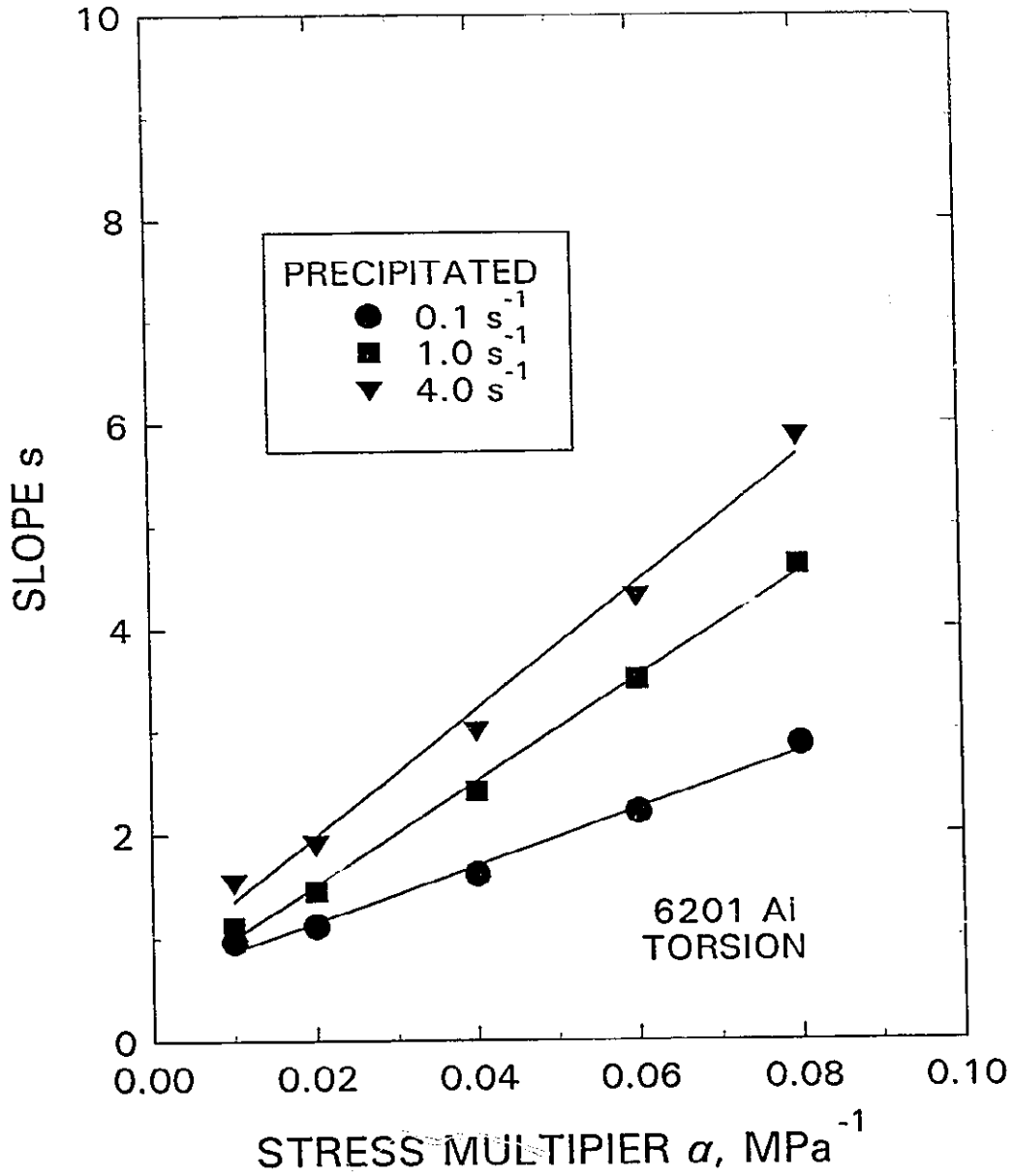

Figure 5.10: Plot of s versus α shows s increasing linearly as α rises but at a higher rate for higher $\dot{\varepsilon}$.

Table 5.2: Values of constitutive constants (n_{avg}, s_{avg} and Q_{HW}) for various stress multipliers (α) for precipiated 6201 Al alloy.

α, (MPa^{-1})	$n_{200°C}$	$n_{300°C}$	$n_{400°C}$	$n_{500°C}$	n_{avg}
0.01	3.6	3.4	6.7	8.6	**5.5±2.1**
0.02	2.2	2.5	6.4	8.5	**3.9±2.6**
0.04	1.2	1.5	4.6	7.6	**3.7±2.4**
0.06	0.8	0.9	3.4	6.6	**2.9±2.1**
0.08	0.6	0.7	2.7	5.6	**2.4±1.8**

α, (MPa^{-1})	$s_{0.1\ s-1}$	$s_{1.0\ s-1}$	$s_{4.0\ s-1}$	s_{avg}
0.01	1.0	1.1	1.6	**1.2±0.2**
0.02	1.1	1.5	1.9	**1.5±0.3**
0.04	1.6	2.4	3.0	**2.4±0.5**
0.06	2.2	3.5	4.3	**3.3±0.8**
0.08	2.9	4.6	5.9	**4.0±1.2**

α, (MPa^{-1})	Q_{HW}, (kJ/mol)
0.01	**128±8**
0.02	**126±13**
0.04	**165±21**
0.06	**192±32**
0.08	**193±41**

The flow stress can be expressed as a function of the product of the strain rate and the Arrhenius term (Equation 3.4). This product is the temperature compensated strain rate, or the Zener-Hollomon parameter (Z). At greater Z, the higher σ originates in fewer thermally activated events per unit strain which arise from either a lower temperature or the shorter time accorded by a high strain rate. With Q_{hw} determined for all the materials tested, it is possible to plot log Z against log sinh $\alpha\sigma$ in order to draw the data into single lines with slopes n and intercepts A (Figure 5.11).

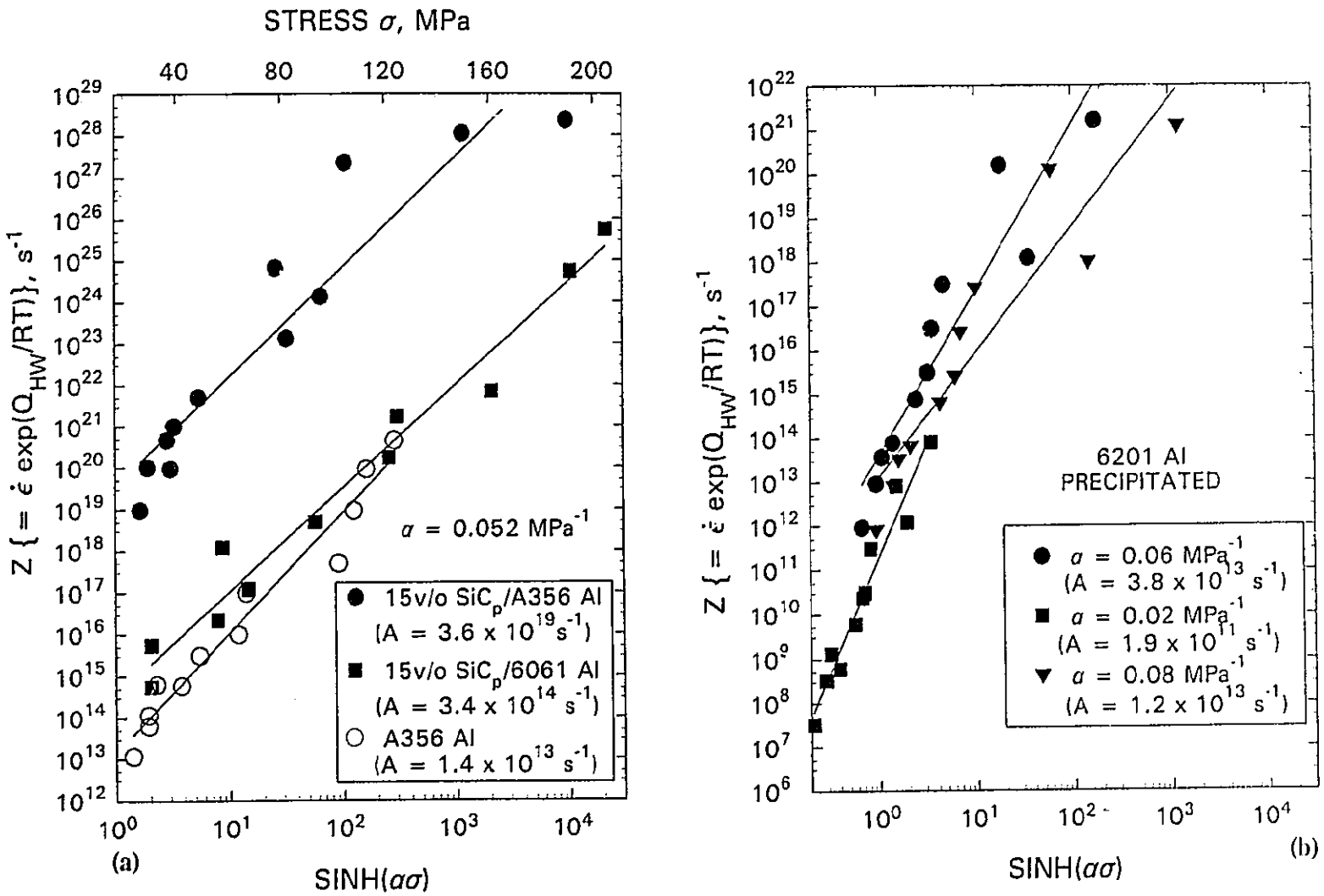

Figure 5.11: Through the use of the Z parameter, the data is organized into a single line: (a) 15v/o SiC_p/6061 Al, 15 v/o SiC_p/A356 and A356 Al for $\alpha = 0.052$ MPa^{-1} and (b) 6201 Al for $\alpha = 0.02$, 0.06 and 0.08 MPa^{-1}.

5.2 Optical Metallography

Optical micrographs of 15v/o SiC_p/6061 Al are shown in Figure 5.12. The as-received structure was generally non-uniform consisting of randomly distributed SiC particles throughout the 6061 Al matrix. Some clustering of the particles was also evident. After testing at 300°C, 1.0 s^{-1}, some particles were aligned in the direction of deformation. Partial or complete fracture was seen in several SiC particles. In addition, some decohesion was also visible. Surface cracking along the matrix-particle interface could also be seen. At higher temperatures, there was evidence of substructure which could be an indication of DRX.

Micrographs of A356 Al shown in Figure 5.13 revealed a cellular type distribution of facetted Si particles (2.5 x 0.5 μm). The fracture surface was irregular exhibiting sharp angular features at 300°C and curved ones at 500°C. Adjacent to the fracture, there were additional short cracks or tears with similar features. Near the fracture, the Si particles gave the appearance of being aligned parallel to the main crack direction. Decohesion was observed with most of the particles especially the larger ones. These observations are in agreement with previous studies by Mayer [60] indicating that the fracture of this material occurs in three stages:

(i) Crack initiation at the eutectic Si particles.

(ii) Propagation of cracks in the interdendritic region.

(iii) Rupture of matrix.

At 300°C, numerous small cracks were observed at the surface but were less frequent at higher temperatures. At 500 and 540°C, some cracks seemed to lie along grain

boundaries with evidence of triple junctions.

In the case of 15v/o SiC_p/A356 Al (Figure 5.14), the SiC particles dominate the field of view. There is a slightly cellular appearance due to the aluminum matrix dendrite cores. The Si particles in the matrix are about one-fifth the size of those in A356. In addition, the Si particles are numerous in regions between neighbouring SiC particles and are in lower density in the center of cells oulined by the SiC particles. The fracture path appears more irregular and the surface more dimpled than A356. The dimples are likely caused by decohesion at particles which later fell out during polishing. At both low and high temperatures, the fissures were in contact with the particles along less than a quarter of the length. A long fissure found at 540°C shows the crack runs mainly through the matrix. In addition, short cracks were often seen in the regions where there were clusters of Si particles (Figure 5.15).

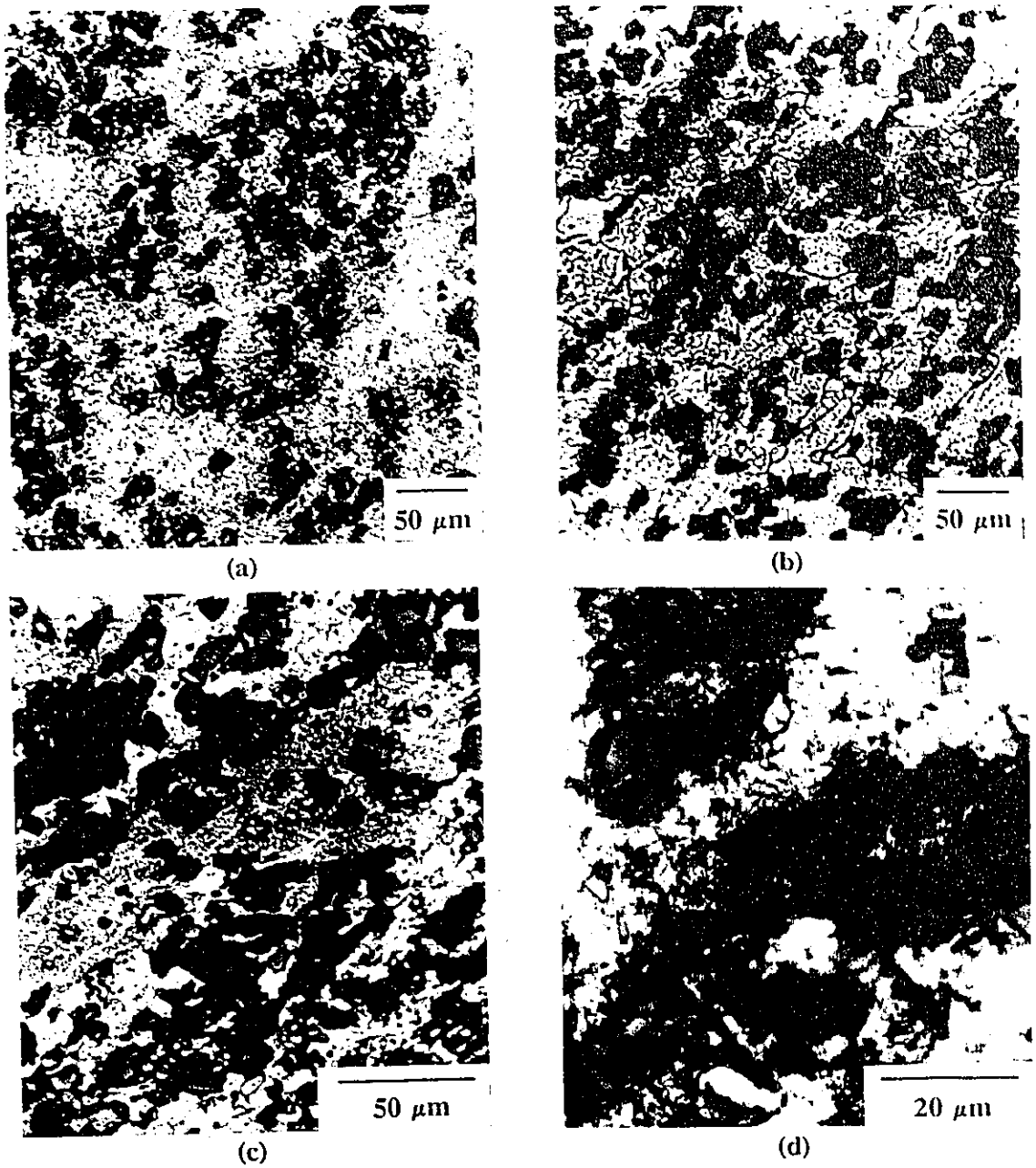

Figure 5.12: Tangential sections of etched 15v/o SiC_p/6061 Al: (a) as-received; SiC particles appear in clusters, (b) 400°C, 1.0 s^{-1}; more even distribution of SiC particles and evidence of substructure, (c) 300°C, 1.0 s^{-1}; particles are aligned in the direction of deformation along which also appears a surface crack and (d) 300°C, 1.0 s^{-1}; partial or complete fracture is seen in some particles surrounding large pore.

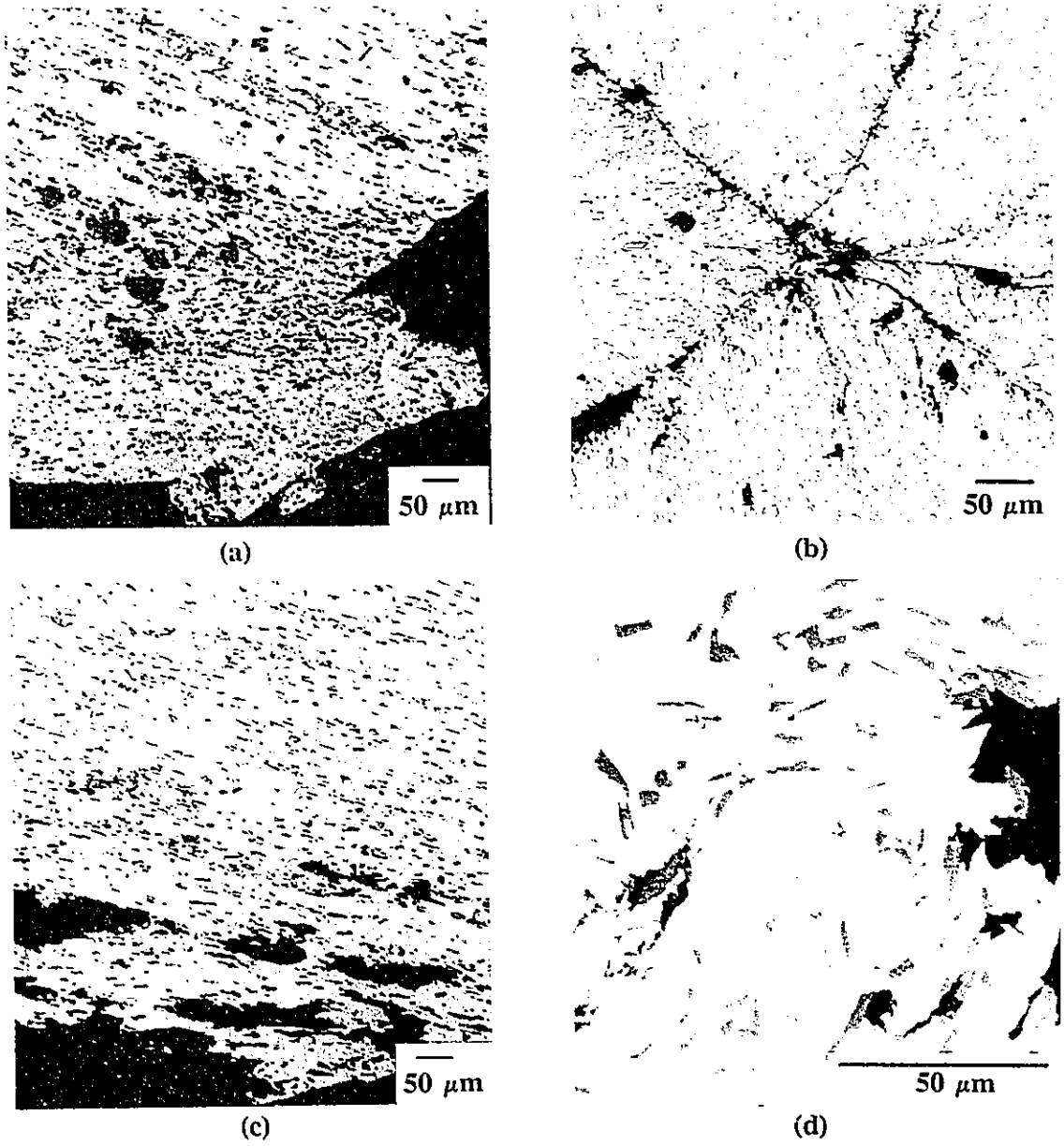

Figure 5.13: Micrographs of unetched sections of A356 Al showing the Si eutectic particles and cracks: (a) longitudinal, 300°C, 1.0 s^{-1}; main fracture surface, decohesion at large particles, aligned fine particles, (b) transverse, 400°C, 1.0 s^{-1}; longitudinal cracks possibly related to a casting defect, (c) longitudinal, 500°C, 1.0 s^{-1}; main and auxilliary fractures, somewhat dimpled appearance and (d) longitudinal, 540°C, 1.0 s^{-1}; Si particles adjacent to fracture path or to decohesions and extended cracks possibly along grain boundary.

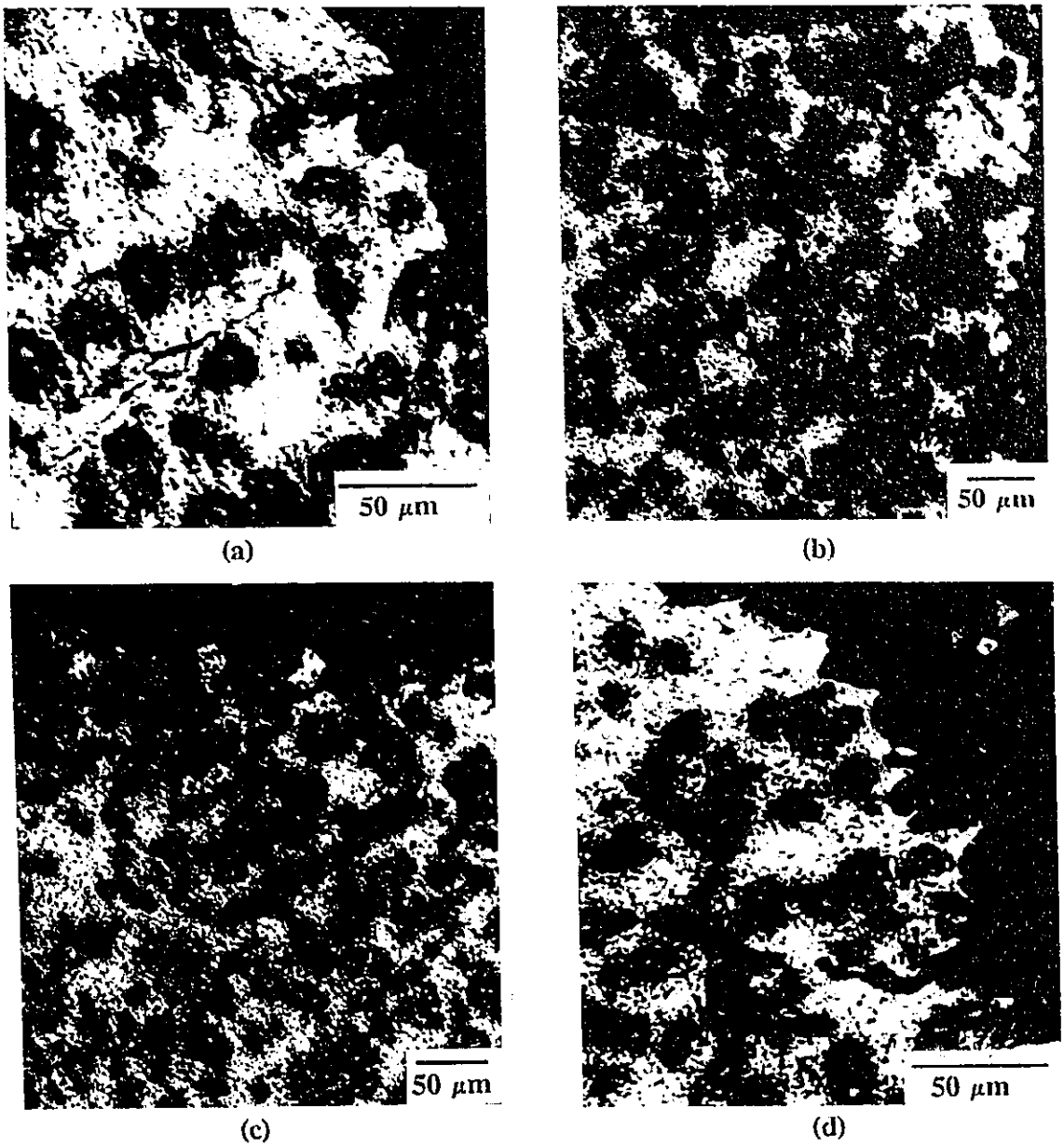

Figure 5.14: Micrographs of unetched longitudinal sections of 15v/o SiC_p/A356 Al showing SiC particles and the cracks: (a) 300°C, 1.0 s^{-1}; main crack irregular and linking up decohesions at SiC particles; cracks in matrix, (b) 400°C, 1.0 s^{-1}; smooth specimen edge showing Al rich dendrites surrounded by Si particles and defined by SiC particles, (c) 400°C, 1.0 s^{-1}; main fracture fairly smooth; bordering on some SiC particles and (d) 500°C, 1.0 s^{-1}; fracture surface strongly dimpled on scale of SiC particles.

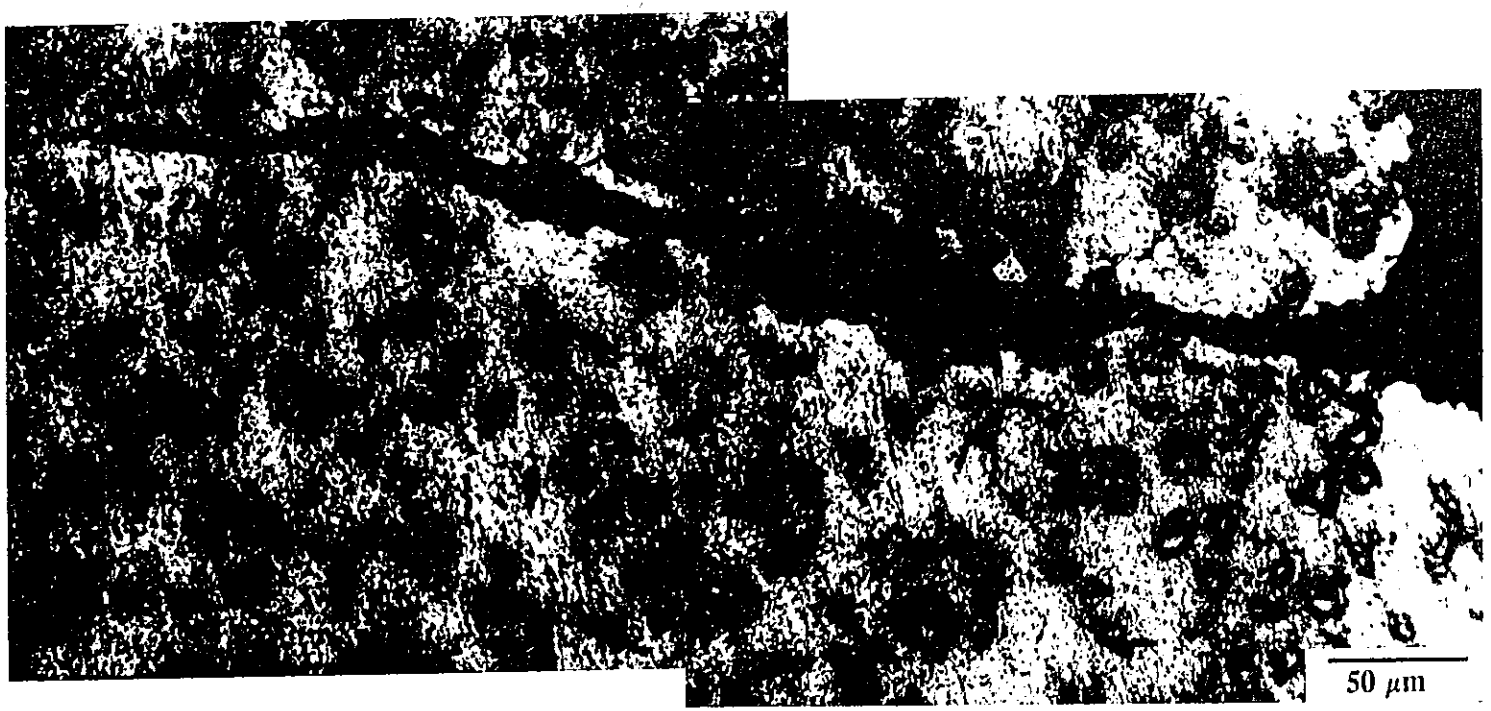

Figure 5.15: Short crack entering from edge of 15v/o SiC_p/A356 Al specimen shows linking up of decohesions at particles by crack progressing through regions of fine Si particles at edge of dendrites.

The microstructures of 6201 Al observed by polarized light, illustrated in Figures 5.16, 5.17 and 5.18 clearly show that the mechanism of softening is DRV and not DRX. In Figure 5.16, at 200°C, 0.1 s^{-1}, three sections are shown: the tangential shows the grains wound around the circumference, the longitudinal section shows elongated grains but the transverse section presents equiaxed grains. At 200°C, the subgrains are too small to be resolved; however, as the temperature rises (0.1 s^{-1}), the subgrains become larger and clearly visible and the grain boundaries become serrated (Figures 5.16b, 5.17). At 600°C, the subgrains are as large as the grain thickness which leads to pinching off where opposite serrations meet. This leads to shortening of the grains and progress toward a more equiaxed structure; because of this, the phenomenon has been named "geometric" DRX although it is entirely by DRV. The effect of rising $\dot{\varepsilon}$ appear in Figure 5.18 for 500°C; the subgrains become smaller and the walls denser. As a consequence of denser substructure at 4.0 s^{-1} and because the quenching was not sufficiently fast, SRX has occurred leading to grains several times the subgrain size.

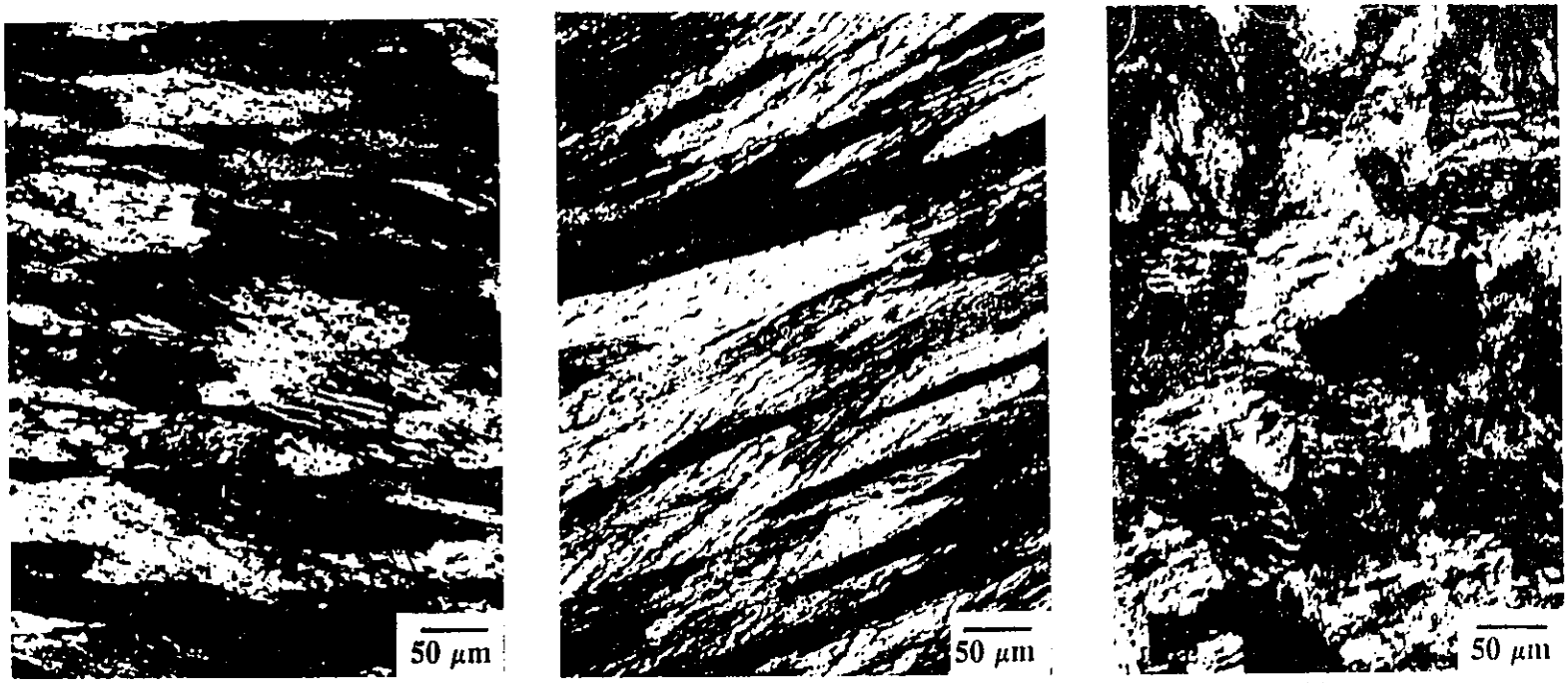

Figure 5.16: Precipitated 6201 Al deformed at 200°C, 0.1 s^{-1}: (a) longitudinal, (b) tangential and (c) transverse sections which indicate that the grains are elongated and wound around the torsion axis as helicoids.

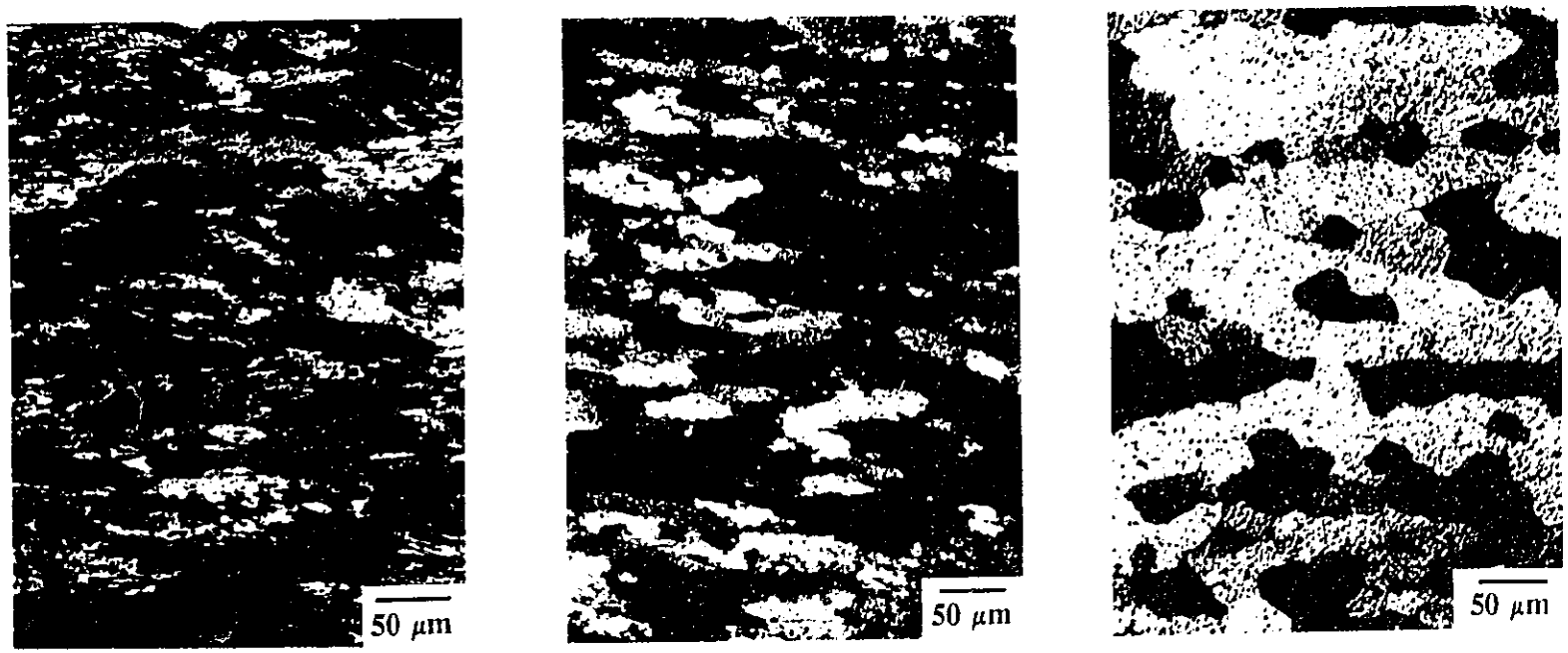

(a) (b) (c)

Figure 5.17: Longitudinal sections close to the surface of 6201 Al: (a) precipitated, 300°C, 0.1 s^{-1}, (b) precipitated, 400°C, 0.1 s^{-1} and (c) solutioned above solvus , 600°C, 0.1 s^{-1}. Subgrains become larger and clearly visible as T rises.

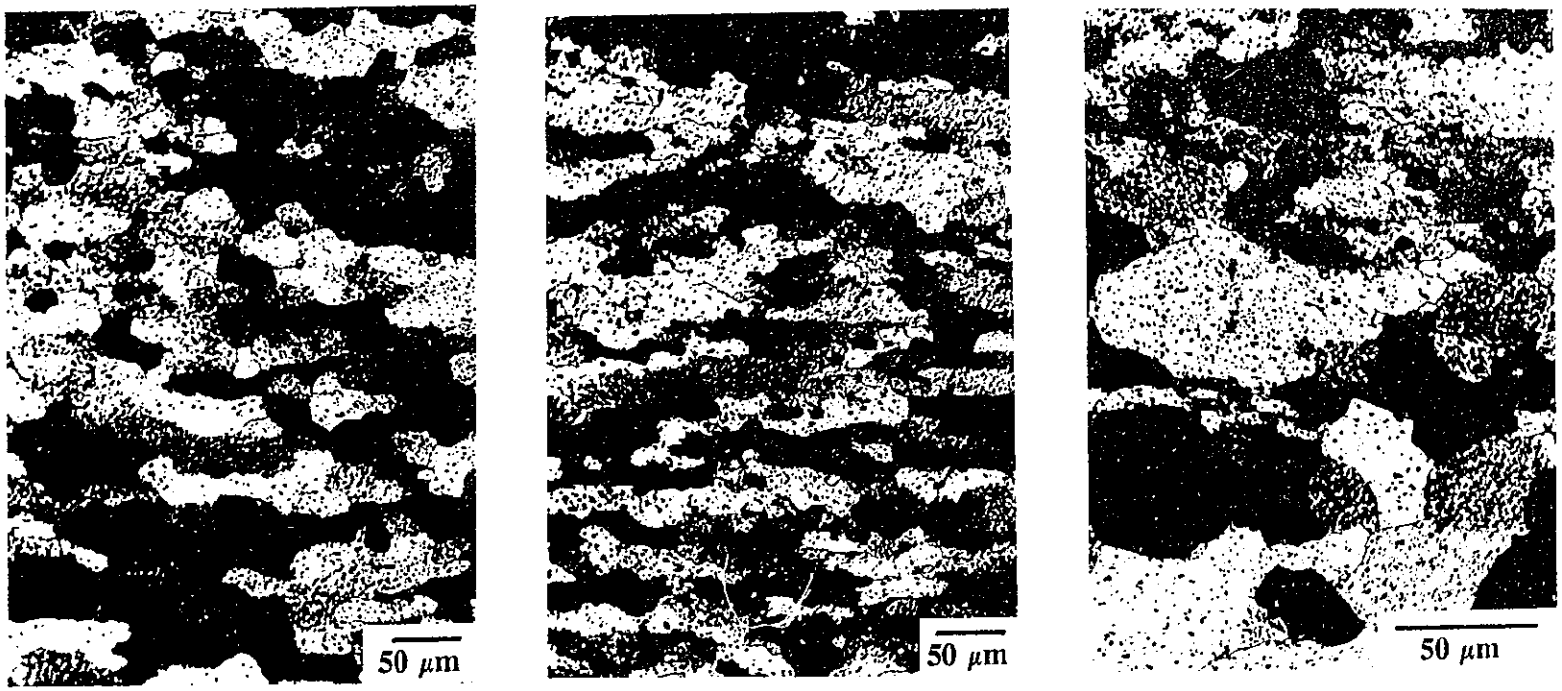

Figure 5.18: Longitudinal sections close to the surface of 6201 Al: (a) precipitated, 500°C, 0.1 s^{-1}, (b) solutioned, 500°C, 1.0 s^{-1} and (c) precipitated, 500°C, 4.0 s^{-1}. The subgrains become smaller as $\dot{\varepsilon}$ increases but at 4.0 s^{-1}, quenching after deformation was insufficiently fast leading to large SRX grains.

6. DISCUSSION

6.1 Continuous Deformation of SiC/Al Composites and Al Matrix Alloys

According to the theory of deformation at high temperatures, aluminum alloys undergo DRV to such extent that they harden monotonically to a steady state regime which is much less than ambient stress levels. Thus, there is no peak in the σ-ε curve except as a result of microstructural changes such as precipitate coarsening or of deformation heating. By contrast, materials which harden more strongly exhibit a peak followed with considerable work softening in the flow curve; this may be indicative of DRX. Although peaks are seen in Figure 5.2 for the composite and the matrix alloy, it is unlikely that DRX is the predominant restoration mechanism but rather DRV [42]. However, microscopic analysis is required to confirm this since there have been reports of DRX occurring in MMCs [37,39]. In the work of Tuler et al. [37], DRX was observed in SiC_p/6061 Al under hot compression. They found at 500°C, 5.0 s^{-1}, a completely recrystallized structure for the 20v/o composite but for the 10 v/o, recrystallization was just beginning in the vicinity of the SiC clusters. They concluded that DRX through particle stimulated nucleation (PSN) occurs at higher temperatures and strain rates. This agrees reasonably well with Humphreys et al. [38] that particle enhanced nucleation is dependent on the volume percentage of particles.

It is apparent from Figure 5.1 that no superplastic behaviour is observed for either 15v/o SiC_p/A356 Al or A356 Al alloy; nor was it observed in 15v/o SiC_p/6061 Al. In order to determine that a material behaves superplastically, m must be greater than 0.3

[7,8,39,53,54]. The value of m for A356 and 6061 Al is in the range (< 0.14) generally observed for other aluminum alloys and is similar for their composites. Pickens et al. [2] determined similar m values for composites and their matrix alloys: at 425°C both 20v/o SiC_p/7090 Al and 7090 Al had equal m values of 0.16 [8,39,54]. Superplastic behaviour is possible if recrystallization has sufficiently refined the grain size of the matrix. Even with fine grains, SiC/Al composites undergo rapid formation of voids which nucleate near or at the SiC particles and which can lead to considerable limitation in ductility [39].

Ductility of the A356 matrix alloy is much lower than 6061 reaching only a maximum ε_f of 5 at 500°C compared to about 20 at 400°C; ε_f of 6061 declined substantially to the point where it was lower than A356 as the temperature approached that for melting (Figure 5.3). The reduced ductility in A356 is likely related to fracture initiation by the Si eutectic particles and to some degree on constraints in the Al due to particles and to the Si solute [42]. The initial rise with temperature for most Al alloys is due to rising DRV and in some cases to precipitate coalescence. The decline at higher temperatures is the result of pore formation at the grain boundaries which enhances fissuring in the presences of rising solute or coarse particles [42,44]. In agreement with the present results, an Al-5Si alloy exhibits rises in tension ductility from 300°C to a maximum at 375°C at 8.0 s^{-1} and from 250 to 325°C at 0.2 s^{-1}. The formation of voids ceased in these ranges somewhat below the present one due to finer Si particles (1-3 μm). In certain materials, the rise in ε_f could result from DRX [59].

The fracture strain of A356 composite is 20 to 30% less than that of its matrix

alloy but is almost double that of the 6061 composite. The composite ductility is diminished due to reduced DRV in the matrix and increased fissure nucleation due to the reinforcements. The addition of SiC to the 6061 Al alloy considerably reduces the ductility because the particles initiate cracking which the matrix strengthened by the Mg and Si solute cannot adequately inhibit. On the other hand, the SiC particles may not increase the effective density of crack initiators in the A356 Al alloy [39]. Microscopic examination has confirmed that the size of the Si particles in the A356 matrix is considerably smaller than in the bulk so that the matrix is likely more ductile than the bulk. Because of the low solute level and the fine particles, the matrix in SiC_p/A356 Al may be more resistant to propagation of the cracks initiated by the SiC particles than the matrix in SiC_p/6061 Al. Microscopic examination by Pickens et al. [2] of 20v/o SiC_p/6061 Al composite produced by P/M revealed voids associated with the SiC particles which could have arisen from clusters of particles or from decohesion. Such void formation at the SiC particles can explain the low ductilities compared to the matrix alloy. The higher ductility that was observed presently in SiC_p/6061 Al compared to reported values [2] arises from less constraint and lower density of nucleation centers due to lower volume percentage of SiC particles. Moreover in the present material, there is an absence of either particle clustering or oxide from powder fabrication [2,8].

The constitutive constants indicate that A356 Al (Q_{HW} = 199 kJ/mol) and 6061 Al (Q_{HW} = 188 kJ/mol) [2] behave similarly to pure Al (Q_{HW} = 150 kJ/mol). Activation energies for alloys increase with rising solute or precipitate content as the operation of DRV becomes more complex. Increases in Q_{HW} from 150 to 265 kJ/mol with rise in Mg

and impurities have been reported [33]. The strengthening of the A356 material is related primarily to the silicon particles and to a lesser degree to the Si dissolved in the Al matrix. The Si particles are sufficiently large and hard in A356 Al that they may cause particle stimulated nucleation (PSN) [39]. It is known that Mg in solution causes significant strengthening to the Al, much more than does Si in solution [42,44].

In previous reports on similar aluminum-matrix composites, both Tuler et al. [37] and Pickens et al. [2] chose to use the power law (Equation 3.2) in their analyses for which plots of ln σ vs 1/T were not linear. They concluded that no single activation energy could be computed because the deformation process was much more complex than in creep. However, using the sinh law (Equation 3.4), there is linear behaviour in the Arrhenius plot (Figure 5.6) such that a single Q_{HW} can be calculated [8,35]. Computation of Q_{HW} showed 263 kJ/mol for A356 composite, higher than 233 for 6061 composite. A high Q_{HW} for the A356 composite can be attributed to the flow stress being similar at 500°C but higher at 300 and 400°C than A356 Al alloy. The SiC particles undoubtedly generate surrounding regions of fine cells which could lead to DRX from PSN [39].

6.2 Continuous Deformation of 6201 Al Alloy

The flow curves (Figure 5.2) rising with increase in strain rate and decline in temperature show the typical dependence on $\dot{\varepsilon}$ and T for materials which dynamically recover [21,33,42,44,46,55]. However, in the solutioned material at 300°C and 1.0 s^{-1}, there was a peak stress of 80 MPa followed by work softening to about 62 MPa. Since

microstructural evidence clearly confirms the absence of dynamic recrystallization, the peak is due partly to the high solute level and partly to dynamic precipitation [42,46]. The softening is due to loss of solute to the particles or the coalescence of particles and thereafter resumption of the normal level of DRV [21,33,42,44,46]. In solutioned 6015 (Figure 3.6), Evangelista et al. [45] observed a much higher peak stress and more rapid softening; since the quantity of Mg_2Si is less than 6201, dynamic precipitation is enhanced either by more rapid heating or by a faster quench previously. A more significant drop at 400°C was also seen by Espedal et al. [21] in Al-0.82Mg-0.64Si. Moreover, Evangelista et al. [45] observed that at lower temperatures the fracture strain was much smaller than the present which is consistent with enhanced cracking at the high peak stress.

As T rises, the ductility of 6201 rises rapidly so that at high T it exceeds 20, the strain limit of the rotary potentiometer (Figure 5.3). Such high fracture strains are consistent with the results of Evangelista et al. [45] At 400 and 500°C, the fracture strain reaches the remarkable level of 150 which is equal to that of pure Al and of Al-2Mg; the solute in 6015 alloy is less than 2%. The ductility arises from intensive DRV which permits grain deformation to accommodate the non-uniform sliding of grain boundaries (GB), thus eliminating the stress concentrations which initiate cracks. The ductility is greater at higher $\dot{\varepsilon}$ because the proportion of ε due to GB sliding is reduced and thus the incidence of GB fissure formation [42].

In the sinh analysis for the precipitated material (Figure 5.7), the constant temperature lines are parallel although at 200°C and 300°C there appear to be some

discrepancies. This could arise because at 200°C there would be more precipitation of Mg_2Si particles from the solute remaining after overaging the specimen, resulting in higher strength. At 300°C and 4.0 s^{-1}, the strength is about double that at 1.0 s^{-1} since the precipitates formed during storage and manipulation had no time during holding or preheating to redissolve at higher $\dot{\varepsilon}$ during testing. Such irregular behaviour at lower test temperatures may be the result of precipitation below the overaging T causing a significant increase in strength [21,42].

The value of the stress exponent n for the precipitated material was calculated to be 3.7 and 2.9 for α = 0.04 and 0.06 MPa^{-1} respectively which is much lower than 4.8 (α = 0.052 MPa^{-1}) for high purity aluminum [49]. This could be the result of the large Mg_2Si precipitates altering the restoration mechanism as has been observed with dispersoids [33,56]. For comparison purposes, partial data was taken from the 6015 Al alloy [45] (flow stresses at 300, 400 and 500°C at 0.042, 0.1 and 0.8 s^{-1}). The strength of 6201 is lower than 6015 at the peak (Figure 5.7) but is comparable to its steady state flow stress (Figure 3.6). The values of n are quite similar for both alloys (2.9 and 2.4 for 6201 and 6015 respectively) for α = 0.06 MPa^{-1}. Since n declines at a much lower rate as α increases (Figure 5.9), it seems reasonable to use values of α between 0.04 and 0.06 MPa^{-1}. Because of the linear increase in s (Figure 5.10), Q_{HW} rises from 165 to 192 kJ/mol with rising α. Similar variation of n, s and Q_{HW} with α has been observed in other alloys [57]. With the approach explained under techniques, the Arrhenius plot for 6015 Al was constructed with constant strain rate lines having a single slope s which is substantially higher than for 6201 Al so that Q_{HW} varies from 285 to 296 kJ/mol for the

range α = 0.04 to 0.06 MPa^{-1} (Table 5.2). These values are much higher than the high T value (170 kJ/mol) published but less than low T (460 kJ/mol) [45]. Evangelista et al. [45] linked the values to two different mechanisms with DRV being inhibited between 300 and 375°C by dynamic precipitation [33,44]. The high T value was thus similar to that for Al in which Q_{HW} = 140-165 kJ/mol is comparable to the activation energy for self-diffusion, which suggests that the rate controlling mechanism is dislocation climb. The present high activation energy is consistent with that of alloys generally in so far a solute or precipitate content make the operation of DRV more complex [33,42,44,55]. Increases in activation energy from 150 to 265 kJ/mol with rise in Mg and impurities (present as particles) have been reported in a review by McQueen and Conrod [33]. In contrast, in pure Al-Mg alloys where deformation was dependent on diffusion of Mg, the creep activation energy Q_c equalled 150 kJ/mol [33,44,58]. Consistent with such simple solute effects, Espedal et al. [21] found that Q_{HW} for dissolved Al-Mg_2Si to be 155 kJ/mol.

6.3 Industrial Applications

About 80% of total metal and alloy production involves hot working. Difficulties such as insufficient ductility at low temperatures or high strain rates have been solved by empirical techniques mainly through the reduction of certain impurities and the specification of working limits. A major goal has been to determine a functional relationship between the parameters so that the flow stress and forming forces can be predicted for any condition which often involves a complex pattern of temperature, strain

rate and strain. Such information on new materials is extremely valuable in assuring that the processing operation will not exceed the capacity of the equipment. In materials developed for high strength, hot ductility is often a problem so it is necessary to know how it varies with temperature and strain rate.

DURALCAN® aluminum composites combine the light weight and strength attributes of aluminum with the stiffness and wear resistance of ceramic to create a material offering unique properties to various engineering communities (automotive, industrial, commercial and recreational). These composites offer low thermal expansion and excellent thermal conductivity. A $30-million plant was built in 1990 in Jonquière, Québec to manufacture 25-million pounds of this material each year. Generally alloys made with ceramic powder are difficult to hot work because the high flow stress leads to extremely high extrusion breakout pressures. In addition, they often have limited hot ductility which can manifest itself as surface break-up during extrusion or cracking during forging or rolling. Studies to improve hot working behaviour of metal matrix composites are difficult to perform for several reasons. Experimental material is extremely expensive and consequently it is often not practical to hot work many billets over a wide range of conditions to optimize hot working parameters. Fortunately, such hot working studies can be performed on hot working simulators using relatively small test specimens such as the hot torsion machine. Hot torsion testing has been successfully used to simulate extrusion and predict the maximum allowable extrusion ratio and also to generate microstructures that correspond to those produced during extrusion. In addition, hot torsion testing has been used to optimize hot rolling parameters for

commercial aluminum alloys. Utilization of torsion testing with its wide range of capabilities could uncover formability schedules which might not be found through less flexible testing techniques.

7. CONCLUSIONS

- The flow stresses decrease uniformly with increasing deformation temperature for both the composites and their matrix alloys. The flow stress for 15v/o SiC_p/A356 Al is generally higher than A356 but the difference is quite small at higher temperatures. In comparison to the 6061 material, A356 material is about 5 to 20% stronger.
- The ductility for 15v/o SiC_p/A356 Al is double that of the 15v/o SiC_p/6061 Al but is 20 to 30% lower than the matrix alloy as the temperature rises. Apparently, the A356 matrix is better able to diminish crack formation and propagation than does the 6061 matrix. The A356 matrix is probably much more ductile than its bulk alloy because of the refinement of the eutectic Si; for the 6061 matrix, there is likely to be no evidence for such improvement and possible diminishment because of increased effects of precipitation due to the high dislocation densities.
- The plots of log $\dot{\varepsilon}$ versus log sinh $\alpha\sigma$ are linear over the range of strain rates tested with slopes fairly independent of temperature. The n value for 15v/o SiC_p/A356 Al and A356 were calculated to be 3.2 and 2.8 respectively. The Arrhenius plots were also linear showing that the activation energies for the composites studied were higher than their matrix alloys. The A356 bulk alloy had similar Q_{HW} to that for pure aluminum.
- The strain rate and temperature dependencies of the strength for 6201 Al in the precipitated condition is suitably represented by the sinh and Arrhenius functions with an activation energy higher than pure Al. The optimum value of the stress multiplier was

determined to be in the range of 0.04 to 0.06 MPa^{-1} where n and Q_{HW} were 3.7, 165 kJ/mol and 2.9, 192 kJ/mol respectively.

- In comparison to 6015, the peak stresses and the values of n and Q_{HW} were lower for 6201; however the steady state flow stresses were similar. The solutioned material exhibited higher strength than precipitated material due to either dynamic precipitation or higher solute levels but at higher temperatures the differences disappeared.

REFERENCES

[1] J. L. Cook and W. R. Mohn, "Whisker-Reinforced MMCs", Engineered Materials Handbook, vol. 1, Composites, ASM International, Metals Park, Ohio, 1987, pp 896-902.

[2] J. R. Pickens, T. J. Langan, R. O. England and M. Liebson, "A Study of the Hot Working Behaviour of SiC-Al Alloy Composites and Their Matrix Alloys by Hot Torsion Testing", Metallurgical Transactions A, vol. 18A, February 1987, pp 303-312.

[3] B. J. Maclean and M. S. Misra, "SiC-Reinforced Aluminum Alloys for Aerospace Applications", Mechanical Behaviour of Metal Matrix Composites, The Metallurgical Society of AIME, Warrendale, PA, 1983, pp 301-320.

[4] M. Hunt, "Making Metal Matrix Composites Stronger and Tougher", Materials Engineering, July 1989, pp 44-46.

[5] M. Hunt, "Aluminum Composites Come of Age", Materials Engineering, January 1989, pp 37-40.

[6] W. C. Harrigan Jr., "Discontinuous Silicon Fiber MMCs", Engineered Materials Handbook, vol. 1, Composites, ASM International, Metals Park, Ohio, 1987, pp 889-895.

[7] M. W. Mahoney and A. K. Ghosh, "Superplasticity in High Strength Powder Aluminum Alloy With and Without SiC Reinforcement", Metallurgical Transactions A, vol. 18A, 1987, pp 653-661.

[8] H. J. McQueen and P. Sakaris, "Mechanical Shaping of Metal Matrix Composites", Composite Structures and Materials, S. V. Hoa and R. Gauvin eds., Elsevier Applied Science, London, 1992, pp 297-306.

[9] D. J. Lloyd, "Particulate Reinforced Composites Produced by Molten Metal Mixing", High Performance Composites for the 1990's, TMS, 1991, pp 33-45.

[10] D. Charles, "Metal Matrix Composites - Ready for Take Off", Metals and Materials, February 1990, pp 78-82.

[11] D. J. Lloyd, Metal Matrix Composites - An Overview", Advanced Structural Materials, Pergamon Press, Oxford, 1989, pp 1-21.

[12] N. Gane, "Developments in Powder Metallurgy", Materials Forum, vol. 13, 1989, pp 81-100.

[13] M. Hunt, "Automotive MMCs: Better and Cheaper", Materials Engineering, October 1989, pp 45-47.

[14] D. J. Lloyd, "The Solidification Microstructure of Particulate Reinforced Aluminum/SiC Composites", Composites Science and Technology, vol. 25, 1989, pp 159-179.

[15] W. C. Harrigan Jr., G. Gaebler, E. G. Davis and E. J. Levin, "The Effects of Hot Rolling on the Mechanical Properties of SiC-Reinforced 6061 Aluminum", Mechanical Behaviour of Metal Matrix Composites, The Metallurgical Society of AIME, Warrendale, PA, 1983, pp 163-180.

[16] R. J. Arsenault, "The Strengthening Mechanisms in Discontinuous SiC/Al Composites", Mechanical and Physical Behaviour of Metallic and Ceramic

Composites, 9th RISO International Symposium on Metallurgy and Materials Science, 1988, pp 333-338.

[17] M. A. Bayoumi, H. Ribes and M. Suery, "Aging Characteristics of SiC-Particle Reinforced Al-SiC Alloys", **Mechanical and Physical Behaviour of Metallic and Ceramic Composites**, 9th RISO International Symposium on Metallurgy and Materials Science, 1988, pp 291-296.

[18] R. DaSilva, D. Caldemaison and T. Bretheau, "Microstructural Behaviour of Al/SiC Composite Materials Subjected to Plastic Deformation: An In-Situ Study", **Mechanical and Physical Behaviour of Metallic and Ceramic Composites**, 9th RISO International Symposium on Metallurgy and Materials Science, 1988, pp 333-338.

[19] K. R. Van Horn, **Aluminum: Physical Metallurgy and Phase Diagrams**, ASM International, Metals Park, Ohio, 1967, pp 123-124.

[20] Properties & Selection of Non-Ferrous Alloys, **ASM Metals Handbook**, 10th Edition, ASM International, Metals Park, Ohio, 1990, pp 29-122.

[21] A. Espedal, H. Gjestland, N. Ryum and H. J. McQueen, "Hot Deformation of Al-Mg-Si Alloys", **Scandinavian Journal of Metals**, vol. 18, 1989, pp 131-136.

[22] P. Sakaris, H. J. McQueen, Q. Meng, Y. Cui and B. Li, "High Temperature Deformation of 6201 Al Alloy In Comparison With 6015 Al Alloy", **Advances in Production and Fabrication of Light Metals**, CIM, Pergamon Press, Oxford, 1992, (in press).

[23] E. A. Starke, "Aluminum Alloys for the 70's", Material Science and Engineering, vol. 29, 1977, pp 99-110.

[24] E. H. Chia, "High Speed Processing of Al-Mg-Si Alloys for Transmission Cables", Company Report, Southwire Company, Carrolton, GA.

[25] K. F. Kobayashi and L. M. Hogan, "The Crystal Growth of Silicon in Al-Si Alloys", Journal of Material Science, vol. 20, 1985, pp 119-125.

[26] L. M. Hogan and D. C. Jenkinson, "The Modification of Aluminum-Silicon Alloys with Strontium", Journal of Crystal Growth, vol. 28, 1975, pp 171-178.

[27] K. Alker and V. Hielscher, "Experiences with Permanent Modifications of an Aluminum-Silicon Casting Alloy", Aluminium, vol. 48, 1972, pp 362-370.

[28] H. J. McQueen, "Deformation Mechanisms in Hot Working", Journal of Metals, vol. 18, no. 4, April 1968, pp 31-38.

[29] H. J. McQueen, W. A. Wong and J. J. Jonas, "Deformation of Aluminum at High Temperature and Strain Rates", Canadian Journal of Physics, vol. 45, 1967, pp 1225-1234.

[30] H. J. McQueen and W. J. M. Tegart, "The Deformation of Metals at High Temperatures", Scientific American, vol. 232, no. 4, April 1975, pp 116-124.

[31] H. J. McQueen, "Dynamic Recovery and Its Relation to Other Restoration Mechanisms", Metallurgia I Odlewnictwo, vol. 5, no. 3, 1979, pp 421-451.

[32] H. J. McQueen, E. Evangelista, M. E. Kassner, "The Classification and Determination of Restoration Mechanisms in Hot Working of Al Alloys", Zeitschrift fur Metallkunde, vol. 82, no. 5, 1991, pp 336-345.

[33] H. J. McQueen and K. Conrod, "Recovery and Recrystallization in the Hot Working of Al Alloys", Microstructural Control in Al Alloy Processing, TMS-AIME, Warrendale, PA, 1986, pp 197-220.

[34] P. Sakaris and H. J. McQueen, "Comparative Hot Workability of SiC_p/A356 and SiC_p/6061 Al Composites and Their Matrices", Metal Matrix Composites - Fabrication and Technology, CIM, Pergamon Press, Oxford, 1992, (in press).

[35] P. Sakaris and H. J. McQueen, "Hot Workability of SiC_p/6061 Al Composites", Aluminum Alloys: Their Physical and Mechanical Properties, ICAA3, vol. 1, Trondheim, 1992, pp 554-559.

[36] Z. Xiong, L. Geng and C. K. Yao, "Investigation of High-Temperature Deformation Behaviour of a SiC Whisker Reinforced 6061 Aluminum Composite", Composites Science and Technology, vol. 39, 1990, pp 117-125.

[37] F. R. Tuler, J. T. Beals, C. Demetry and D. Zhao, "Deformation Mechanism Mapping of SiC/Al Metal Matrix Composites", Cast Reinforced Metal Composites, ASM International, Chicago, IL, 1988, pp 321-325.

[38] F. J. Humphreys, "Deformation and Annealing Mechanisms in Discontinuously Reinforced Metal-Matrix Composites", Mechanical and Physical Behaviour of Metallic and Ceramic Composites, 9th RISO International Symposium on Metallurgy and Materials Science, 1988, pp 51-74.

[39] F. J. Humphreys, W. S. Miller, and M. R. Djazeb, "Microstructural Development During Thermomechanical Processing of Particulate Metal-Matrix Composites", Material Science and Technology, vol. 6, 1990, pp 1157-1166.

[40] K. Kannikeswaran and R. Y. Lin, "Trace Elements Effects on Al-SiC Interfaces", Journal of Metals, 1987, pp 17-19.

[41] T. G. Nieh, C. A. Henshall and J. Wadsworth, Scripta Metallurgica, vol. 18, 1984, pp 1405-1412.

[42] H. J. McQueen, "Effect of Solutes and Precipitates on Hot Working Behaviour of Al Alloys", Hot Deformation of Aluminum Alloys, TMS-AIME, Warrendale, PA, 1991, pp 105-120.

[43] P. Sakaris and H. J. McQueen, "Hot Workability of 6201 Al Alloy", Aluminum Alloys: Their Physical and Mechanical Properties, ICAA3, vol. 2, Trondheim, 1992, pp 276-281.

[44] H. J. McQueen, "Micromechanisms of Dynamic Softening in Aluminum Alloys During Hot Working", Hot Deformation of Aluminum Alloys, TMS-AIME, Warrendale, PA, 1991, pp 31-54.

[45] E. Evangelista, A. Forcellesee, F. Gabrielli and P. Mengucci, "Hot Workability of Some Heat Treatable Aluminum Alloys, Hot Deformation of Aluminum Alloys, TMS-AIME, Warrendale, PA, 1991, pp 121-139.

[46] M. M. Farag and C. M. Sellars, "Analysis of Double Maximum Flow Patterns in Axisymmetric Extrusion of H30 Aluminum Alloy", Metals Technology, vol. 2, 1975, pp 220-228.

[47] S. Fulop, K. Cadien, M. J. Luton, H. J. McQueen, "A Servo-Controlled Hydraulic Torsion Machine for Hot Working Studies", Journal of Testing and Evaluation, vol. 5, 1977, pp 419-426.

[48] Operators Manual Material Testing System No. 910.30, MTS System Corporation, Minneapolis, MN, 1972.

[49] K. Conrod and H. J. McQueen, "Hot Working Characteristics of Al-0.65%Fe and Al-0.5%Fe-0.5%Co Conductor Alloys", Aluminum Alloys: Physical and Mechanical Properties, Wharley, UK, 1986, pp 435-447.

[50] F. Weill and G. Wyon, "Superplastic Behaviour of Fine Grained Aluminum Alloys Whose Grain Boundaries Have Been Enriched by Gallium", Strength of Metals and Alloys, ICSMA 5, vol. 1, 1979, pp 387-396.

[51] B. Verlinden, P. Wouters, H. J. McQueen, E. Aernoudt, L. Delaey and S. Cauwenberg, "Effect of Different Homogenization Treatments on the Hot Workability of Aluminum Alloy AA2024", Material Science and Engineering, A123, 1990, pp 229-237.

[52] T. Sheppard, S. J. Patterson and M. G. Tutcher, "On the Development of Structure During the Extrusion Process", Microstructural Control in Al Alloy Processing, TMS-AIME, Warrendale, PA, 1986, pp 123-154.

[53] C. A. Stanford-Beale and T. W. Clyne, "Extrusion and High Temperature Deformation of Fibre-Reinforced Aluminum", Composites Science and Technology, vol. 35, 1989, pp 121-157.

[54] J. Pilling, "Superplasticity in Aluminum Base Metal Matrix Composites", Scripta Metallurgica, vol. 23, 1989, pp 1375-1380.

[55] H. J. McQueen and N. Ryum, "Hot Working and Subsequent Static Recrystallization of Al and Al-Mg Alloys", Scandinavian Journal of Metals,

vol. 14, 1985, pp 183-194.

[56] H. J. McQueen, E. Evangelista, J. Bowles and G. Crawford, "Hot Deformation and Dynamic Recrystallization of Al-5Mg-0.8Mn", Metal Science, vol. 18, 1984, pp 395-402.

[57] H. J. McQueen and P. Sakaris, "Influence of Stress Multiplier in Sinh Equation on Constitutive Constants for Al Alloys with Mg and Dispersoids", Aluminum Alloys: Their Physical and Mechanical Properties, ICAA3, vol. 2, Trondheim, 1992, pp 179-184.

[58] H. J. McQueen and M. E. Kassner, "Behaviour of Al-Mg Alloys in Hot Working and Superplasticity", Superplasticity in Aerospace II, TMS-AIME, 1991, pp 189-206.

[59] K. P. Rao, S. M. Doraivelu, H. Md. Roshan and Y. V. R. K. Prasad, "Deformation Processing of an Aluminum Alloy Containing Particles: Studies on Al-5Pct Si Alloy 4043", Metallurgical Transactions A, vol. 14A, 1983, pp 1671-1679.

[60] P. Mayer, "Effect of Strain Rate on Mechanical Properties of Aluminu-Silicon Carbide Composites", Metal Matrix Composites - Processing, Microstructure and Properties, 12th Riso International Symposium on Material Science, 1991, pp 515-522.

APPENDIX A

BASIC Program (SIMULB) for MTS Torsion Unit

```
10 REM            SIMULATION OF ROLLING
45 REM        MAY 1986 VERSION BY FRANCISCO BORATTO
90 DIM C1(17),D1(17),Q9(17)
100 DIM A(110,17),B(110,17),A1(110),B1(110)
120 DIM E(17),T(17),D(17),G(90),C2(17),D2(17),T2(17)
130 DIM CNTR(3)
140 PRINT "DO YOU WANT TO RUN A TEST (RU) OR RECALL DATA (RE) ";
145 INPUT A$
160 IF A$="RE" THEN 2600
165 IF A$="RU" THEN 170
167 GO TO 130
170 CNTR(3)
175 PRINT "ENTER SPECIMEN INFORMATION :"
176 PRINT
180 PRINT "SAMPLE#";\INPUT C$
200 PRINT "RADIUS (MM) ";\INPUT R
220 PRINT "GAUGE LENGTH (MM) ";\INPUT L
240 PRINT "MAX TORQUE (IN.LB) ";\INPUT M
260 PRINT "MAX TWIST (TURNS) ";\INPUT M2
300 OPEN "SCH.DAT" FOR INPUT AS FILE #1
310 INPUT #1:N
320 FOR I=0 TO N
330 INPUT #1:T2(I),T(I)
335 INPUT #1:E(I),D(I)
340 NEXT I
350 CLOSE #1
360 OPEN "RATE.DAT" FOR INPUT AS FILE #1
370 FOR J=0 TO N
380 INPUT #1:Q9(J)
390 NEXT J
400 CLOSE #1
620 CNTR(3)
630 MSW1(1)\FG1(0)
640 PRINT "CHECK THE FOLLOWING :"
642 PRINT
660 PRINT "DC ERROR IS 0"
680 PRINT "REMOTE/LOCAL SWITCH TO REMOTE"
700 PRINT "SPAN 1 IS AT ZERO"
720 PRINT "STROKE CONTROL"\PRINT
740 PRINT "PRESS RETURN TO CONTINUE"
742 PRINT
744 INPUT F$\PRINT
760 PRINT "TURN OFF THE HYDRAULICS"\PRINT
780 PRINT "SET 'SPAN 1' TO 10"
```

```
800 PRINT
802 PRINT "PRESS RETURN TO CONTINUE"
806 PRINT INPUT F$\PRINT
840 REM                 DUMP CHECK
880 EDMP
900 SDMP(1,A)\IF A=0 THEN 980
920 PRINT "DUMP CARD PROBLEM. UNABLE TO FINISH TEST."
940 PRINT \PRINT "TURN OFF THE HYDRAULICS."
960 STOP
980 DACQ(0,K9,1,0)
1000 FOR I=K9 TO 0 STEP -1
1020 FG1(I)
1040 NEXT I
1060 GOSUB 2960
1080 PRINT "IS TEST READY (Y/N)"; INPUT D$
1100 IF D$<>"Y" THEN 1080
1105 PRINT "ZERO LOAD";\INPUT D1$
1110 PRINT "PRESS RETURN TO START TEST"\INPUT D1$
1112 PRINT "TEST RUNNING"
1115 GOSUB 4000
1120 MSW1(1)\CNTR(3)
1140 Z2=5.00000E-03*L*SQR(3)/2/PI/R*2047/M2
1160 FOR J=1 TO N
1180 PRINT J"TH PASS RUN"
1200 X(1)=20.47/E(J)-E(J-1)*D(J)
1220 Y=E(J)*L/2/PI/R*2048/M2*SQR(3)
1240 X(2)=Y\X(4)=Y
1260 X(3)=204.7*D(J)\X(5)=2047
1280 X(6)=Y-Z2
1300 GOSUB 3200
1320 DACQ(3,A1,0,V)\DACQ(3,B1,1,V)
1340 X=6\FG1(X,1,5,0)
1360 STAR
1380 BUF1(Z)
1400 IF Z>-1 THEN 1380
1420 QUIT
1440 PRINT J"TH PASS FINISH"
1460 X(1)=2200/T(J)
1480 X(2)=X(6)
1500 X=2
1520 V1=100*T(J)
1540 DACQ(3,C1,0,V1)\DACQ(3,D1,1,V1)
1560 FG1(X,1,7,7)
1580 STAR
1600 BUF1(Z)
1620 IF Z>-1 THEN 1600
1640 QUIT
1660 FOR I=1 TO 100
1680 A(I,J)=-A1(I)\B(I,J)=B1(I)
1700 A1(I)=0\B1(I)=0\NEXT I
1720 FOR I=101 TO 110
```

```
1740 I1=I-100\A(I,J)=-C1(I1)\B(I,J)=D1(I1)\C1(I1)=0\D1(I1)=0\NEXT I
1760 A(0,J)=A1\IF A1<100 THEN 1780\A(0,J)=100
1780 NEXT J
1785 PRINT "TURN OFF THE HYDRAULICS"
1800 PRINT "DO YOU WANT TO PRIN THE DATA (Y/N) ";\INPUT W$
1820 IF W$<>"Y" THEN 1920
1840 CNTR(3)
1860 PRINT "SAMPLE#: "C$
1880 PRINT "EQU STRESS", "EQU STRAIN", "TIME", "PASS"
1900 PRINT "(MNT/M^2)",,"(SEC.)"
1920 C2(0)=0
1940 FOR J=1 TO N
1960 C2(J)=0
1980 GOSUB 3200
2000 FOR I=1 TO A(0,J)
2020 C2(0)=C2(0)+V/1000
2040 C2(J)=C2(J)+V/1000
2060 IF W$<>"Y" THEN 2100\GOSUB 3260
2080 PRINT Y,X,C2(0),I,J
2100 NEXT I
2120 FOR I=101 TO 110
2140 C2(0)=C2(0)+T(J)/10
2160 IF W$<>"Y" THEN 2200\GOSUB 3260
2180 PRINT Y,X,C2(0),I,J
2200 NEXT I
2220 NEXT J
2240 PRINT "DO YOU WANT TO KEEP THIS EXP (Y/N)"\INPUT U$
2260 IF U$<>"Y" THEN 2940
2280 FOR J=1 TO N
2300 G(J)=E(J)*100\G(J+17)=T(J)*100\G(J+34)=D(J)*100
2320 G(J)=INT(G(J)+.51)\G(J+17)=INT(G(J+17)+.51)\G(J+34)=INT(G(J+34)+.51)
2340 G(J+51)=A(0,J)\G(68+J))=T2(J)
2360 NEXT J
2380 G(86)=R*100\G(87)=L*100\G(88)=M\G(89)=M2\G(90)=N
2400 OPEN "DX1:"&C$ FOR OUTPUT AS FILE #1
2420 AOUT (G,1,0,E1)
2440 FOR J=1 TO N
2460 Q=(J-1)*2+1\P=Q+1
2480 FOR I=1 TO 110
2500 A1(I)=A(I,J)\B1(I)=B(I,J)
2520 NEXT I\A1=0\B1=0
2540 AOUT(A1,1,Q,E2)\AOUT(B1,1,P,E3)
2560 NEXT J
2580 CLOSE #1
2590 STOP
2600 CNTR(3)
2605 PRINT "RECALLING DATA"
2607 PRINT
2640 PRINT "SAMPLE #?";\INPUT C$
2660 OPEN "DX1:"&C$ FOR INPUT AS FILE #1
2680 AINP(G,1,0,E1)
```

```
2700 FOR J=1 TO G(90)
2720 Q=(J-1)*2+1\P=Q+1
2740 AINP(A1,1,Q,E2)\AINP(B1,1,P,E3)
2760 FOR I=1 TO 110
2780 A(I,J)=A1(I)\B(I,J)=B1(I)
2800 NEXT I
2820 E(J)=G(J)/100\T(J)=G(J+17)/100\D(J)=G(J+34)/100
2840 A(0,J)=G(J+51)\T2(J)=G(J+68)
2860 NEXT J
2880 CLOSE #1
2900 R=G(86)/100\L=G(87)/100\M=G(88)\M2=G(89)\N=G(90)
2920 E(0)=0\T(0)=0\D(0)=0\GOSUB 2960\GO TO 1800
2940 PRINT \PRINT "TURN OFF THE HYDRAULICS"\PRINT "------------------------"
2942 STOP
2960 CNTR(3)
2980 PRINT TAB(20)"SIMULATION OF ROLLING"
2985 PRINT TAB(20)"---------------------"
3000 PRINT " "\PRINT "SAMPLE#: "C$
3020 PRINT \PRINT "TORQUE RANGE: "M;" (IN.LB)";
3025 PRINT TAB(34)"ROTATION RANGE: ";M2;" (TURNS)"
3040 PRINT "SAMPLE RADIUS: ";R;" (MM)";
3045 PRINT TAB(34)"SAMPLE LENGTH: ";L;" (MM)"
3060 PRINT "AUSTEN. TEMP.: ";T2(0);" (C)";
3065 PRINT TAB(34)"SOAKING TIME:10 MIN"
3080 PRINT " "\PRINT "THE CONDITION OF TEST :"
3100 PRINT "PASS","STRAIN","TIME","STRAIN RATE","TEMP."
3105 PRINT "----","------","----","----------","-----"
3120 FOR J=0 TO N
3140 PRINT J,E(J),T(J),D(J),T2(J)
3160 NEXT J
3165 PRINT
3166 PRINT "DO YOU WANT TO CORRECT STRAIN RATES (Y/N) ";\INPUT Q$
3167 IF Q$="Y" THEN GOSUB 7000
3168 IF Q$="Y" THEN 2960
3170 PRINT "DO YOU WANT TO MODIFY THIS SCHEDULE (Y/N) ";\INPUT Q$
3172 IF Q$="Y" THEN GOSUB 6000\GOTO 2960
3174 PRINT "DO YOU WANT TO SAVE THIS SCHEDULE (Y/N) ";\INPUT Q$
3175 IF Q$="Y" THEN GOSUB 5000
3180 RETURN
3200 V=INT(10*((E(J)-E(J-1)/D(J)+.018.1/D(J)))
3220 IF V<1 THEN V=1
3240 RETURN
3260 X=B(I,J)/2047*M2*2*P1*R/L/SQR(3)
3280 Y=A(I/J)/2047*M*101.967/R^3
3290 REM
3300 RETURN
4000 DACQ(0,Q5,1,0)
4010 Q6(1)=52
4020 Q6(2)=Q5
4030 Q6=2
4040 FG1(Q6,1,7,7)
```

```
4050 STAR
4060 BUF1(Z)
4070 IF Z>-1 THEN 4060
4080 QUIT
4090 ETURN
5000 REM SUBROUTINE TO FILE SCHEDULE IN SCH.DAT
5010 OPEN "SCH.DAT" FOR OUTPUT AS FILE #1
5020 PRINT #1:N
5030 FOR I=0 TO N
5040 PRINT #1:T2(I),",",T(I)
5045 PRINT #1:E(I),",",D(I)
5050 NEXT I
5060 CLOSE #1
5080 RETURN
6000 CNTR(3)
6060 PRINT "HOW MANY INTERRUPTIONS ";\INPUT N
6070 PRINT \PRINT "ENTER THE TEMPERATURES :"
6080 FOR I=0 TO N
6090 PRINT "T2(";I;")";\INPUT T2(I)
6100 NEXT I
6110 PRINT
6112 CNTR(3)
6115 PRINT "ENTER THE REST TIME AFTER PASS :"
6120 FOR I=0 TO N
6130 PRINT "T(";I;")";\INPUT T(I)
6140 NEXT I
6150 PRINT
6155 CNTR(3)
6160 PRINT "ENTER THE CUMULATIVE STRAIN VALUES :"
6170 FOR I=0 TO N
6180 PRINT "E(";I;")";\INPUT E(I)
6190 NEXT I
6195 PRINT
6197 CNTR(3)
6200 PRINT "ENTER THE STRAIN RATES :"
6210 FOR I=0 TO N
6220 PRINT "D(";I;")"\INPUT D(I)
6230 NEXT I
6240 RETURN
7000 REM
7010 FOR I=1 TO N
7020 D(I)=D(I)*Q9(I)
7030 NEXT I
7040 RETURN
```

APPENDIX B

Flow Chart of BASIC Program (SIMULB)

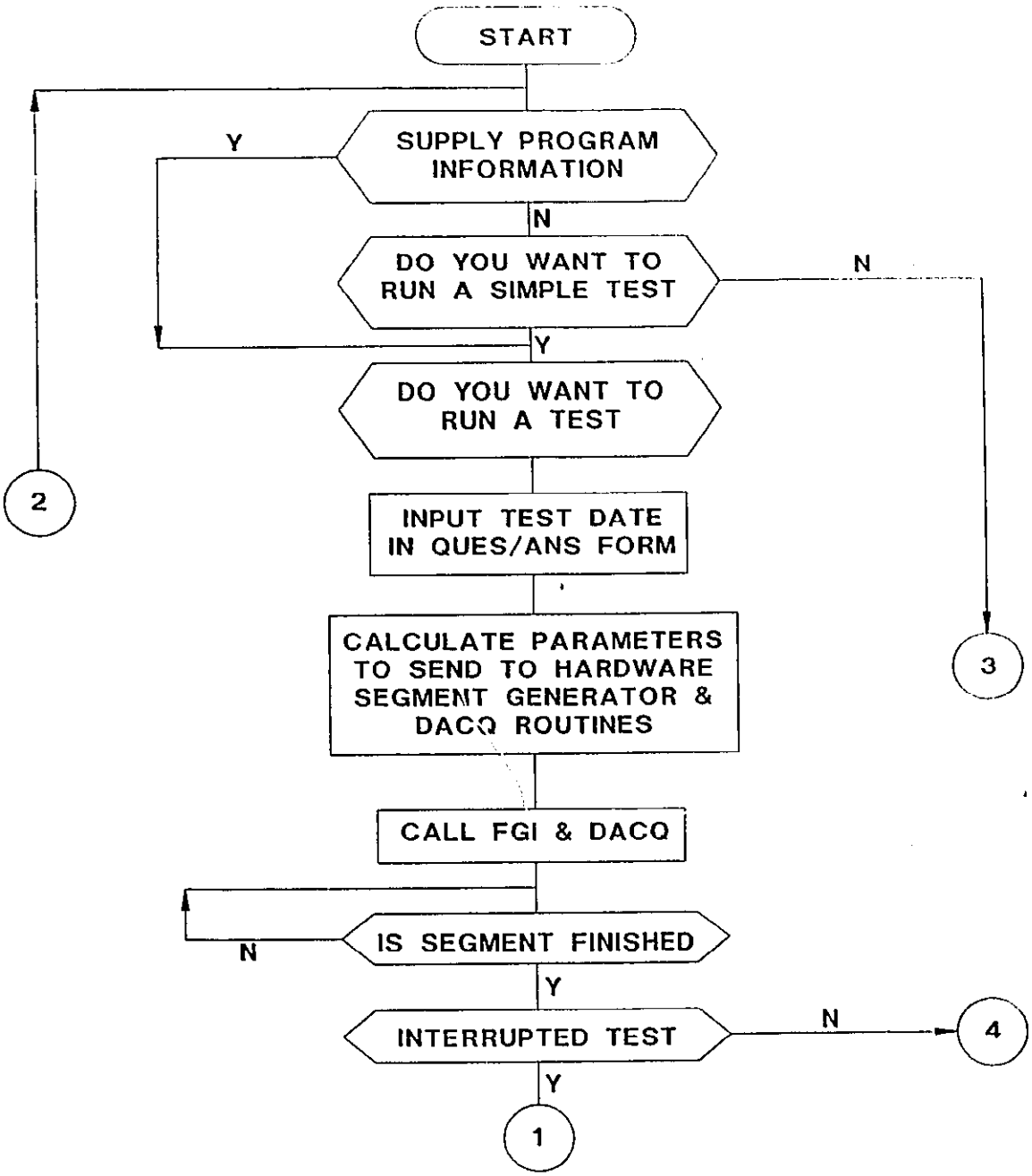

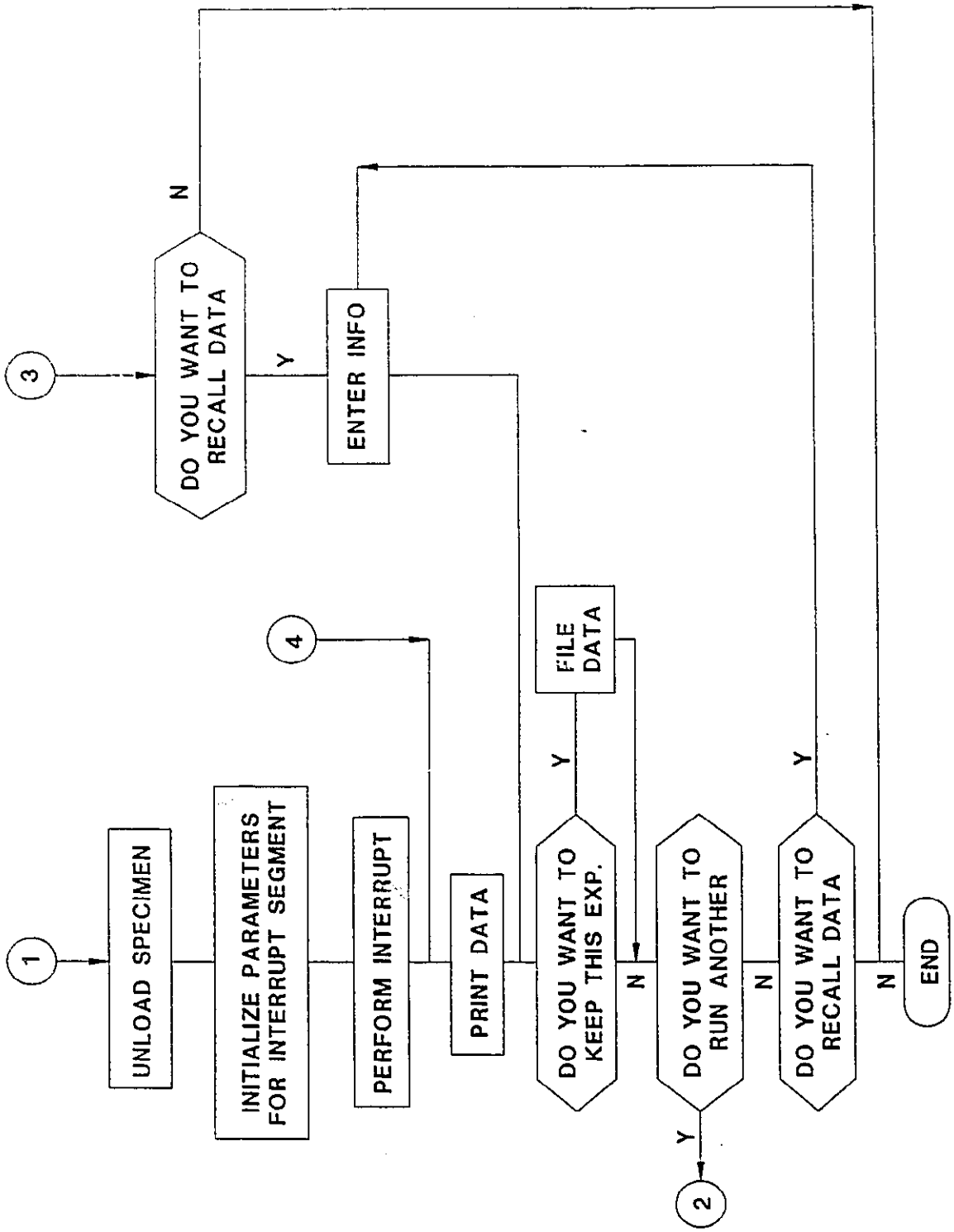
1
UNLOAD SPECIMEN
INITIALIZE PARAMETERS FOR INTERRUPT SEGMENT
PERFORM INTERRUPT
4
PRINT DATA
DO YOU WANT TO KEEP THIS EXP.
Y
FILE DATA
N
DO YOU WANT TO RUN ANOTHER
Y
2
N
DO YOU WANT TO RECALL DATA
Y
N
END
3
DO YOU WANT TO RECALL DATA
N
Y
ENTER INFO